Design and Integration of Ion-Exchangable Polymeric Materials for High-performance Fuel Cells and Water Electrolyzers

고성능 연료전지 및 수전해용
이온 교환성 고분자 설계 및 융합

2023 년 8 월

서울대학교 대학원

재료공학부

정 지 윤

Design and Integration of Ion-Exchangable Polymeric Materials for High-performance Fuel Cells and Water Electrolyzers

고성능 연료전지 및 수전해용
이온 교환성 고분자 설계 및 융합

지도교수 안 철 희

이 논문을 공학박사학위논문으로 제출함
2023 년 7 월

서울대학교 대학원
재료공학부
정 지 윤

정 지 윤 의 공학박사학위논문을 인준함
2023 년 7 월

위 원 장 _____유 웅 열_____ (인)

부위원장 _____안 철 희_____ (인)

위   원 _____권 민 상_____ (인)

위   원 _____선 정 윤_____ (인)

위   원 _____이 성 수_____ (인)

Abstract

Design and Integration of Ion−Exchangable Polymeric Materials for High−performance Fuel Cells and Water Electrolyzers

Jiyoon Jung

Department of Materials Science and Engineering

Seoul National University

As the transition to a hydrogen economy that utilizes hydrogen as an energy source is accelerating away from a fossil fuel−oriented energy system, the importance of renewable energy technology for revitalizing hydrogen production and use is emerging. Water electrolyzers and fuel cells are the basis for a sustainable hydrogen economy. Water electrolysis is a technology that produces hydrogen from water using electricity, and a fuel cell is a device that produces electricity from hydrogen fuel.

Among water electrolysis technologies, anion exchange membrane water electrolyzers (AEMWEs) are attracting attention as a next−generation water electrolyzers because it can produce high−purity hydrogen through the use of non−platinum group metal based electrodes. Anion exchange membranes (AEMs) are key component of AEMWEs, and its main role is to transfer hydroxide and prevent crossover of gas generated from both the anode and cathode. The ionomer present on the electrode catalyst layer also affects the water electrolysis performance, serving as a binder and effectively delivering hydroxide ions from the catalyst layer to the membrane.

In Chapter 2, anion exchange membranes for water electrolysis with improved mechanical strength and alkaline stability were developed. In order to increase mechanical strength, interpenetrating cationic network membranes were prepared, and pyrrolidinium and piperidinium, which have high alkaline stability, were introduced as cationic groups. The developed membranes showed improved alkaline stability and durability compared to existing commercially available anion exchange membranes.

In Chapter 3, polydiallylammonium-based anion exchange membranes and ionomer for AEMWEs were developed. Diallylammonium produces a pyrrolidinium anion exchange groups with excellent alkaline stability through cyclization polymerization. In addition, polydiallylammonium ionomers with a wide range of ion exchange capacities were synthesized by adjusting by varying side chain functional groups, and the effect of the ion exchange capacities on AEMWE performance was confirmed. Also, the greater the hydrophobicity of ionomers, the faster the emission of generated H_2 gas and the higher current density was shown because the reaction site was not blocked with H_2 gas.

High-temperature proton exchange membrane fuel cells (HT-PEMFCs) exhibit reduced carbon monoxide poisoning and increased catalytic activity due to its higher operation temperature. However, Nafion, a widely utilized, commercially available proton exchange membrane, shows rapid decrease in proton conductivity at high temperatures due to low humidity. Another type of high temperature polymer electrolyte membrane is phosphoric acid doped-polybenzimidazole, which is widely studied as a proton exchange membrane for HT-PEMFC, but suffers from phosphate poisoning of the platinum catalyst. Therefore, the development of membranes and ionomers that can be stably applied to HT-PEMFCs is necessary. In Chapter 4, ionomers and proton exchange membranes containing protonated phosphonic acid groups were developed for HT-PEMFCs. The protonated phosphonic acid group is capable of proton transport even at high temperature and low humidity. The parameters of the dispersion solvent that affect the

microporous structure of the ionomer were identified, and the effect of the microporous structure of the ionomer on the fuel cell was confirmed. Developed proton exchange membranes with protonated phosphonic acid group exhibited better mechanical properties and maintained high proton conductivity than those of Nafion at high temperature and low humidity.

Table of Contents

List of Tables

List of Figures

Chapter 1. Introduction

1.1. Anion exchange membrane water electrolyzers

With the increase in energy demand, there has been a significant rise in the use of fossil fuels, which in turn leads to environmental pollution and global warming due to the emission of greenhouse gases such as nitrogen oxides and carbon dioxide.[1] As a result, there is growing interest in hydrogen as a cleaner and sustainable energy source. Hydrogen is an environmentally friendly energy source as it releases water as a by−product of electrochemical reactions.[2] There are various methods to produce hydrogen energy, including steam reforming of natural gas, biomass, and electrolysis of water. Recently, there has been a surge in interest in water electrolysis technology that produces green hydrogen.[3]

1.1.1. Water electrolyzers

In water electrolysis, a reduction reaction occurs at the cathode and an oxidation reaction occurs at the anode. Depending on the type of electrolyte, it is largely divided into alkaline electrolyzers (AWE), proton exchange membrane water electrolyzers (PEMWE), and anion exchange membrane water electrolyzers (AEMWE),[4] the characteristics of each are listed in Table 1−1.

Table 1-1. Type of water electrolyzers

	AWE	PEMWE	AEMWE
Reaction	HER : $2H_2O + 2e^- \rightarrow H_2 + 2OH^-$ OER : $2OH^- \rightarrow \frac{1}{2}O_2 + H_2O + 2e^-$	HER : $2H^+ + 2e^- \rightarrow H_2$ OER : $H_2O \rightarrow \frac{1}{2}O_2 + 2H^+ + 2e^-$	HER : $2H_2O + 2e^- \rightarrow H_2 + 2OH^-$ OER : $2OH^- \rightarrow \frac{1}{2}O_2 + H_2O + 2e^-$
Electrolyte	NaOH, KOH solution	proton exchange membrane (Nafion)	anion exchange membrane
Temperature	70~90 ℃	50~80 ℃	40~60 ℃
Pros	• Free of PGMs and titanium based catalysts	• High current density (1000 – 2000 mA/cm²) • Low gas permeation • Higher efficiency	• Non–PGM catalysts • Wide range of active • DI water, low alkaline concentration • Low ohmic resistances • Low gas permeation • high hydrogen production rate
Cons	• H₂ crossover • Electrolyte blow–out ↗ Limited current density range ↗ low hydrogen production rate • High alkaline concentration	• High cost – PGM catalysts (cathode : Pt, anode : iridium, membrane : Nafion) • Acid corrosion tolerant hardware need	

2

Alkaline water electrolyzers (AWEs) use a porous membrane and do not require a platinum group metal (PGM) catalyst because they use alkaline electrolytes of NaOH or KOH solution.[5] However, gas crossover occurs due to the use of a porous diaphragm, and current density decreases due to leakage of the electrolyte, thereby reducing water electrolysis efficiency. PEMWE uses a proton exchange membrane (PEM) such as Nafion as an electrolyte and shows a high current density of 1,000~2,000 mA/cm^2.[6] In addition, the use of dense PEM shows low gas permeation and high hydrogen production efficiency. However, there is a problem that it is expensive due to the use of expensive Nafion electrolyte and PGM catalysts such as Pt and IrO_2. AEMWE combines the advantages of AWEs and PEMWEs, uses a dense anion exchange membrane (AEM), and has low gas permeation and high hydrogen production rate while enabling non-PGM catalysts by using an alkaline solution.[7]

AEMWE consists of a device for producing hydrogen comprising of a gas diffusion layer (GDL) and a membrane electrode assembly (MEA). Figure 1-1(a) shows a schematic diagram of AEMWE. In a MEA, the actual reaction that determines the performance of water electrolysis takes place and consists of electrode, AEM and ionomer. As shown in the reaction equation below, hydrogen evolution reaction (HER) occurs at the cathode and oxygen evolution reaction (OER) occurs at the anode.[8]

$$Cathode : 2H_2O + 2e^- \rightarrow H_2 + 2OH^-$$
$$Anode : 2OH^- \rightarrow \tfrac{1}{2}O_2 + H_2O + 2e^-$$
$$Overall : 2H_2O \rightarrow 2H_2 + O_2$$

(a)

AEMWE

$2e^-$ ↑   ↓ $2e^-$

KOH, O_2 ←   OH⁻   → H_2

H_2O

KOH, H_2O →   **AEM**

GDL   GDL

Catalyst layer   Catalyst layer

Anode   Cathode

$2OH^- → 1/2O_2 + H_2O + 2e^-$ $2H_2O + 2e^- → H_2 + 2OH^-$
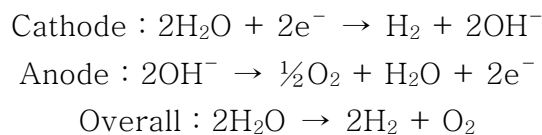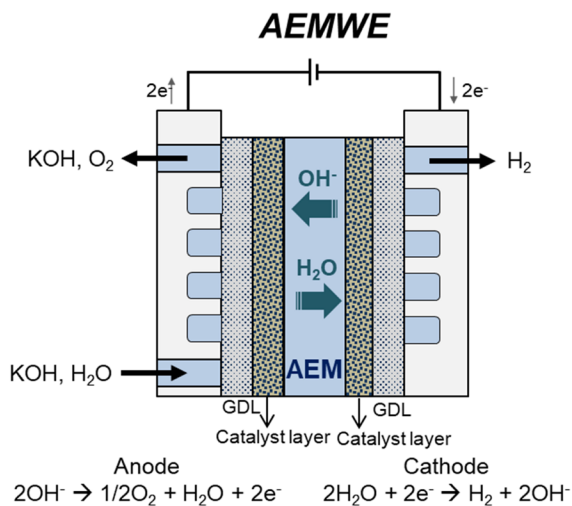
(b) Aryl-ether backbone degradation

OH⁻
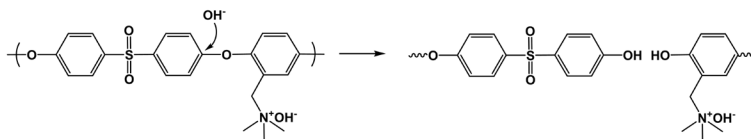
Quaternary ammonium degradation

OH⁻ SN_2 reaction

OH⁻   Hofmann elimination

Ammonium hydroxide

(c)   OH

Neutralization

Acidic phenol
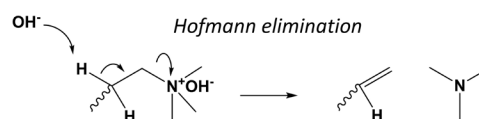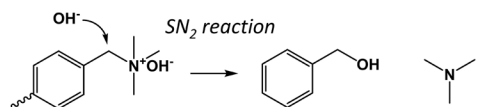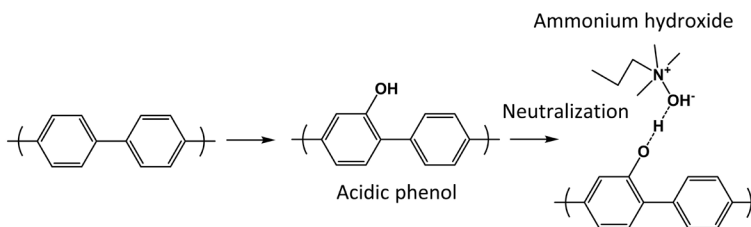
Figure 1-1. (a) Schematic illustration of AEMWEs (b) Degradation mechanism of AEMs and AEIs (c) Phenyl adsorption problem of AEIs

1.1.2. Membranes for AEMWEs

AEM is a key component of an AEMWE's MEA, and its main role is to transfer hydroxide from the cathode to the anode, and at the same time, it prevents the crossover of generated gases. In order to effectively deliver the hydroxide, it is advantageous to have high ionic conductivity and high ion exchange capacity (IEC), which represents an ion exchange group equivalent per repeating unit.[9] Because AEMWE operates in an alkaline environment, high alkaline stability of AEMs is required.[10]

The alkaline stability of AEM can be largely divided into the backbone and side chain of the polymer, and the main degradation mechanism is shown in Figure 1-1(b). The aryl-ether group in the backbone is a structure to be avoided because it is easily attacked by hydroxide and degradation occurs.[11] In order to increase the alkaline stability of the backbone, there are many studies on aryl-ether free polymer.[11] Since quaternary ammonium (QA) is an electron withdrawing group, the side chain containing the QA group can also be attacked by nucleophilic hydroxide.[12] β-hydrogen is a major degradation site of the QA group, and Hofmann elimination is likely to occur, and SN2 degradation by nucleophile (OH$^-$) attack can also occur through α-hydrogen.[13] Therefore, α,β-hydrogen-free polymer is a way to increase the alkaline stability. However, since the synthesis of the QA group generally proceeds through the SN2 reaction using a primary halide, α-hydrogen is essential. There are many difficulties in the synthesis of α,β-hydrogen-free polymers because the S_N2 reaction does not occur well if a tertiary halide is used to avoid α,β-hydrogen, and also unwanted elimination reaction can occur.

On the other hand, a study that conducted an alkaline stability test according to the type of QA groups was reported.[14] As a result of the alkaline stability test under the harsh conditions of 160℃ and 1M NaOH, the ring-shaped QA has excellent alkaline stability. In particular, the 6-azaspiro[5.5]undecanium (ASU) group

has two hexagonal rings centered on the nitrogen atom, so nucleophiles cannot easily approach it due to the steric hindrance, thus showing the excellent alkaline stability.

1.1.3. Ionomers for AEMWEs

Ionomer exists on the catalyst layer and effectively delivers the hydroxide to the catalyst layer while serving as a binder. Requirements of AEM and AEI in AEMWEs are almost similar, they should have high IEC, high ionic conductivity, and good alkaline stability.[15] However, unlike AEM, mechanical properties are not very important in AEI. Also, the benzene ring in the ionomer has an oxidation stability issue on the OER catalyst surface.[16] When the phenyl group is adsorbed on the OER catalyst, phenol is formed due to electrochemical oxidation, and the local pH decreases due to the neutralization of ammonium hydroxide.[17] Therefore, research on benzene-free ionomer is needed.

1.2. Proton exchange membrane fuel cells

1.2.1. Proton exchange membrane fuel cells

Fuel cell is an eco-friendly hydrogen power generation technology that produces electricity by using a chemical reaction between hydrogen and oxygen and generates water as a reaction product.[18] Fuel cells are classified into alkaline fuel cell (AFC), polymer electrolyte membrane fuel cell (PEMFC), phosphoric acid (PAFC), molten carbonate fuel cell (MCFC), and solid oxide fuel cell (SOFC) depending on the type of electrolyte.[19] Table 1-2 lists each feature.

Among them, PEMFCs using PEM as an electrolyte have high power density, excellent durability, and operate at relatively low temperatures.[20] Figure 1-2 (a) shows the schematic illustration of PEMFC. At the anode, H_2 gas is oxidized to generate

two protons and electrons, and at the cathode, O_2 gas reacts with protons and electrons to produce water. The membrane electrode assembly (MEA) of PEMFCs is composed of PEM, electrode containing ionomer, and gas diffusion layer (GDL).[21]

Table 1-2. Type of water fuel cells

	AFC	PEMFC	PAFC	MCFC	SOFC
Electrolyte	KOH solution	proton exchange membrane (Nafion)	Phophoric acid	Molten mixture	Ceramic
Charge carrier	OH⁻	H⁺	H⁺	CO_3^{2-}	O^{2-}
Temperature	60~230 ℃	50-100 ℃	150~250 ℃	650 ℃	600~900 ℃
Electrical efficiency	60~70 %	40~ 60 %	45~55 %	45~55 %	45~60 %

1.2.2. Membranes for PEMFCs

In PEMFC, PEM separates the cathode and anode, prevents gas crossover, and transfers protons from the anode to the cathode. For excellent performance and durability, PEMs should have high proton conductivity, oxidation stability, and mechanical properties.[22]

The most widely used PEM to date for LT-PEMFCs is Du Pont's Nafion,[23] and the chemical structure of Nafion is shown in Figure 1-2 (b). Nafion is a perfluorinated polymer composed of a polytetrafluoroethylene (PTFE) backbone and a side chain with a sulfonic acid group at the end, and has excellent thermal, chemical, and mechanical properties.[24] However, Nafion is expensive and its ionic conductivity decreases at high temperatures where water is scarce. Therefore, it is necessary to develop a PEM in which proton conduction occurs well even in a low humidity environment.

In HT-PEMFCs, polybenzimidazole (PBI) has been touted as the polymer of choice due to its excellent thermal and chemical stability.[25] The chemical structure of PA doped PBI (PA-PBI) is shown in Figure 1-2 (c). The interactions that govern the ability of PBI to "hold" phosphoric acid are classically deemed an "acid-base interaction".[26] But due to the nature of having to hold a large amount of liquid phosphoric acid, PA-PBIs easily suffers from a

7

large loss in conductivity arising from PA leaching under water condensing conditions of temperatures lower than 140 °C, mildly humidifying conditions, high gas flow rates, or even high water vapor forming conditions of high current density. And as the proton conductivity of PA−PBIs greatly depends on acid doping level,[27] maintaining a high level of PA content in the membrane is a crucial component of designing a good membrane and obtaining optimal membrane electrode assembly cell performance.

(a) **PEMFC**

(b)

(c)
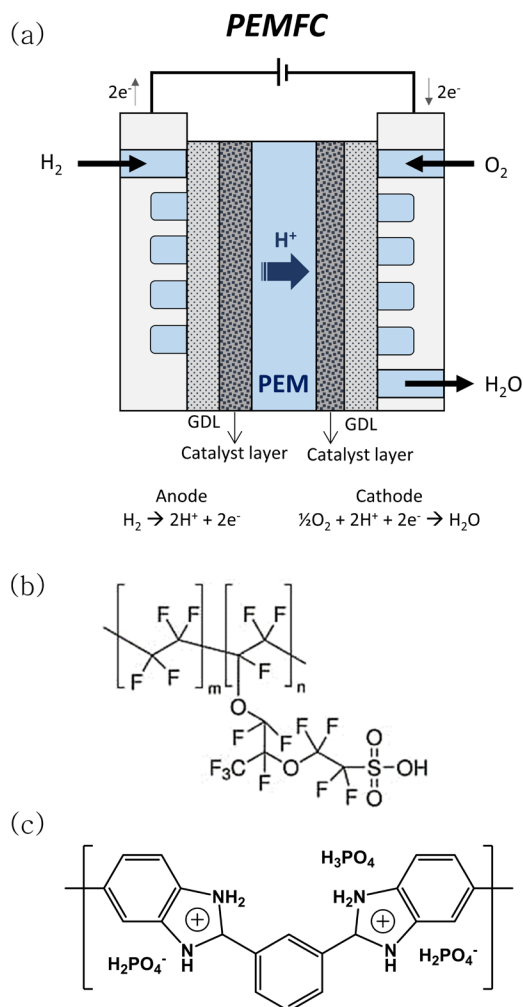
Figure 1−2. (a) Schematic illustration of PEMFCs, structure of (b) Nafion and (c) PA−PBI

1.2.3. Ionomers for PEMFCs

Ionomer is thinly coated on the catalyst layer, and it serves as a binder to prevent separation of the catalyst layer, at the same time improves performance by allowing protons to be delivered to the catalyst layer. Since the electrochemical reaction occurs at the triple phase boundary (TPB) of the electrolyte, electrode, and reaction gas, it is important to reduce the interfacial resistance of the TPB.[28] The ionomeric binder in a HT−PEMFC requires many of the same characteristics as the membrane including proton conductivity and thermal stability. However, in addition to these traits, the binder should provide high accessibility of reactant gases while limiting electrode flooding triggered by phosphoric acid redistribution,[29] which in turn is only possible through a hydrophobic interconnected network for good mass transfer. Finding the best balance between anhydrous proton conductivity with phosphoric acid with mass transfer properties has and will be the key to optimizing MEA performance.

Polytetrafluoroethylene (PTFE) has been the most widely applied binder material optimized for HT−PEMFC electrode performance due to its hydrophobicity and thermal stability.[30] The absence of proton conductivity is somewhat mitigated by excess phosphoric acid in the PA−PBI membrane which is known to migrate into the catalyst layer, causing a major tradeoff relationship with phosphate poisoning of Pt catalysts and mass transport properties. Notably, PTFE acts as an both electrical and ionic insulator in the electrode; consequently, cell performance generally decreases with increasing PTFE binder content, because the binder obstructs reaction pathways, such as those involving the movement of phosphoric acid and oxygen to the Pt particles to form the idealize TPB.

Polybenzimidazole (PBI) has also been used as ionomeric binder in HT−PEMFCs, but with varying levels of success.[31] While providing high anhydrous proton conductivity analogous to the

membrane properties, when exposed to the PA-doped PBI membrane in MEA configuration, the hydrophilicity hinders mass transport properties while giving rise to possible high levels of phosphate poisoning of the Pt catalyst.[32]

1.3. Research objectives

Chapter largely contains studies on anion exchange membranes and anion exchange ionomers for anion exchange membrane water electrolyzers, and proton exchange membranes and proton exchange ionomers for high temperature proton exchange membrane fuel cells.

In chapter 2, in order to increase the alkaline stability, mechanical strength and durability of anion exchange membranes, IPN membranes with cationic network were fabricated and evaluated using ethylene vinyl alcohol with good mechanical properties.

In chapter 3, anion exchange membranes and ionomers synthesized using diallylammonium cyclopolymerization were investigated. Both AEMs and AEIs showed excellent alkaline stability, high ionic conductivity and AEMWE performance. In addition, the ion exchange capacity (IEC) of the ionomers was adjusted over a wide range to confirm the ionomer's IEC effect on the performance.

In chapter 4, protonated phosphonic acid ionomers and membranes for HT-PEMFC capable of proton conduction even at high temperature and low humidity were developed. The parameters of the dispersion agent affecting the microporous structure of the ionomer were identified, and the performance tests of HT-PEMFC according to the microporous structure were compared.

1.4. References

[1] Bareiß, K., de la Rua, C., Möckl, M., & Hamacher, T. , **2019**, *Applied Energy*, *237*, 862-872.

[2] Nowotny, J., & Veziroglu, T. N. , **2011**, *International Journal of Hydrogen Energy*, *36*(20), 13218-13224.

[3] Kumar, S. S., & Lim, H., **2022**, *Energy Reports*, *8*, 13793-13813.

[4] Feng, Q., Liu, G., Wei, B., Zhang, Z., Li, H., & Wang, H., **2017**, *Journal of Power Sources*, *366*, 33-55.

[5] Marini, S., Salvi, P., Nelli, P., Pesenti, R., Villa, M., Berrettoni, M.,& Kiros, Y., **2012**, *Electrochimica Acta*, *82*, 384-391.

[6] Ni, M., Leung, M. K., & Leung, D. Y., **2006**, *Proceeding of the WHEC*, *16*.

[7] Cho, M. K., Lim, A., Lee, S. Y., Kim, H. J., Yoo, S. J., Sung, Y. E., ... & Jang, J. H., **2017**, *Journal of Electrochemical Science and Technology*, *8*(3), 183-196.

[8] Pérez-Alonso, F. J., Adán, C., Rojas, S., Peña, M. A., & Fierro, J. L. G., **2014**, *international journal of Hydrogen Energy*, *39*(10), 5204-5212.

[9] Overton, P., Li, W., Cao, X., & Holdcroft, S., **2020**, *Macromolecules*, *53*(23), 10548-10560.

[10] Cha, M. S., Park, J. E., Kim, S., Han, S. H., Shin, S. H., Yang, S. H., ... & Lee, J. Y., **2020**, *Energy & Environmental Science*, *13*(10), 3633-3645.

[11] Noh, S., Jeon, J. Y., Adhikari, S., Kim, Y. S., & Bae, C., **2019**, *Accounts of chemical research*, *52*(9), 2745-2755.

[12] Mohanty, A. D., & Bae, C., **2014**, *Journal of Materials Chemistry A*, *2*(41), 17314-17320.

[13] Espiritu, R., Golding, B. T., Scott, K., & Mamlouk, M., **2017**, *Journal of Materials Chemistry A*, *5*(3), 1248-1267.

[14] Marino, M. G., & Kreuer, K. D., **2015**, *ChemSusChem*, *8*(3), 513-523.

[15] Cossar, E., Murphy, F., Walia, J., Weck, A., & Baranova, E. A.,

2022, *ACS Applied Energy Materials*, *5*(8), 9938−9951.

[16] Leonard, D. P., Lehmann, M., Klein, J. M., Matanovic, I., Fujimoto, C., Saito, T., & Kim, Y. S., **2023**, *Advanced Energy Materials*, *13*(3), 2203488.

[17] Li, D., Matanovic, I., Lee, A. S., Park, E. J., Fujimoto, C., Chung, H. T., & Kim, Y. S., **2019**, *ACS applied materials & interfaces*, *11*(10), 9696−9701.

[18] Shin, J., Hwang, W. S., & Choi, H., **2019**, *Technological Forecasting and Social Change*, *143*, 239−248.

[19] Pan, J., Lu, S., Li, Y., Huang, A., Zhuang, L., & Lu, J., **2010**, *Advanced Functional Materials*, *20*(2), 312−319.

[20] Proietti, E., Jaouen, F., Lefèvre, M., Larouche, N., Tian, J., Herranz, J., & Dodelet, J. P., **2011**, *Nature communications*, *2*(1), 416.

[21] Chen, M., Zhao, C., Sun, F., Fan, J., Li, H., & Wang, H., **2020**, *ETransportation*, *5*, 100075.

[22] Tseng, C. Y., Ye, Y. S., Cheng, M. Y., Kao, K. Y., Shen, W. C., Rick, J., ... & Hwang, B. J., **2011**, *Advanced Energy Materials*, *1*(6), 1220−1224.

[23] Nimir, W., Al-Othman, A., Tawalbeh, M., Al Makky, A., Ali, A., Karimi-Maleh, H., ... & Karaman, C., **2023**, *International Journal of Hydrogen Energy*, *48*(17), 6638−6656.

[24] Teng, H., **2012**, *Applied Sciences*, *2*(2), 496−512.

[25] Li, X., Ma, H., Wang, H., Zhang, S., Jiang, Z., Liu, B., & Guiver, M. D., **2015**, *RSC Advances*, *5*(66), 53870−53873.

[26] Lee, A. S., Choe, Y. K., Matanovic, I., & Kim, Y. S., **2019**, *Journal of Materials Chemistry A*, *7*(16), 9867−9876.

[27] Yang, J., Liu, C., Gao, L., Wang, J., Xu, Y., & He, R., **2015**, *Rsc Advances*, *5*(122), 101049−101054.

[28] Dusastre, V., & Kilner, J. A., **1999**, *Solid state ionics*, *126*(1−2), 163−174.

[29] Mack, F., Morawietz, T., Hiesgen, R., Kramer, D., & Zeis, R., [1] Bareiß, K., de la Rua, C., Möckl, M., & Hamacher, T. , **2019**, *Applied Energy*, *237*, 862−872.

[30] Mack, F., Morawietz, T., Hiesgen, R., Kramer, D., Gogel, V., &

Zeis, R., **2016**, *International Journal of Hydrogen Energy*, *41*(18), 7475–7483.

[31] Yusof, M. S. M., Jalil, A. A., Ahmad, A., Triwahyono, S., Othman, M. H. D., Abdullah, T. A. T., ... & Nabgan, W., **2019**, *International Journal of Hydrogen Energy*, *44*(37), 20760–20769.

[32] Jung, J., Ku, J., Park, Y. S., Ahn, C. H., Lee, J. H., Hwang, S. S., & Lee, A. S., **2022**, *Polymer Reviews*, *62*(4), 789–825.

Chapter 2. Interpenetrating cationic network membranes for AEMWEs

2.1 Introduction

2.1.1 Methods to improve the mechanical properties of membranes

AEM should have high ionic conductivity, alkaline stability, and mechanical strength, all of which are directly related to the durability of AEMWEs.[1] There are roughly four ways to improve the mechanical strength of AEM. First, polymer crosslinking can increase dimensional stability during water uptake.[2] Crosslinking can be accomplished through double bonds reaction through a radical initiator, a ring opening reaction of epoxy groups, and S_N2 reaction between halides and amines, and there are various other methods.[3] Second, manufacturing a composite membrane by coating a polymer on a substrate with high mechanical strength increases physical properties. Polypropylene (PP), polyethylene (PE) and polytetrafluoroethylene (PTFE) are widely used as substrates.[5] Third, there is a method of manufacturing composite membranes including various inorganic nanoparticle fillers such as SiO_2, TiO_2, and ZrO_2.[6] The last method is to fabricate a blending membrane, semi−interpenetrated membrane (sIPN), and interpenetrated membrane (IPN) by mixing with a polymer that can improve mechanical properties.[6] Examples of polymers that can improve the mechanical strength include poly(vinyl alcohol (PVA), polybenzimidazole (PBI), polyimide (PI), and poly(vinylidene fluoride) (PVDF).

2.1.2 Ion-solvating materials

Ion-solvating materials can form a semi-solid by dissolving a liquid alkali electrolyte.[8] Ion-solvating membranes exhibit high hydroxide conductivity as a homogeneous ternary electrolyte part of polymer-water-KOH is formed, and exhibits the mechanical properties of a polymer membrane.[9] However, the ionic conductivity is lower than that of AEM, which directly transfers ions through cations. Representative examples of ion-solvating materials include KOH doped PBI and PVA,[9] the chemical structure of several ion-solvating materials is in Figure 2-1(a). Under alkaline conditions, PBI interacts with hydroxide by Bronsted acid-base chemistry to generate anionic ionenes,[10] enabling hydroxide transport. Ion-solvating PBI AEMs have excellent mechanical strength and gas-tightness. However, when exposed to high KOH concentration and high temperature for a long time, degradation occurs through nucleophilic attack at the C2 position of the PBI group.[11],[12] PVA is also capable of hydroxide transport through the Grotthuss mechanism under alkaline conditions and mechanism is shown in Figure 2-1(b).[13] There are several papers on blending or IPN anion exchange membranes using PVA[R], but they do not show good mechanical strength during water uptake due to the abundant hydrophilic hydroxyl groups in PVA.

Ethylene vinyl alcohol (EVOH) is a new ion-solvating material. EVOH is composed of a hydrophobic ethylene part and a hydrophilic vinyl alcohol part.[14] EVOH is an semi-impermeable polymer and absorbs water well due to the vinyl alcohol part. In addition, there is an ethylene group in the backbone, which increases dimensional stability by reducing swelling during uptake compared to PVA.

(a)

KOH doped PBI   PVA   EVOH

(b)
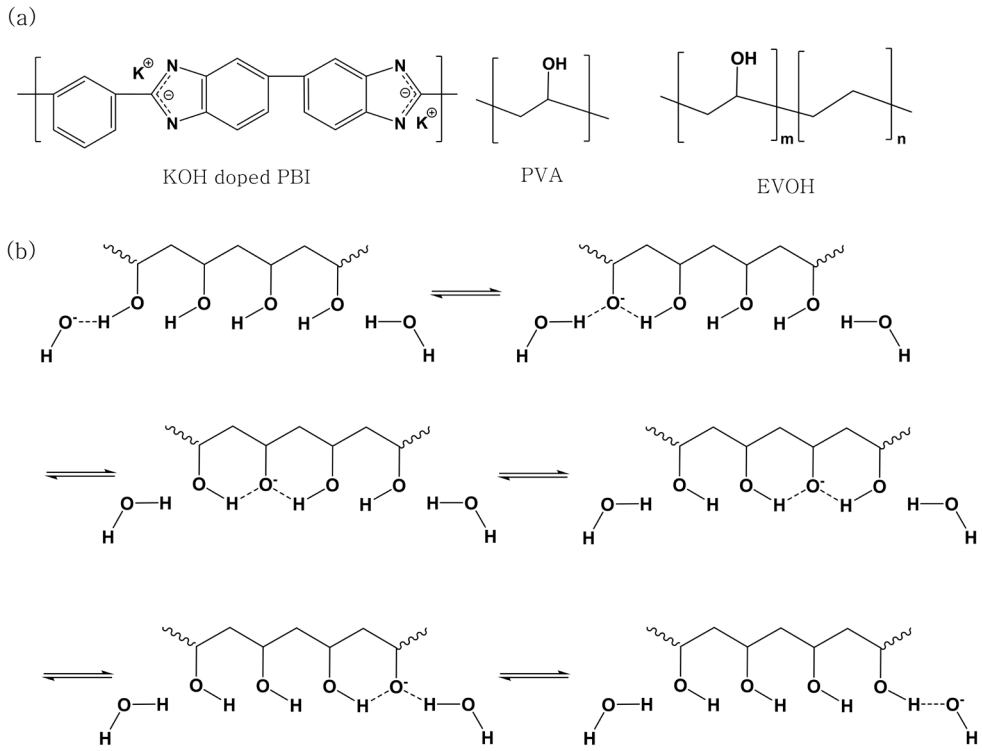
Figure 2-1. (a) Chemical structure of ion-solvating materials
(b) Hydroxide transfer through Grotthuss mechanism of PVA under
alkaline conditions

2.1.3 Menshutkin reaction

Important part of AEM and AEI is the cationic group capable of ion transport. Menshutkin reaction is one of the reactions that can generate cationic group,[15] and Figure 2−2(a) shows the mechanism. The Menshutkin reaction is a S_N2 reaction and reacts faster in high polarity solvents than in low polarity solvents.[16] The Menshutkin reaction occurs well in the 1° halide substrate, but the reaction doesn't occur well in the 3° halide substrate due to steric hindrance, and rather, the elimination reaction may occur. Therefore, it is important to select an appropriate halide substrate and tertiary amine.

2.1.4 Cyclopolymerization of diallylamine

The cyclopolymerization of diallylamine occurs through the mechanism of initiation, intramolecular cyclization, and linear propagation,[17] and the mechanism is shown in Figure 2−1(b). After cyclopolymerization of diallylamine monomer, five−membered pyrrolidinium rings are generated.[18] These pyrrolidinium based quaternary ammoniums have good alkaline stability[19], so it can be applied to the fabrication of AEM. Because cationic diallylammonium monomers undergo polymerization better than neutralized diallylamine[20], diallylamine monomer reacts in aqueous HCl to form ammonium forms.

(a)

(b)
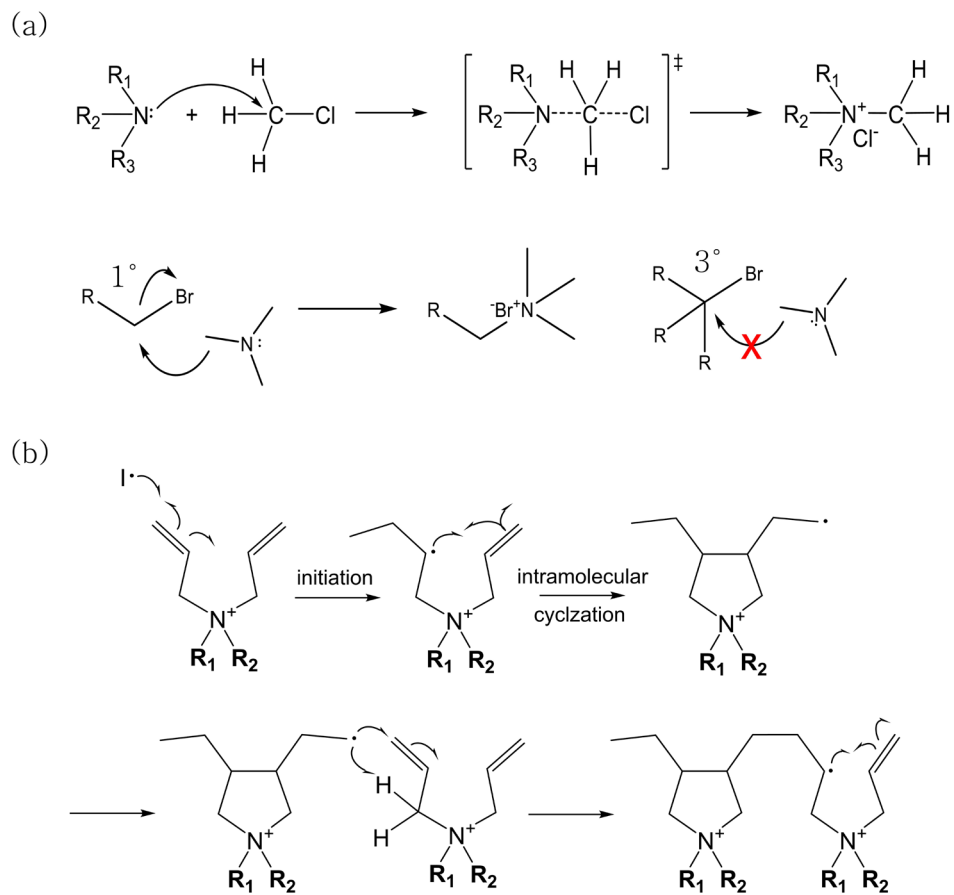
Figure 2-2. (a) Menshutkin reaction (b) Cyclopolymerization mechanism of diallylamine monomers

2.1.5 References

[1] Zhang, J., Zhang, K., Liang, X., Yu, W., Ge, X., Shehzad, M. A., ... & Xu, T., **2021**, *Journal of Materials Chemistry A*, *9*(1), 327−337.

[2] Devi, R. R., Ali, I., & Maji, T. K., **2003**, *Bioresource technology*, *88*(3), 185−188.

[3] Sibaja, B., Pereira Matheus, C., Ballestero Mendez, R., Vega Baudrit, J., & Auad, M. L., **2017**, Synthesis and Characterization of Interpenetrating Polymer Networks (IPNs) from Acrylated Soybean Oil and a−Resorcylic Acid: Part 1. Kinetics of Network Formation.

[4] Teo, A. J., Mishra, A., Park, I., Kim, Y. J., Park, W. T., & Yoon, Y. J., **2016**, *ACS Biomaterials Science & Engineering*, *2*(4), 454− 472.

[5] Xu, Z. L., Yu, L. Y., & Han, L. F., **2009**, *Frontiers of Chemical Engineering in China*, *3*, 318−329.

[6] Couture, G., Alaaeddine, A., Boschet, F., & Ameduri, B., **2011**, *Progress in Polymer Science*, *36*(11), 1521−1557.

[7] Wan, Y., Creber, K. A., Peppley, B., Bui, V. T., & Halliop, E., **2005**, *Polymer international*, *54*(1), 5−10.

[8] Kraglund, M. R., Carmo, M., Schiller, G., Ansar, S. A., Aili, D., Christensen, E., & Jensen, J. O., **2019**, *Energy & environmental science*, *12*(11), 3313−3318.

[9] Aili, D., Yang, J., Jankova, K., Henkensmeier, D., & Li, Q., **2020**, *Journal of Materials Chemistry A*, *8*(26), 12854−12886.

[10] Aili, D., Yang, J., Jankova, K., Henkensmeier, D., & Li, Q., **2020**, *Journal of Materials Chemistry A*, *8*(26), 12854−12886.

[11] Hu, B., Huang, Y., Liu, L., Hu, X., Geng, K., Ju, Q., ... & Li, N., **2022**, *Journal of Membrane Science*, *643*, 120042.

[12] Kraglund, M. R., Carmo, M., Schiller, G., Ansar, S. A., Aili, D., Christensen, E., & Jensen, J. O., **2019**, *Energy & environmental science*, *12*(11), 3313−3318.

[13] Zhang, K., McDonald, M. B., Genina, I. E., & Hammond, P. T., **2018**, *Chemistry of Materials*, *30*(18), 6420−6430.

[14] Phillips, A. K., & Moore, R. B., **2005**, *Polymer*, *46*(18), 7788−

7802.

[15] Mohanty, A. D., Lee, Y. B., Zhu, L., Hickner, M. A., & Bae, C., **2014**, *Macromolecules*, *47*(6), 1973-1980.

[16] Sola, M., Lledos, A., Duran, M., Bertran, J., & Abboud, J. L. M., **1991**, *Journal of the American Chemical Society*, *113*(8), 2873-2879.

[17] Solomon, D. H., & Hawthorne, D. G., **1976**, *Journal of Macromolecular Science-Reviews in Macromolecular Chemistry*, *15*(1), 143-164.

[18] Umoren, S. A., Solomon, M. M., Ali, S. A., & Dafalla, H. D., **2019**, *Materials Science and Engineering: C*, *100*, 897-914.

[19] Sun, Z., Lin, B., & Yan, F., **2018**, *ChemSusChem*, *11*(1), 58-70.

[20] Tuzun, N. S., Aviyente, V., & Houk, K. N., **2003**, *The Journal of Organic Chemistry*, *68*(16), 6369-6374.

2.2 EVOH supported cationic network IPN membranes using Menshutkin reaction for AEMWEs

2.2.1 Introduction

In order to manufacture AEM, complex synthetic processes or expensive catalysts are required, which are obstacles to commercialization. For example, in the case of free radical polymerization using vinyl monomers, oxygen interferes with polymerization, so it is very important to remove and control oxygen.[1] In addition, in some cases, expensive Grubbs polymerization catalysts or dangerous super acids are used, so it is necessary to develop AEMs that can be easily manufactured for commercialization.[2-4]

In this study, AEM was fabricated in a simple way through one-step fabrication and crosslinking using Menshutkin reaction of commercially available monomers. In order to increase the alkaline stability, a monomer capable of forming ring structure with piperidinium[5] was selected. In addition, to increase the mechanical strength, ion-solvating materials, EVOH, was used to make an IPN membrane. These EVOH supported cationic network IPN membranes can be manufactured in a very simple way, and are expected to have good alkaline stability and mechanical properties.

2.2.2 Experimental

Materials

1,3,5-Tris(bromomethyl)benzene (97%), 4,4'-trimethylenebis (1-methylpiperidine)(98%), poly(vinyl alcohol-co-ethylene) (EVOH, ethylene 32 mol %), and poly(vinyl alcohol) (PVA) with Mw of 89,000-93,000 g/mol were supplied by Sigma Aldrich Chemical Co. Ltd and used as received. Glutaraldehyde (GA, 25 wt% solution in water), dimethyl sulfoxide (DMSO, 99.5 %), ethanol (99.5 %), potassium oxide (KOH), n-propyl alcohol (NPA)

and hydrochloric acid (HCl, 35~37 %) were obtained from Daejung and used as received.

For membrane electrode assembly fabrication, platinum ruthenium (Pt–50 wt%, Ru–25 wt%, 047371.06) on high surface area advanced carbon support, and iridium(IV) oxide (99.99 wt%, 043396.06), cobalt nanopowder (99.8%, 46347) were received from Alfa Aesar. FAA–3–50 membrane and ionomer were received from FumaTech.

EVOH supported cationic network IPN membrane preparation

For the fabrication of the AEMs, a total of three solutions of two monomer solutions and an EVOH solution were prepared. 1,3,5–Tris(bromomethyl)benzene (1.0 g, 2.80 mmol) and 4,4′ – Trimethylenebis(1–methylpiperidine) (1.0 g, 4.20 mmol) were dissolved in 9 g of DMSO, respectively. In another vial, 20 g of 10 wt% EVOH/DMSO solution was prepared. After mixing the three solutions at once, well–mixed solution was casted on a glass plate. The solvent was evaporated while crosslinking through Menshutkin reaction took place within the EVOH matrix for 24 hrs in a convection oven at 80℃. After that, the cast membranes were placed in a vacuum oven at 100℃ for 48 hrs to evaporate off residual DMSO solvent. Then, the cross–linked membrane was removed from the glass plate and PiP/50EVOH was obtained. In the same way, PiP/60, 70, and 80 EVOH were obtained by adjusting the ratio of the PiP cation network and EVOH. Fabrication process of PiP/xEVOH is shown in Figure 2–3(a).

To increase the dimensional stability of the anion exchange membrane, the hydroxide group of EVOH was cross–linked with glutaraldehyde. 5% GA solution was prepared by diluting the 25% GA aqueous solution with ethanol, and pH was adjusted to 3 with HCl.[6] Synthesized IPN membrane was immersed at 70℃ for 24 hrs. IPN membrane was finally obtained through washing and drying. Crosslinking mechanism of PVA parts is shown in Figure 2–3(b).

(a)

(b)
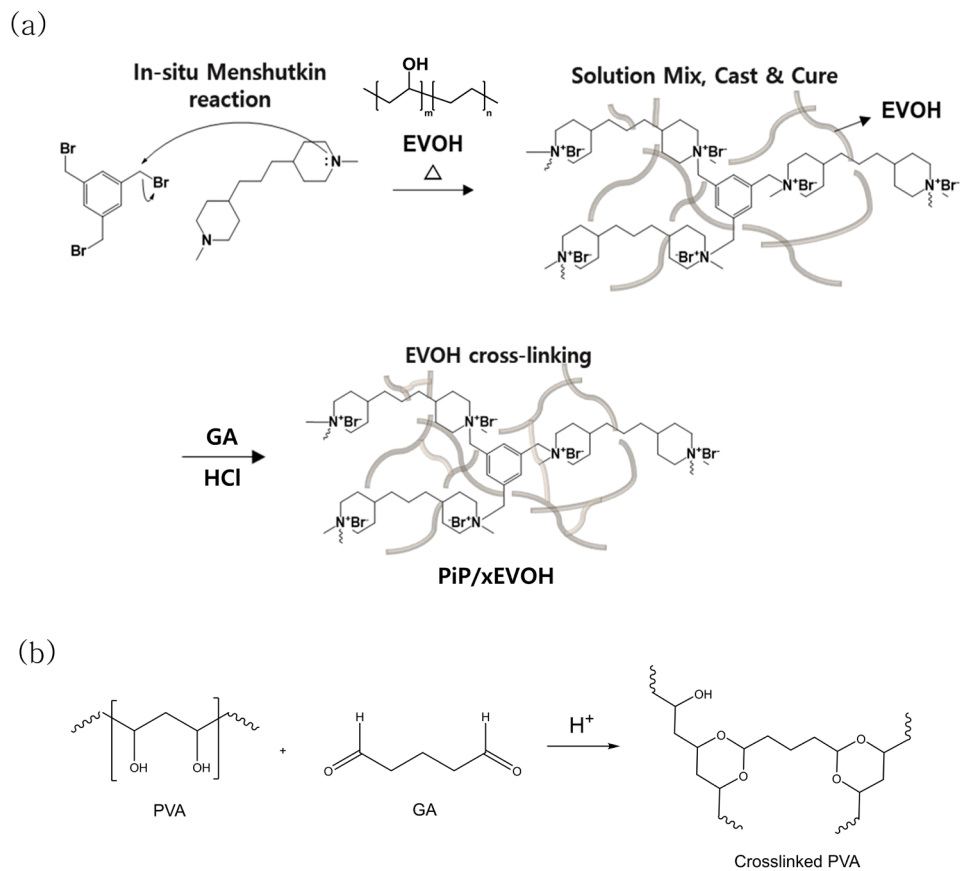
Figure 2-3. (a) Fabrication process of PiP/xEVOH membranes (b) PVA crosslinking mechanism with GA

Characterization and measurements

Fourier-transform infrared spectroscopy (FT-IR) spectra was obtained using PerkinElmer FT-IR system (Spectrum-GX) to analyze the structure of AEMs. The thermal stability of the PiP/xEVOH membranes were examined by using TA Instrument TGA 2950 with heating rate of 10 ℃/min under N_2 atmosphere. Mechanical property of the AEMs were characterized using universal tensile machine (Tinius Olsen H5K-T). Membrane samples (4cm*0.5cm) were prepared to measure the mechanical strength and tested at stretching speed of 10 mm/min.

Ion exchange capacity (IEC) value was determined by the back titration. OH^- form membranes were immersed in 0.01 M HCl solution for 24 hrs. The HCl solution was titrated with 0.01 M KOH solution after adding three drops of phenolphthalein/EtOH indicator solution. The IEC (meq g^{-1}) was calculated based on the following equation:

$$IEC = (V_{HCl}*C_{HCl} - V_{NaOH}*C_{NaOH})/W_{dry}$$

Where VHCl and VNaOH are volume of HCl and NaOH, respectively. CHCl and CNaOH are the concentration of HCl and NaOH, respectively. Wdry is the weight of the dried membranes.

The swelling ratio (SR) and water uptake (WU) were evaluated after immersing the membrane in water at room temperature for 24 hrs. After removing the membrane from the water, excess water on the surface was carefully wiped off and the weight and length was measured for comparison. After membrane was completely dried, the weight and length of the dried membrane were also measured. As the result, SR and WU were calculated according to the following formula:

SR = ((Lwet -Ldry)/Ldry)*100
WU= ((Wwet-Wdry)/Wdry) *100

The KOH uptake rate is also tested in the same way. After the

preparation of the membrane, the membrane was immersed in 1M KOH solution at room temperature for 24 hrs. The weight of the membrane was measured after removing the excess KOH solution on the surface of the membrane. After washing several times with water and drying, the weight of dried membrane was measured and compared. KOH uptake was calculated using the following equation.

KOH uptake $= ((m_{wet,KOH}-m_{dry})/m_{dry})*100$

The ohmic resistance of the AEMs were measured in water and 0.1M-5M KOH solution at different temperature by two-electrode electrochemical impedance spectroscopy (EIS, SI 1260, Solartron) over the frequency range from 10 Hz to 10 MHz with an amplitude of 20 mV. Before measurement, all OH- form membranes were immersed in distilled water for at least 24 hrs to equilibrate in water. Hydroxide conductivity was calculated by the following equation:

$\sigma = L/(R \times W \times d)$

where L was the distance between two electrodes (cm), R was the measured ohmic resistance (Ω), W was the width of the membrane (cm) and d was the width of the membrane (cm).

MEA fabrication and electrolysis performance

PiP/xEVOH based MEAs ($1cm^2$ active area) were fabricated by the catalyst coated substrate (CCS) method. 50 wt% PtRu/C was used as anode and IrO_2, Co were used as cathode catalysts, respectively. Catalyst inks were prepared by dispersing each catalyst powder over the TMA-70 ionomer which was synthesized,[7] chemical structure and NMR spectra are shown in Figure 2-4(a) and (b). (4.65 wt% TMA-70 solution in n-propanol : aqueous 5:5 wt co-solution, the ionomer to carbon (I/C) weight ratio is 0.5, and for the OER catalyst layer the binder content was 10wt%) in an aqueous solution of n-propanol and little

amount of water, followed by ultrasonic treatment for more than 20 min with maintaining water temperature less than 35℃ to prevent catalyst agglomeration. The prepared catalyst inks were directly sprayed onto the gas diffusion layer (GDL) set on a 70℃ pre-heated hotplate. GDLs 39 BB (Fuel Cell Store), and Pt coated Ti paper (Giner) were used for the cathode and anode respectively. Cathode catalyst loading amount is 0.6 $mgPt \cdot cm^{-2}$, and anode catalyst loading amount is 2.0 $mgIr \cdot cm^{-2}$, 0.7 $mgCo \cdot cm^{-2}$. The fabricated CCS was dried at room temperature for more than 1 h to remove residual solvent in the catalyst layers. Prior to single cell application, the PiP/xEVOH membranes were sandwiched by the fabricated electrode without hot-pressing process. Polarization curves were obtained on Scribner electrolyzer cell with power supplied by Biologic potentiostat (SP-200) attached with power booster (HCV-3048) with electrolyte supplied with peristaltic pump.

Figure 2-4. (a) Chemicals structure and ^{1}H-NMR spectra (b) ^{19}F-NMR spectra for TMA-70 ionomers
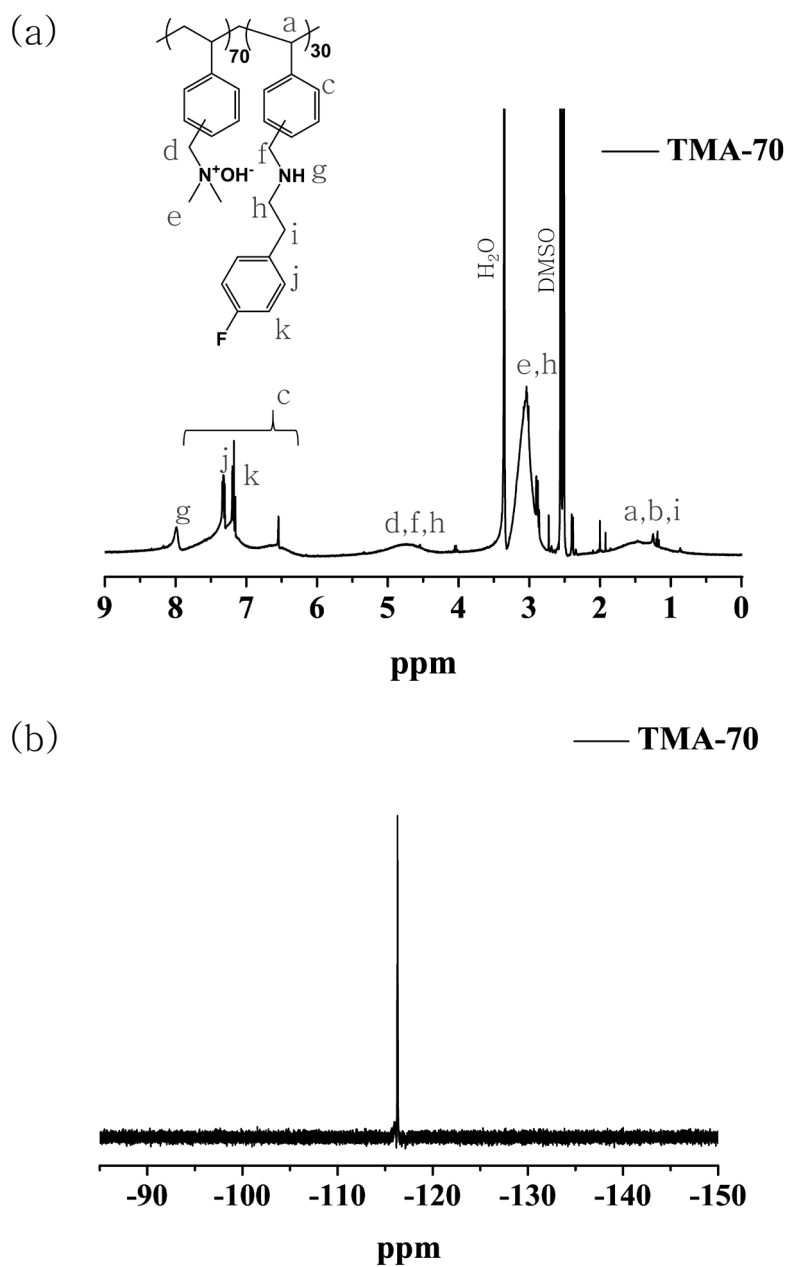
2.2.3 Results and discussion

Preparation and characterization of membranes

One of the advantages of PiP/xEVOH is that IEC can be easily controlled by adjusting the content of cationic group and EVOH. A membrane with only 100% of cationic PiP network, theoretically has IEC 4.10 mmol/g, and when only EVOH is 100%, it has zero IEC because there is no ion exchange group. In this study, AEMs with a theoretical IEC ranging from 0.82 to 2.05 were fabricated by adjusting the EVOH content in the PiP/xEVOH membrane from 50 to 80 wt%. PiP/xEVOH was flexible and yellowish, and Figure 2-5 shows SEM images of the PiP/xEVOH cross section. Even when the EVOH content increased from 50 wt% to 80 wt%, a dense structure was shown without any phase separation.
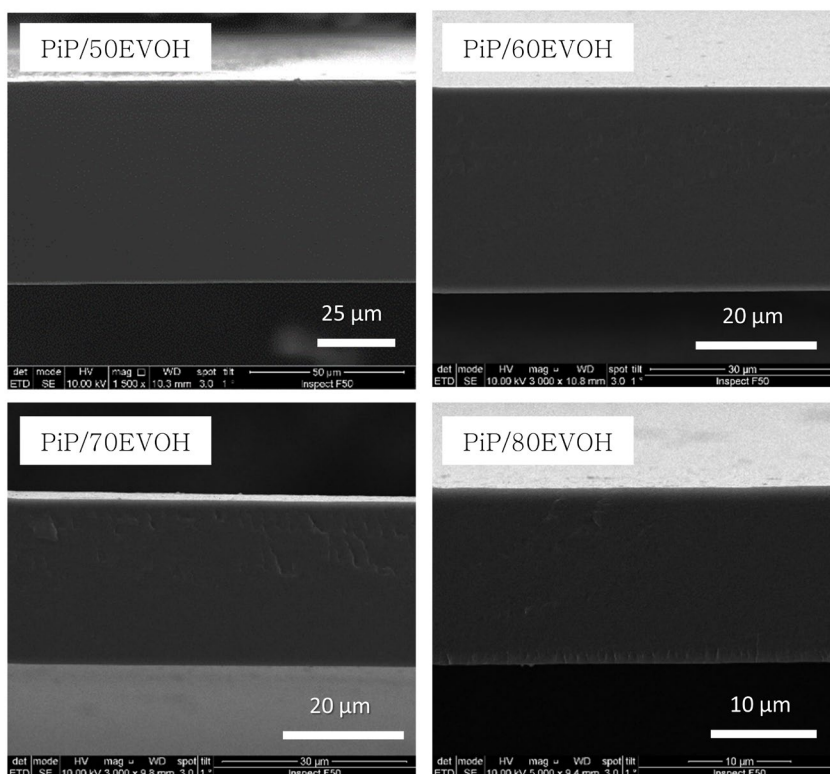
Figure 2-5. SEM images of PiP/xEVOH membrane (cross section)
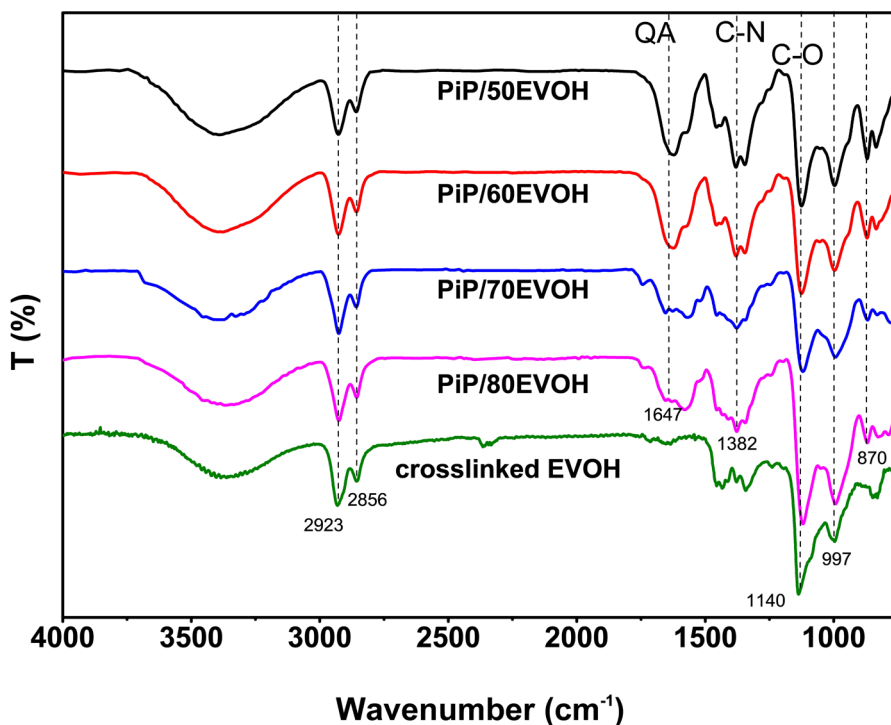
Figure 2-6. FT-IR spectra for PiP/xEVOH

Figure 2-6 shows FT-IR spectra of cross-linked EVOH film and PiP/xEVOH membrane with EVOH content of 50-80 wt%. Hydroxyl group was observed at ~3000 cm^{-1} due to the EVOH in all membranes.[8] EVOH related peaks were observed at 2923 cm^{-1} (antisymmetric stretching of CH$_2$), 2856 cm^{-1} (Symmetric stretching of CH$_2$), 1140 cm^{-1} (C-O), 1150-1085 cm^{-1} (C-O-C) and 997 cm^{-1} (-COCO-, acetal group).[9-11] In the PiP/xEVOH membrane, peak of 1647 cm^{-1} indicating the stretching vibration of quaternary ammonium groups increased as the PiP content increased. Also PiP/xEVOH membrane related peaks are observed at 1382 cm^{-1} (C-N) and 870 cm^{-1} (aromatic C-H and C=C stretch).[12]
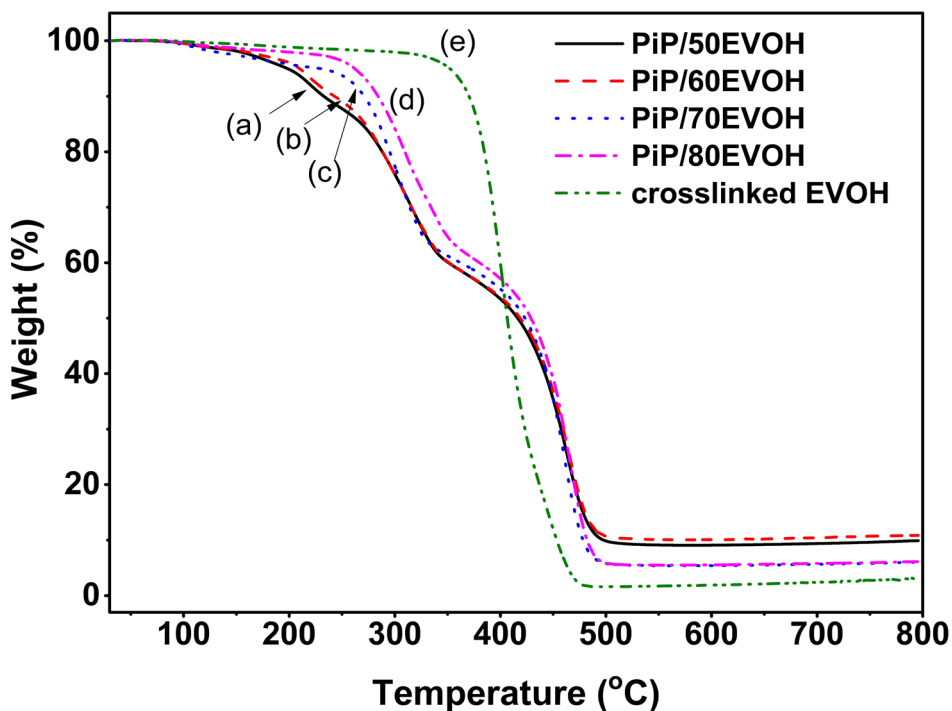
Figure 2-7. TGA curves for (a) PiP/50EVOH (b) PiP/60EVOH (c) PiP/70EVOH (d) PiP/80EVOH (e) crosslinked EVOH

As the operating temperature of AEMWE is 60-80℃, the AEMs should have thermal stability over 100℃.[13] The thermal stability of cross-linked EVOH and PiP/xEVOH membrane was analyzed by TGA as depicted in Figure 2-7. Crosslinked EVOH showed high thermal stability up to 300℃ and thermal degradation of EVOH backbones started at 310℃. Moreover, all the PiP/xEVOH AEMs were stable up to 200℃, and exhibited excellent thermal stability. The T_{d5} (5 wt% degradation temperature) is 198℃, 209℃, 228℃, 262℃, and 350℃ for PiP/50,60,70,80 EVOH and crosslinked EVOH, respectively. In PiP/xEVOH, the decomposition of piperidinium cations started around 200℃, which is characteristic of ammonium functionalized polymers.
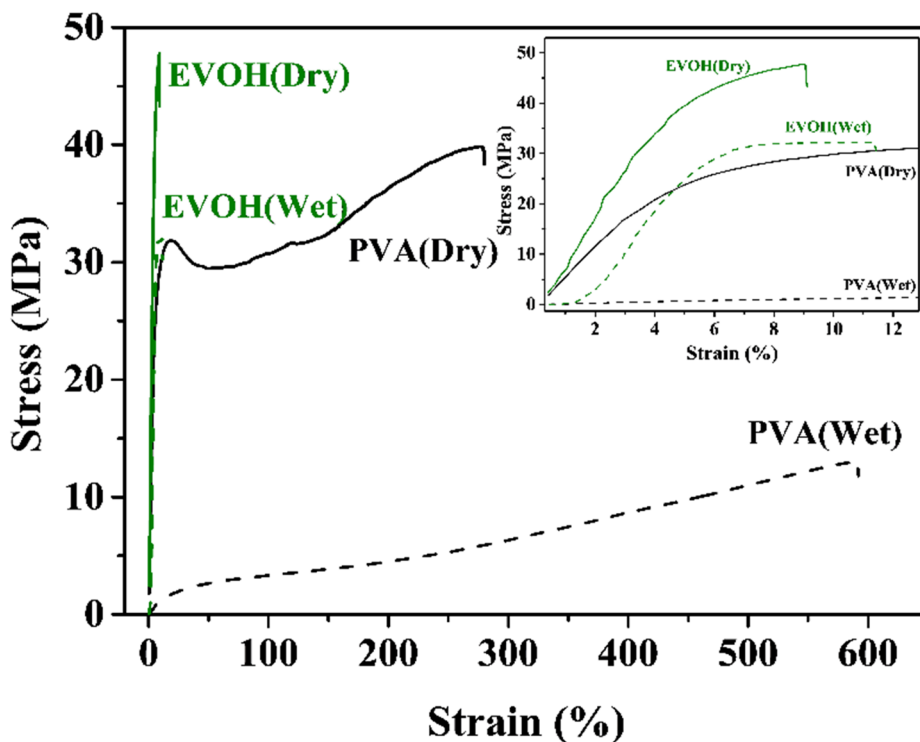
Figure 2-8. Stress-strain curves for crosslinked PVA and crosslinked EVOH freestanding film

In order to justify use of EVOH over PVA, mechanical properties are initially tested. Figure 2-8 shows stress-strain curves for crosslinked PVA and crosslinked EVOH freestanding films. PVA film showed high elongation at break of 278% and tensile strength of 39.8 MPa under dry conditions. EVOH showed a relatively low elongation at break of 9.1%, but showed a higher tensile strength of 47.8 MPa. At the dry conditions, the elongation at break of PVA increased to 583%, but the tensile strength was decreased by 12.9 MPa, while the wet EVOH film showed a slight increase in elongation at break and excellent tensile strength of 32.2 MPa. Thus, the higher mechanical strength under both dry and wet conditions as well the relatively lower drop-off in tensile strength when wet was the main reasoning and rationale behind the selection of EVOH over PVA as IPN counterpart.
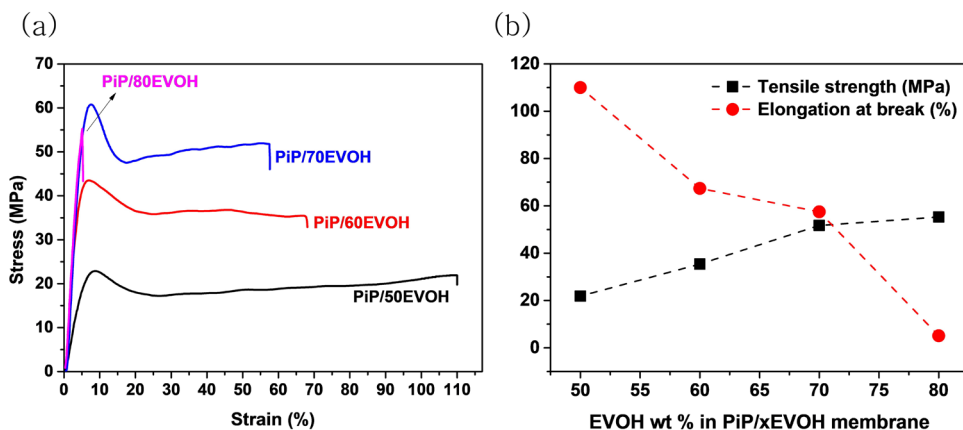
Figure 2-9. (a) Stress-strain curves for PiP/xEVOH (b) Summary of mechanical properties for PiP/xEVOH

Figure 2-9(a), (b) shows the stress-strain curves and tensile strength values, respectively for PiP/xEVOH membranes. PiP/xEVOH membranes showed excellent mechanical strength that ranged from 21.9-55.3 MPa. PiP/80EVOH showed highest tensile strength of 55.3 MPa but showed low elongation at break of 5.1% due to the low elongation at break of EVOH freestanding film as shown in the Figure 2-8. As the EVOH content increased, tensile strength increased while elongation at break decreased as expected. Moreover, Figure 2-10 compares the mechanical properties between PiP/60PVA and PiP/60EVOH, and PiP/60EVOH has higher tensile strength of 35.4 MPa than that of PiP/60PVA.

Table 2-1. Hydration properties of FAA-3, crosslinked PVA and EVOH, and PiP/xEVOH

Sample	IEC[a] (mmeq g^{-1})	Water uptake (%)[b]	Swelling ratio (%)[c]	KOH uptake (%)[d]	Ionic conductivity (mS cm^{-1})[e] 25 ℃	70 ℃
FAA-3	2.01	41.6	13.5	80.2 ± 0.8	23.4	59.6
crosslinked PVA	-	19.3 ± 1.1	0.7 ± 0.7	19.3 ± 0.1	-	-
crosslinked EVOH	-	8.4 ± 0.1	4.2 ± 0.5	7.3 ± 1.3	-	-
PiP/50EVOH	1.46	37.9 ± 0.2	11.2 ± 0.6	60.9 ± 1.1	41.4	66.6
PiP/60EVOH	1.38	35.5 ± 1.5	10.9 ± 0.2	53.1 ± 8.4	35.2	54.4
PiP/70EVOH	0.88	20.3 ± 0.4	4.6 ± 1.0	28.8 ± 0.7	26.8	51.6
PiP/80EVOH	0.70	17.2 ± 0.4	4.4 ± 0.7	14.7 ± 4.3	21.2	49.3
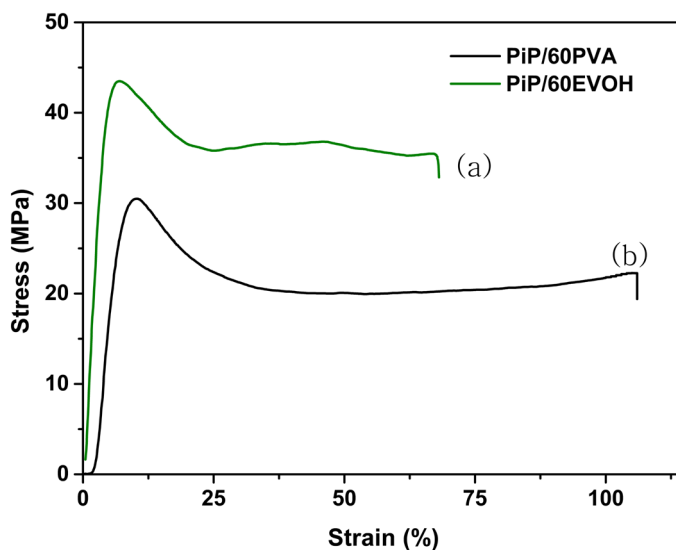
Figure 2-10. Stress-strain curves for (a) PiP/60PVA (b) PiP/60EVOH

Hydration properties of membranes

Table 2-1 lists experimental IEC, water uptake, swelling ratio, KOH uptake and hydroxide conductivity of FAA-3, crosslinked PVA, crosslinked EVOH, and PiP/xEVOH. FAA-3 is commercially available AEM, although the exact structure is not known, consists of polyaromatic backbone and side chain with QAs.[14] FAA-3 is fully AEM, has an IEC of 2.01, and has been compared with PiP/xEVOH.

Figure 2-11 show the water uptake, swelling ratio and KOH uptake of PiP/xEVOH according to the EVOH content. The lower the EVOH content, that is, the higher the cationic PiP content, the higher the absorption and swelling characteristics. PiP/50EVOH with the lowest EVOH content showed a water uptake of 37.9%, a swelling ratio of 11.2%, and a KOH uptake of 60.9%.
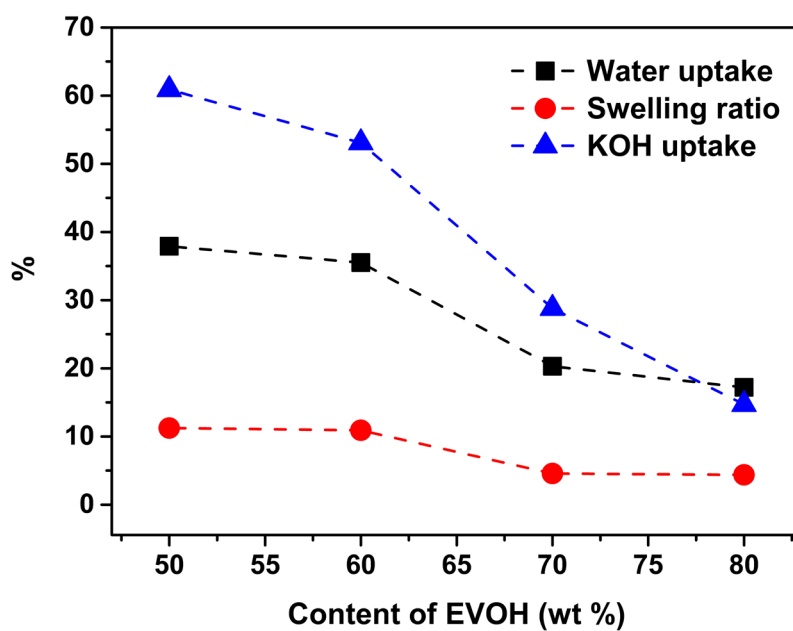
Figure 2-11. Water uptake and swelling ratio and KOH uptake of PiP/xEVOH
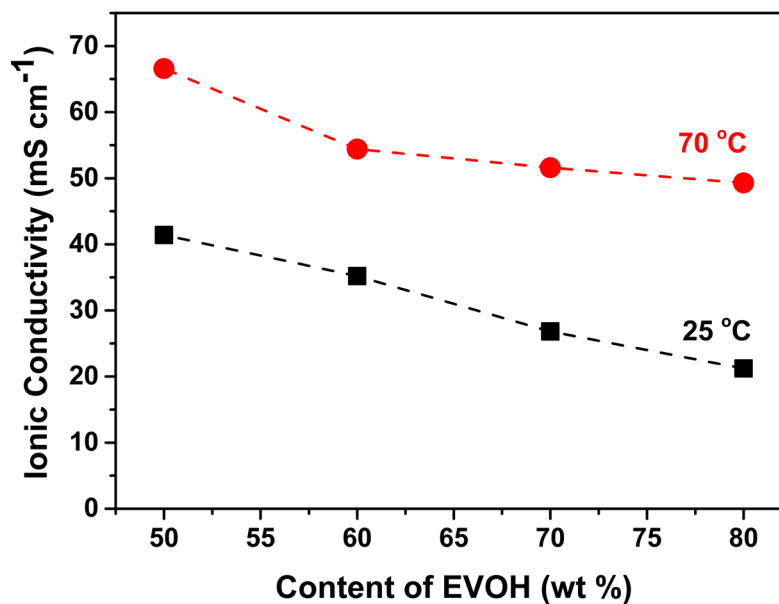
Figure 2-12. Hydroxide conductivity of PiP/xEVOH
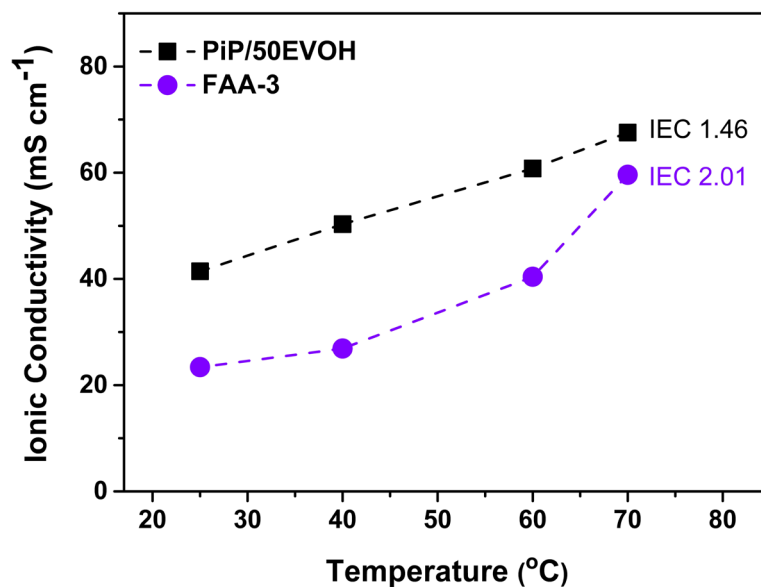
Figure 2-13. Hydroxide conductivity of PiP/50EVOH and FAA-3 at different temperature

Hydroxide conductivity

The hydroxide conductivity of PiP/xEVOH at 25℃ and 70℃ is plotted in Figure 2-12. Similar to the uptake characteristics, the higher the cationic content, the higher the ionic conductivity. PiP/50EVOH showed the highest hydroxide conductivity of 66.6 mS/cm at 70 ℃. Figure 2-13 shows the change in ionic conductivity of PiP/50EVOH with increasing temperature and comparison with FAA-3.

As the temperature increased, the hydroxide conductivity increased. FAA-3 was expected to have higher ion conductivity as a fully anion exchange membrane, however the ionic conductivity of PiP/50EVOH was higher than that of FAA-3 at all temperatures. PiP/50EVOH is an IPN membrane, but its water uptake properties are almost similar to FAA-3, and EVOH has no cationic group, but it can transfer some hydroxide like PVA's hydroxide transfer through Grotthuss mechanism.[15]
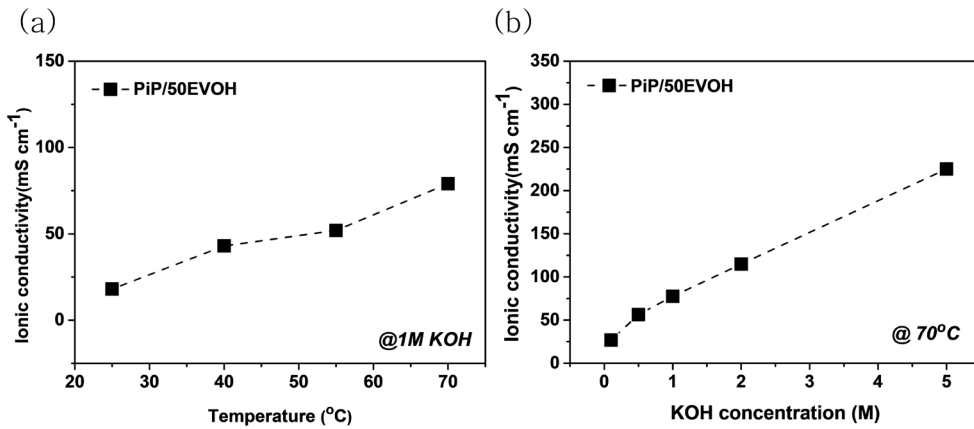
Figure 2-14. (a) Hydroxide conductivity by temperature of PiP/50EVOH membrane in 1M KOH solution. (b) Hydroxide conductivity of PiP/50EVOH membrane according to KOH concentration.

It is interesting to compare the hydroxide conductivity under real alkaline conditions because the operation of AEMWEs is carried out in a KOH environment. Figure 2-14(a) shows the hydroxide conductivity by temperature of PiP/50EVOH measured in 1M KOH solution. Similar to the measurement in water, the hydroxide conductivity increased as the temperature increased, and an ionic conductivity of 79 mS/cm was measured at 70℃. Figure 2-14(b) shows the hydroxide conductivity according to the KOH concentration. It can be seen that as the KOH concentration increases, the amount of hydroxide that can be delivered in the solution increases and the conductivity increases.

(a)   (b)
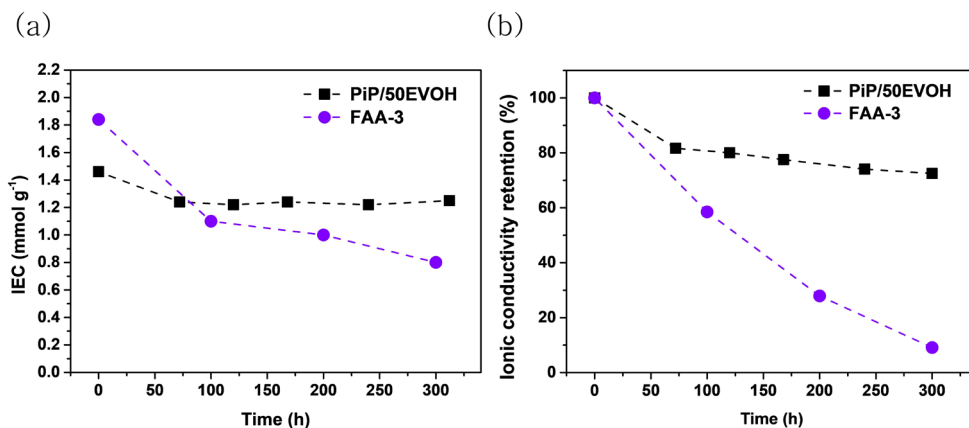
Figure 2−15. Alkaline stability of PiP/50EVOH and FAA−3 in 1M KOH at 70 ℃ for 300 hrs (a) Ion exchange capacity (b) ionic conductivity retention

Alkaline stability

Figure 2−15 (a), (b) shows the alkaline stability evaluation results of PiP/50EVOH and FAA−3. To see how well it maintains the cationic group in an alkaline environment, the membrane was immersed in 1M KOH solution at 70℃, and how well the IEC and ionic conductivity were maintained for each immersion time was compared. For FAA−3, a commercialized film, both IEC and ionic conductivity rapidly decreased over time, and it can be seen that a lot of degradation occurred around the QA group. On the other hand, PiP/50EVOH showed a slight decrease in IEC and ionic conductivity at the beginning of immersion, but maintained a constant level afterwards. As a result, it was confirmed that QA of ring−shaped piperidinium had excellent alkaline stability.

AEMWEs cell performance

  Figure 2-16 (a)-(e) shows the LSV curves of PiP/xEVOH and FAA-3, and Figure 2-16 (f) shows the ohmic resistance of the MEA. All four developed PiP/xEVOH AEMs (x = 50, 60, 70, 80) were tested and their cell performance compared under conditions of 1.0 M KOH circulating electrolyte at 70℃. Initial performance of polarization curves showed that the lowest content of EVOH with PiP/xEVOH series exhibited the best cell performance, among four different contents, with maximum current density of 1.78 A/cm2 at 2.0V. In addition, the current densities of other EVOH contents were 1.61 A/cm2 (x=60), 1.50 A/cm2 (x=70), and 0.61 A/cm2 (x=80) A/cm2 at 2.0 V respectively. The single cell performance results were consistent with the trend of ionic conductivity at 70 ℃, and hence reflected in the ohmic resistance trend in electrochemical impedance spectroscopy (EIS) analysis at 1.5 V, 1.8 V, and especially at 2.1 V. In AEMWE performance, MEA with commercially available FAA-3 membrane which is fully anion exchange membrane showed slightly higher performance than MEA with PiP/50EVOH membrane. A complete AEM has much higher IEC and a faster rate of ion transport through abundant cationic groups, leading to good performance.[16]
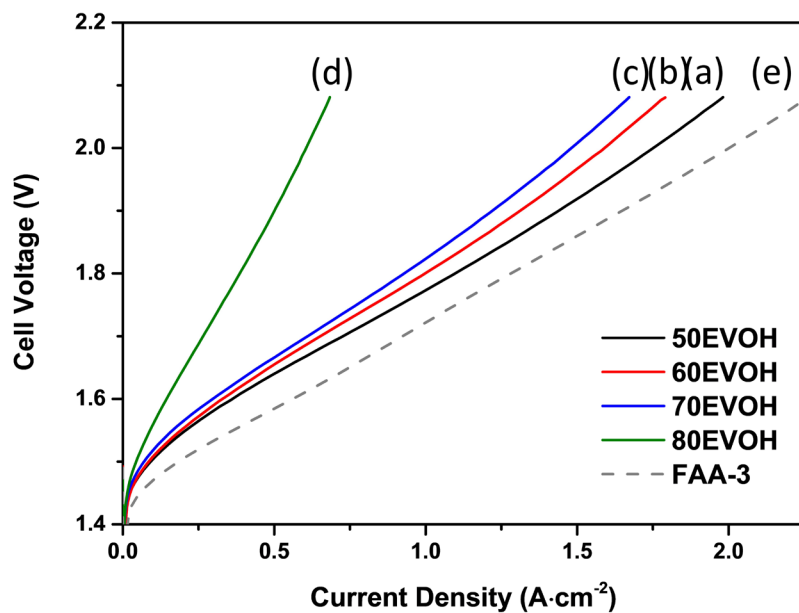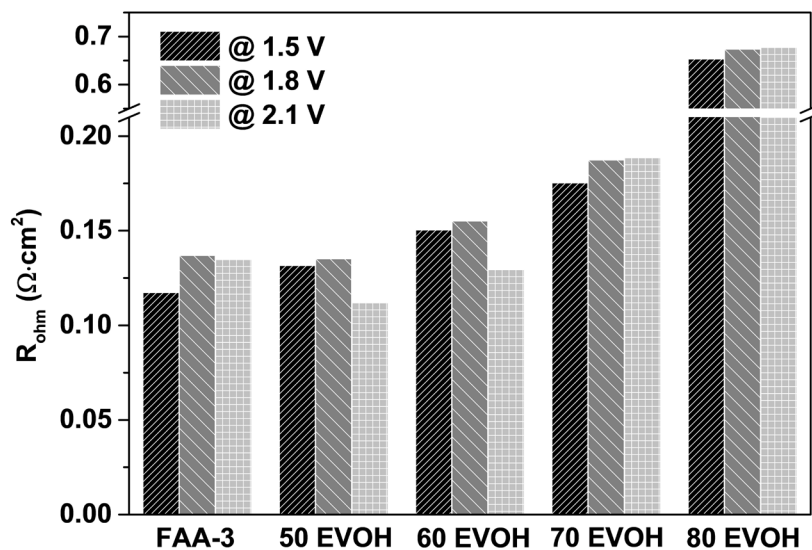
Figure 2-16. Linear sweep voltammetry(LSV) curve of (a) PiP/50EVOH (b) PiP/60EVOH (c) PiP/70EVOH (d) PiP/80EVOH (e)FAA-3, (f) ohmic resistance of each membrane's electrochemical impedance spectroscopy(EIS) nyquist plot.
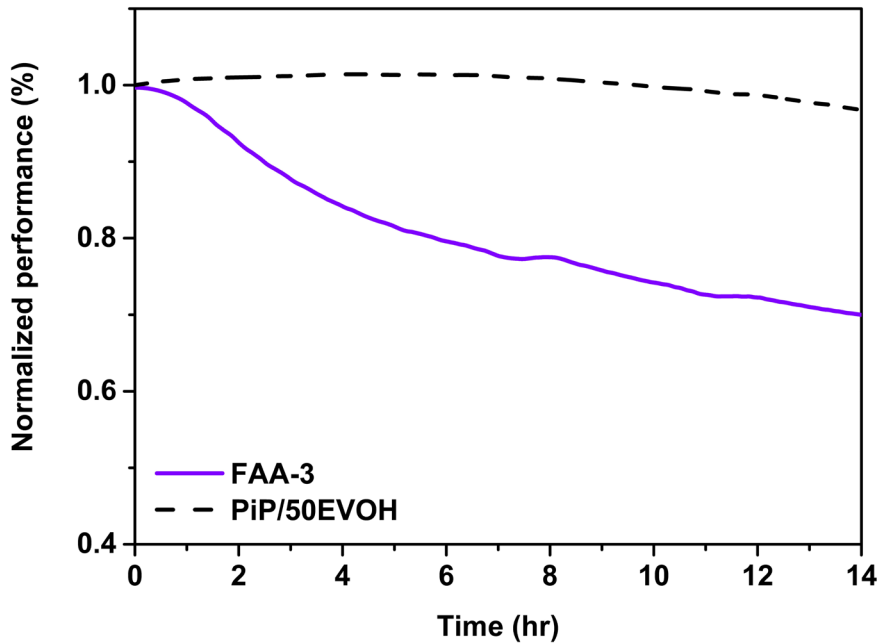
Figure 2-17. Comparison of the stability of PiP/50EVOH and FAA-3 AEMWE. Single cell stability test of PiP and FAA-3 at constant voltage of 1.6 V at 70℃.

After the single cell performance evaluation, the PiP/50EVOH MEAs were held at 1.6 V for a short-term durability test and result is shown in Figure 2-17. The PiP/50EVOH was stably operated compared to FAA-3 membrane for 14 hrs due to time constraints. While the PiP/50EVOH MEA maintained its initial current density very well without degradation, the FAA-3 cell exhibited gradual cell performance decrease within a few hours. PiP/50EVOH membrane showed better durability than commercially available FAA-3 membrane due to the alkaline stable ring structure of quaternary ammonium group and stable conductivity under corrosive alkaline electrolyte circulating conditions.

(a)

(b)

1.2 A cm^{-2} @ 2.0V
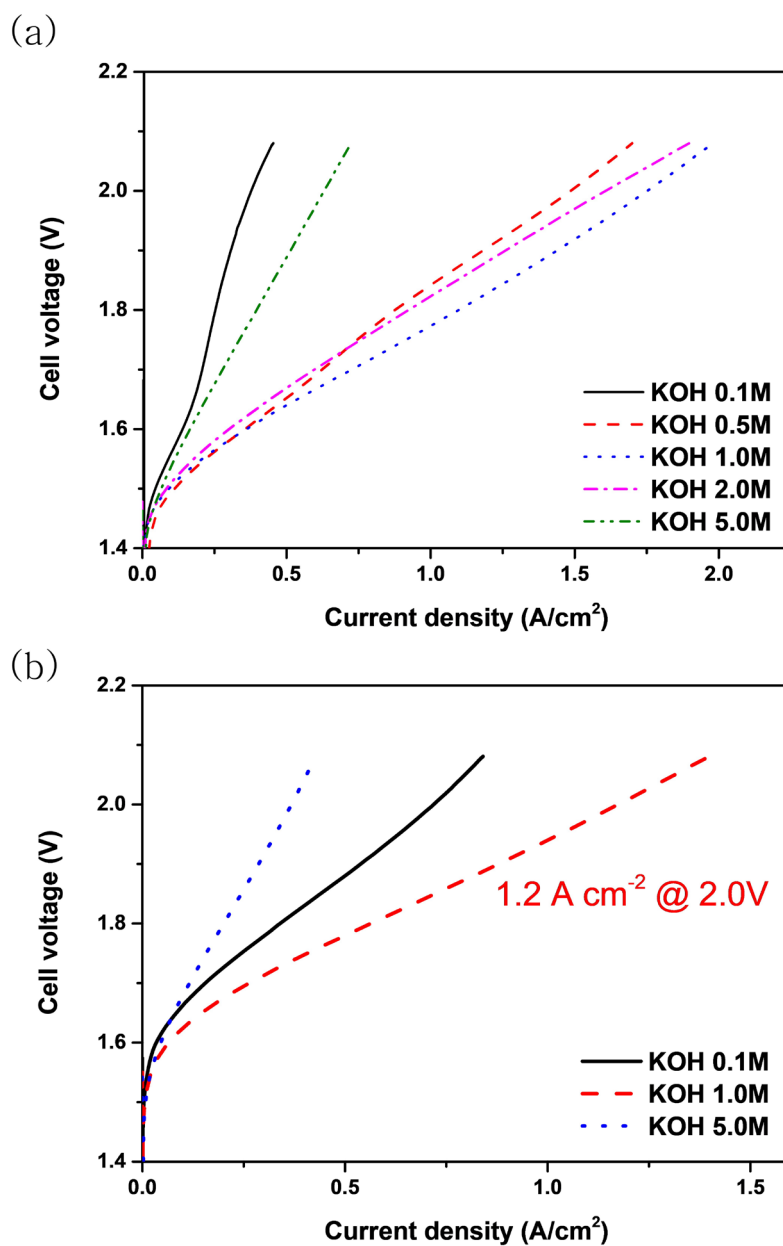
Figure 2-18. LSV curve with PiP/50EVOH comparing to concentration of electrolyte (a) with IrO$_2$, (b) non-PGM cobalt catalyst on anode

Furthermore, MEA performance showed a high dependence on electrolyte concentration as shown in Figure 2-18(a). Even though the ionic conductivity trend increased with the concentration of potassium hydroxide doping and submersion condition, this trend was only reflected in cell performance until the electrolyte concentration was 1.0 M. After the concentration increase more than 2.0M, the polarization curves showed decreased performance. This was attributed to previous reports in which an increase in KOH concentration results in decrease in the ohmic resistance of the anion exchange membrane and increase in the reaction kinetics of OER and HER, resulting in improved AEMWE performance.[17] However, this effect is limited in a high-concentration KOH solution. At high KOH concentration, water structure on electrode-electrolyte interface change which leads to performance decay.[18] As the KOH concentration increases, tetrahedrally coordinated water which has the highest water dissociation energy increases as the KOH concentration increases, and high viscosity may adversely affect OER and HER kinetics.

As shown in Figure 2-18(b), non-PGM catalyst cobalt OER catalyst was also tested with a low loading content of $0.7mgCo/cm^2$. The dependence on electrolyte concentration was similar to the MEAs fabricated with IrO2 PGM OER catalyst. Under 1M KOH conditions, the MEA fabricated with non-PGM catalyst cobalt exhibits an excellent current density of $1.2A/cm^2$ at 2.0V and 70℃, which was not significantly lower than that of the best PGM OER performance under identical testing conditions, $1.78A/cm^2$ at 2.0V and 70℃.

(a)
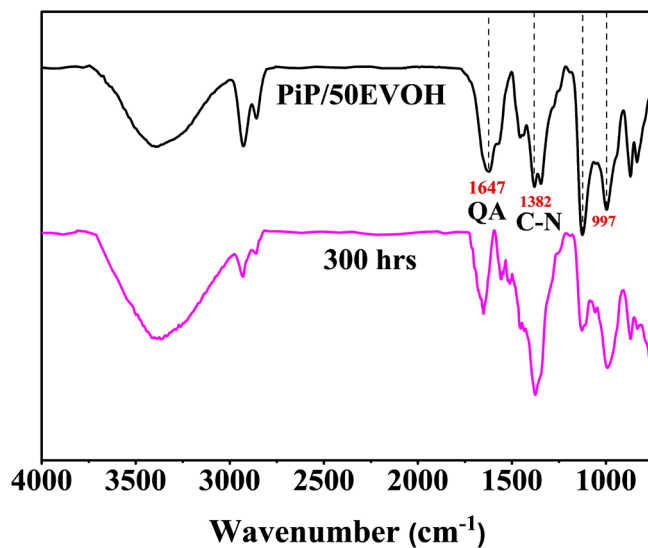
(b)   Major degradation mechanism
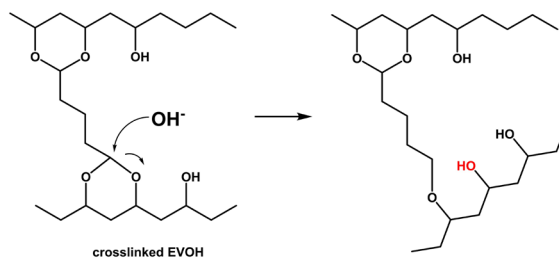
Minor degradation mechanism
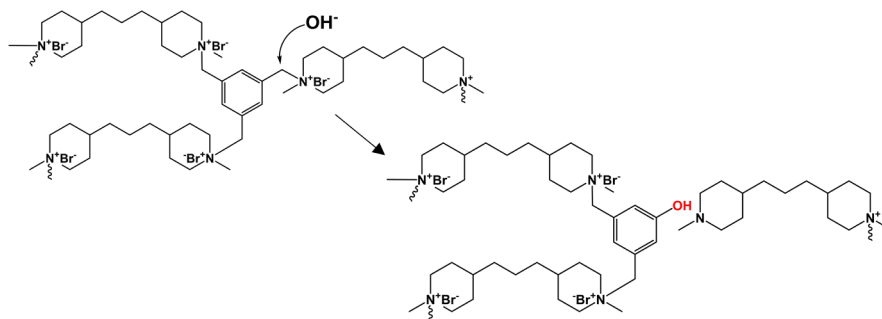
Figure 2-19. (a) FT-IR spectra for PiP/50EVOH after immersing in 1M KOH at 70 ℃ for 300h (b) Major and minor degradation mechanism of PiP/xEVOH membranes.

Degradation mechanism of membranes in alkaline condition

In order to understand the degradation mechanism of PiP/50EVOH, FT−IR analysis was performed before and after 300 h of immersion in 1M KOH at 70℃. FT−IR spectra are shown in Figure 2−19(a). After 300 hrs, the QAs peak decreased slightly, and the C−N peak at $1382cm^{-1}$[19] was broadened, confirming that degradation of QAs occurred. In addition, $997cm^{-1}$ peak increased due to the generation of secondary and primary alcohol, and $1127cm^{-1}$ peak was decreased which means the C−O−C[20] in EVOH was destroyed. Degradation of the acetal group of EVOH is the major degradation mechanism, as QAs and EVOH are somewhat damaged under alkaline conditions, but there is no significant decrease in ionic conductivity or IEC. Based on this, the major and minor degradation mechanisms are shown in Figure 2−19(b).

2.2.4 Conclusions

EVOH−supported cationic network IPN membranes were prepared via in−situ Menuki coat and cure method. The IEC was able to be controlled by adjusting the EVOH content and PiP/50EVOH has an IEC of 1.46mmol/g. The PiP/xEVOH membranes are capable of high KOH uptake of 60.9% while maintaining excellent mechanical strength of 21.9−55.3MPa. PiP/50EVOH showed excellent ionic conductivity of 66.6 mS/cm at 70℃. Also, PiP/50EVOH which β hydrogens of cation groups exist inside the ring shows better alkaline stability than FAA−3.[21] Under 1M KOH conditions, MEA with PiP/50EVOH membrane exhibits a current density of 1.78 A/cm^2 at 2.0V and 70℃. This study also showed the performance of 1.2A/cm^2 at 2.0V with a non−PGM cobalt OER catalyst, which was a small drop off from the PGM IrO_2 catalyst. Consequently, considering the simple membrane fabrication and the excellent alkaline stability, our EVOH−supported cationic network IPN membranes will open up opportunities as alternative anion exchange membrane materials for various applications.

2.2.5 References

[1] Mogilevich, M. M., **1979**, *Russian Chemical Reviews*, *48*(2), 199.

[2] Yasir, M., Liu, P., Tennie, I. K., & Kilbinger, A. F., **2019**, *Nature Chemistry*, *11*(5), 488-494.

[3] Li, W., Shen, Z., & Zhang, Y., **2001**, *European Polymer Journal*, *37*(6), 1185-1190.

[4] Guzman-Gutierrez, M. T., Nieto, D. R., Fomine, S., Morales, S. L., Zolotukhin, M. G., Hernandez, M. C. G., ... & Wilks, E. S., **2011**, *Macromolecules*, *44*(2), 194-202.

[5] Zhou, X., Wu, L., Zhang, G., Li, R., Hu, X., Chang, X., ... & Li, N., **2021**, *Journal of Membrane Science*, *631*, 119335.

[6] Mansur, H. S., Sadahira, C. M., Souza, A. N., & Mansur, A. A., **2008**, *Materials Science and Engineering: C*, *28*(4), 539-548.

[7] Li, D., Park, E. J., Zhu, W., Shi, Q., Zhou, Y., Tian, H., ... & Kim, Y. S., **2020**, *Nature Energy*, *5*(5), 378-385.

[8] Reis, E. F. D., Campos, F. S., Lage, A. P., Leite, R. C., Heneine, L. G., Vasconcelos, W. L., ... & Mansur, H. S., **2006**, *Materials Research*, *9*, 185-191.

[9] Zhang, H. B., Lin, G. D., Zhou, Z. H., Dong, X., & Chen, T., **2002**, *Carbon*, *40*(13), 2429-2436.

[10] Wang, X., Su, M., Liu, C., Shen, C., & Liu, X., **2020**, *Journal of Renewable Materials*, *8*(1), 89.

[11] Garrido, L. H., Schnitzler, E., Zortéa, M. E. B., de Souza Rocha, T., & Demiate, I. M., **2014**, *Journal of Food Science and Technology*, *51*, 2640-2647.

[12] Chen, Y., Mastalerz, M., & Schimmelmann, A., **2012**, *International Journal of Coal Geology*, *104*, 22-33.

[13] Du, N., Roy, C., Peach, R., Turnbull, M., Thiele, S., & Bock, C., **2022,** *Reviews*, *122*(13), 11830-11895.

[14] Kang, S. Y., Park, J. E., Jang, G. Y., Kim, O. H., Kwon, O. J., Cho, Y. H., & Sung, Y. E., **2022**, *Journal of Hydrogen Energy*, *47*(15), 9115-9126.

[15] Santos, F., Tafur, J. P., Abad, J., & Romero, A. J. F., **2019**,

Journal of Electroanalytical Chemistry, *850*, 113380.

[16] Li, Z., Li, C., Long, C., Sang, J., Tian, L., Wang, F., ... & Zhu, H., **2020**, *Journal of Polymer Science*, *58*(16), 2181−2196.

[17] Razmjooei, F., Farooqui, A., Reissner, R., Gago, A. S., Ansar, S. A., & Friedrich, K. A., **2020**, *ChemElectroChem*, *7*(19), 3951−3960.

[18] Guha, A., Sahoo, M., Alam, K., Rao, D. K., Sen, P., & Narayanan, T. N., **2022**, *Iscience*, *25*(8), 104835.

[19] Sivakumar, P. K., Kumar, S., Kumar, R. M., Kanagadurai, R., & Sagadevan, S. , **2016**, *Materials Research*, *19*, 937−941.

[20] Moosavinejad, S. M., Madhoushi, M., Vakili, M., & Rasouli, D., **2019**, *Maderas. Ciencia y tecnología*, *21*(3), 381−392.

[21] Arges, C. G., Parrondo, J., Johnson, G., Nadhan, A., & Ramani, V., **2012**, *Journal of Materials Chemistry*, *22*(9), 3733−3744.

2.3 Polydiallylammonium and EVOH based cationic network IPN membranes

2.3.1 Introduction

For anion exchange properties, a combination of ammonium network forming precursors, polymeric structure consist of quaternary ammonium groups with cyclic and aromatic main chains were synthesized. Crosslinking of two types of diallylamine based monomer, first of which is diallyldimethylammonium chloride (DADMAC) which is commercially available and the other contains a benzene ring in the center (BTMDAA), occurs through cyclopolymerization of the diallylammonium groups, and quaternary ammonium for ion transport is formed simultaneously. The selection of precursors was due to diallyl based ammonium monomers form a five−membered pyrrolidinium ring with excellent alkaline stability[1] through cyclopolymerization, and BTMDAA provides a cross−linked structure and improves dimensional stability of AEMs with the presence of a benzene ring in the center. By utilizing this chemistry within the various contents of the ion−solvating polymer matrix, anion exchange membranes with tunable ion−solvating / anion exchange properties, most notably, mechanical properties and IEC, can be easily tuned in one−step. This optimization of ion−solvating/anion−exchange properties has been also verified with AEMWEs test, in which 1:1 blending ratio (BD3/50EVOH) showed the highest activity (1.57 A/cm^2 at 2.0 V). In particular, 300 h of static alkaline stability test along with electrochemical operation in AEMWEs under 1.0M KOH at 70℃ presented remarkable retention of IEC and ionic conductivity, even superior AEMWEs durability compared to commercialized FAA−3 membrane. This is presumably due to the fact that alpha−carbon and beta−hydrogens of the quaternary ammonium groups are mostly present inside the ring which suppresses hydroxide ion attack due to the steric hindrance, for excellent alkaline stability.[2]

2.3.2 Experimental

Materials

For the synthesis and fabricate the membrane, 1,3,5-Tris(bromomethyl)benzene (97%), 2,6-di-tert-butyl-4-methylphenol (99%), diallyldimethylammonium chloride (DADMAC, 60% in water), 2,2'-azobis(2-methylpropionamidine) dihydrochloride (AAPH,97%), poly(vinyl alcohol-co-ethylene) (EVOH, ethylene 32 mol%), and poly(vinyl alcohol) (PVA) with Mw of 89,000-93,000 were supplied by Sigma Aldrich Chemical Co. Ltd. Diallylmethylamine (98%) was supplied by Thermo Fisher Scientific Inc. Glutaraldehyde (GA, 25wt% solution in water), dimethyl sulfoxide (DMSO, 99.5 %), tetrahydrofuran (THF, 99.5 %), ethanol (99.5%), potassium oxide (KOH), n-propyl alcohol (NPA) and hydrochloric acid (HCl, 35~37%) were obtained from Daejung.

For membrane electrode assembly fabrication, platinum ruthenium (Pt-50wt%, Ru-25wt%, Alfa 047371.06) on high surface area advanced carbon support, and iridium(IV) oxide (99.99 wt%, Alfa 043396.06), cobalt nanopowder(99.8%, 46347) were received from Alfa Aesar. The commercial FAA-3-50 membrane obtained from FumaTech which has a thickness of 45-55 μm.

Synthesis of BTMDAA

1,3,5-tris(bromomethyl)benzene (5.82g, 0.016mol) and 2,6-di-tert-butyl-4-methylphenol (0.72g, 0.003mol) as an inhibitor were added to a 100 mL round-bottom-flask. DMSO (50mL) was added as a solvent and dissolved them homogeneously using a magnetic bar. After that, diallylmethylamine (18.14g, 0.163 mol) was added slowly and the reaction was carried out at 80℃ for 72 hours in an Ar atmosphere[3]. After the reaction, the solution was cooled to room temperature and slowly poured into cold THF. The precipitate was separated via Buchner funnel, and residual solvent was evaporated at room temperature for 24 hours in a vacuum oven. An ivory powder (BTMDAA) (10.44 g, 93 % crude yield) was obtained.

^{1}H NMR (D$_2$O, ppm): 7.85 (s, 3H), 6.15 - 6.02 (m, 6H), 5.76 - 5.64 (m, 12H), 4.59 (s, J = 15.0 Hz, 6H), 4.06 - 3.81 (m, 12H), 2.98 (s, 9H), 13C NMR (DMSO-d6, ppm): 139.96, 129.72, 128.31, 126.29, 64.04, 63.08, 46.70.

BD$_3$/xEVOH semi-IPN membrane fabrication

5wt% BTMDAA/DMSO solution 20 g (1g, 1.45mmol BTMDAA) was placed in vial and DADMAC 60% aqueous solution 1.69 g (0.7g, 4.35mmol DADMAC) was added. Afterwards, 15.3g (1.7g EVOH) of 10wt% EVOH/DMSO solution was added to the well-mixed solution. 85mg of AAPH which is initiator was dissolved in a small amount of water, added to the above solvent, and mixed homogeneously. The blending solution was casted on the glass plate and cyclopolymerization was performed at 80℃ while the solvent is slowly evaporated. The glass plate was then placed in a vacuum oven at 100℃ for 48 hrs to remove all residual DMSO. Semi-IPN anion exchange membrane of BD$_3$/50EVOH was obtained by separating the membrane from the glass plate. In the same way, BD$_3$/60-80 EVOH semi-IPN can be prepared by adjusting the contents of BD$_3$ and EVOH.

BD$_3$/xEVOH IPN membrane fabrication

To increase the dimensional stability of the membrane, the hydroxide group of EVOH was partially cross-linked with GA. A 5% GA solution was prepared by diluting the 25% GA aqueous solution with ethanol and hydrochloric acid was used as catalyst. The synthesized semi-IPN membrane was immersed in GA/HCl solution (pH 3) at 70℃ for 24 hrs[4]. IPN membrane was finally obtained through washing and drying.

Characterization methods of the membranes

^{1}H NMR and ^{13}C NMR spectra were measured in D$_2$O or DMSO-d6 at 25℃ on a Bruker Ascend™ 400 (^{1}H NMR: 400 MHz, ^{13}C NMR: 400MHz) to confirm successful synthesis of BTMDAA. Structure analysis of AEMs were performed using Fourier

transform infrared spectrometer (FT−IR, PerkinElmer FT−IR system, Spectrum−GX). The thermal stability of the BD_3/xEVOH membranes were measured using thermogravimetric analysis (TGA, TA Instrument, TGA 2950) from 25 to 800℃ with heating rate of 10 ℃/min under N_2 atmosphere. Mechanical strengths of the AEMs were evaluated via tensile strength measurements (Tinius Olsen H5K−T). The dimensions of the AEMs were 4cmx0.5cm and tested at strain speed of 10 mm/min.

Ion exchange capacity (IEC) of the AEMs were determined by the acid−base titration according to the following procedure. OH^- form membranes were dried at 80℃ for overnight before titration to obtain accurate dry weight. All samples were immersed in 0.01M HCl solution for 24 hrs. The solution was titrated with 0.01M KOH solution using three drops of phenolphthalein/EtOH indicator solution. The IEC (mmeq/g) was calculated based on the following equation:

$$IEC = (V_{HCl}*C_{HCl} - V_{NaOH}*C_{NaOH})/W_{dry}$$

where V_{HCl} and V_{NaOH} are volume of HCl and NaOH, respectively. C_{HCl} and C_{NaOH} are the concentration of HCl and NaOH, respectively. W_{dry} is the mass of the dried membranes.

The swelling ratio (SR) and water uptake (WU) were defined as the ratio of the mass and length change, respectively, before and after the equilibration of the membrane in water for 24 hrs.

The KOH uptake rate is also determined in the same way. After the preparation of the dry membrane, the membrane was immersed in 1M KOH solution at room temperature for 24 hrs. The mass of the samples was measured after removing the excess KOH solution. After washing several times with water and drying, the mass of dried membrane was measured and compared. KOH uptake was calculated using the following equation.

$$KOH\ uptake = ((m_{wet,KOH} - m_{dry})/m_{dry})*100$$

The ohmic resistance of the AEMs were measured in water and 0.1M−5M KOH solution at different temperature by two− electrode electrochemical impedance spectroscopy (EIS, SI 1260,

Solartron) over the frequency range from 10 Hz to 10 MHz with an amplitude of 20 mV. Before measurement, all OH^- form membranes were immersed in distilled water for at least 24 hrs to equilibrate in water. Hydroxide conductivity was calculated by the following equation:

$$\sigma = L/(R \times W \times d)$$

where L was the distance between two electrodes (cm), R was the measured ohmic resistance (Ω), W was the width of the membrane (cm) and d was the width of the membrane (cm).

MEA fabrication and water electrolysis performance

BD_3/xEVOH based MEAs (1 or 5 cm^2) were fabricated by the catalyst coated substrate (CCS) method. 50 wt% PtRu/C was used as cathode and IrO_2, Co were used as anode catalysts, respectively. Catalyst inks were prepared by dispersing each catalyst powder over the TMA-70 ionomer which was synthesized using a literature procedure[5]. 4.65 wt% TMA-70 solution in n-propanol / water (1:1 wt) solution, the ionomer to carbon (I/C) weight ratio is 0.5) in an aqueous solution of n-propanol and little amount of water, followed by ultrasonic treatment for more than 20 min with maintaining water temperature less than 35℃ to prevent catalyst agglomeration. The prepared catalyst inks were directly sprayed onto the gas diffusion layer (GDL) set on a 70℃ pre-heated hotplate. GDLs 39 BB (Fuel Cell Store), and Pt coated Ti paper (Giner) were used for the cathode and anode respectively. Cathode catalyst loading amount is 0.6 $mgPt/cm^2$, and anode catalyst loading amount is 2.0 $mgIr/cm^2$, 0.7 $mgCo/cm^2$. The fabricated CCS was dried at room temperature for more than 1 h to remove residual solvent in the catalyst layers. Prior to single cell application, the BD_3/xEVOH membrane sample was sandwiched by fabricated electrode without hot-pressing process.

2.3.3 Results and Discussion

Synthesis of BTMDAA precursor

BTMDAA was synthesized through the Menshutkin reaction of diallylmethylamine and 1,3,5−Tris(bromomethyl)benzene, and chemical structure, ^{1}H−NMR, and ^{13}C−NMR spectra for BTMDAA were shown in Figure 2−20. BTMDAA is a precursor that can form a complex cationic network through cyclopolymerization of diallylamine groups. The crosslinked network provided by BTMDAA served to increase the dimensional stability of the membrane.

Membrane fabrication

In our initial pretests, when the cationic network formed using only BTMDAA, the crosslinking density was too high and the flexibility of AEM was low. Therefore, DADMAC was used to increase the flexibility of the membrane. However, when the DADMAC content was too high, problem of low dimensional stability of the membrane occurred. So the input mol ratio of BTMDAA and DADMAC was fixed at 1:3 and the formed cationic network was named BD_3. IPN membranes with variously controlled BD_3 and EVOH contents were fabricated, and we named the BD_3/xEVOH membrane according to x wt% EVOH content.

Figure 2−21 shows the overall fabrication process of BD_3/xEVOH IPN anion exchange membrane. The BD_3/xEVOH sIPN membrane was successfully fabricated by the cyclopolymerization reaction between the DADMAC and BTMDAA. The EVOH content in the membrane was adjusted from 50 to 80wt%, and EVOH was crosslinked using GA to improve dimensional stability.
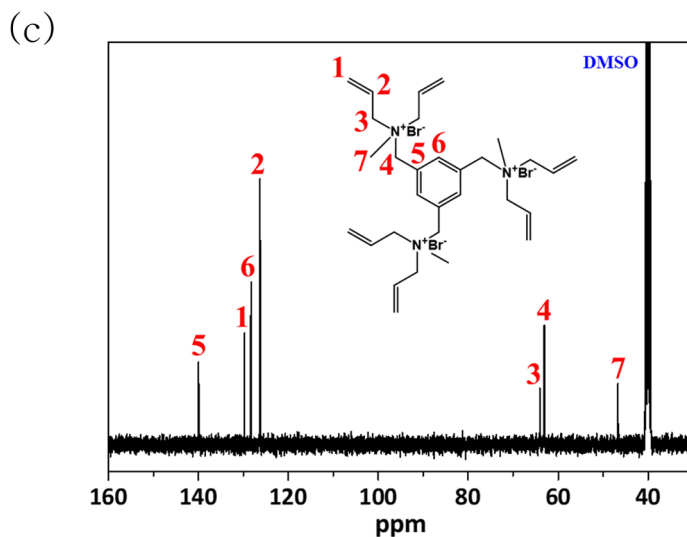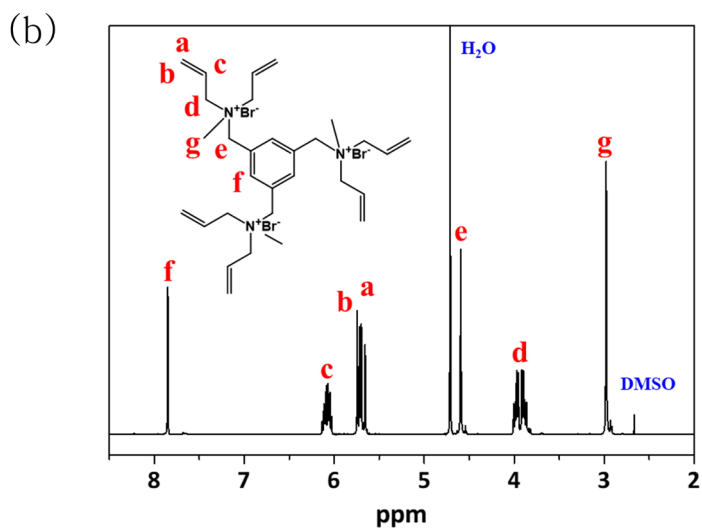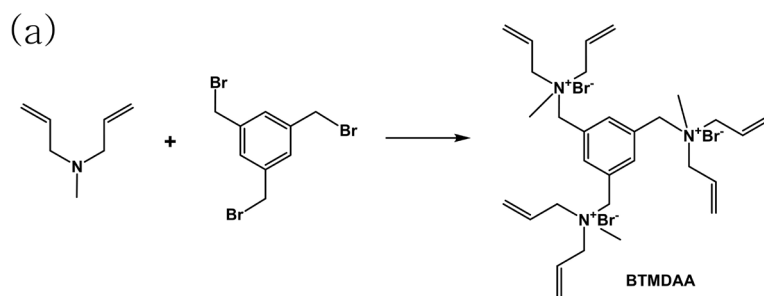
Figure 2-20. (a) Synthesis mechanism for BTMDAA (b) ^{1}H-NMR spectra (c) ^{13}C-NMR spectra for BTMDAA
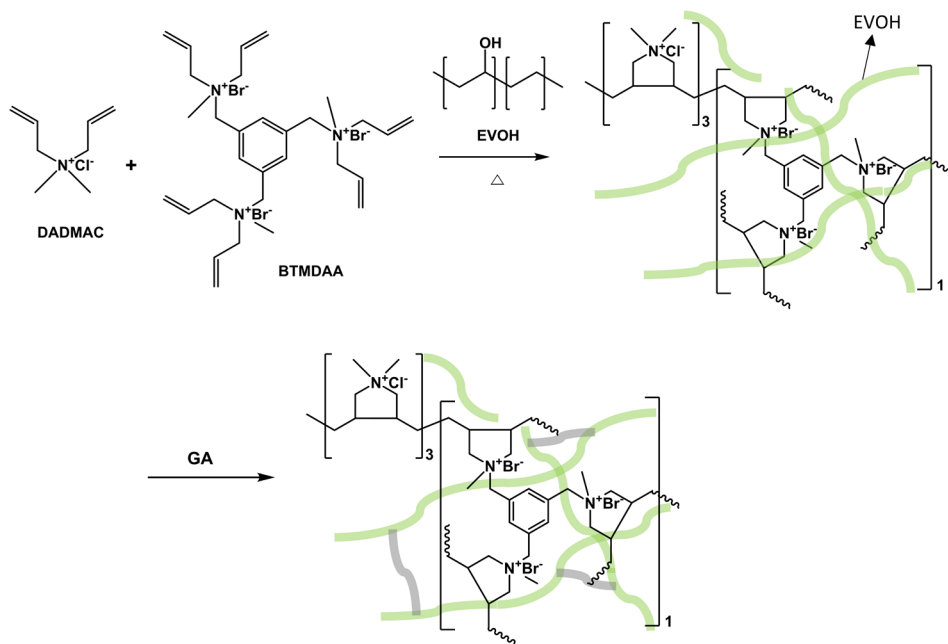
Figure 2-21. Fabrication process of BD₃/xEVOH membranes
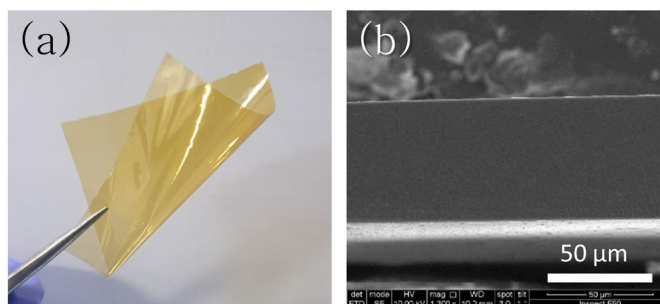
Figure 2-22. (a) Membrane image (b) SEM image (cross section) of BD₃/50EVOH

All IPN membranes exhibit excellent membrane forming ability, and as shown in Figure 2-22(a), obtained yellowish transparent IPN membrane is flexible and easy to handle. Figure 2-22(b) shows the cross-view of BD_3/50EVOH membrane, which possessed a homogeneous and dense structure. It is noteworthy to point out that EVOH contents below 50wt% had poor mechanical properties, and thus unsuitable for membrane electrode assembly tests.

Characterization of membranes

Figure 2-23 shows the FT-IR spectra for crosslinked EVOH membrane and BD_3/xEVOH membrane with various content of EVOH. In the range of 3,300~3,500 cm^{-1}, hydroxide peaks were observed in all membrane due to the hydroxide groups of EVOH. Other crosslinked EVOH related peaks were indicated at 2931 cm^{-1} (antisymmetric stretching of CH_2), 2856 cm^{-1} (Symmetric stretching of CH_2), 1150~1085 cm^{-1} (C-O-C), 1135 cm^{-1} (C-O), and 998 cm^{-1} (-COCO-, acetal group)[6],[7]. The FT-IR peaks of all the cationic network compounds were showed at 1382 cm^{-1} (C-N), 870 cm^{-1} (aromatic C-H and C=C stretch) and 1647 cm^{-1} (quaternary ammonium), indicating the formation of homogeneous ammonium networks within the ion-solvating polymer matrix.

The thermal stabilities of crosslinked EVOH and IPN membranes with various EVOH content were evaluated by TGA and the results are displayed in Figure 2-24. The 5% mass loss temperature of crosslinked EVOH is 352℃ and all IPN membranes are thermally stable up to 200℃. Considering the working temperature of AEMWE, these IPN membranes exhibited suitable thermal stability for AEMWE application.
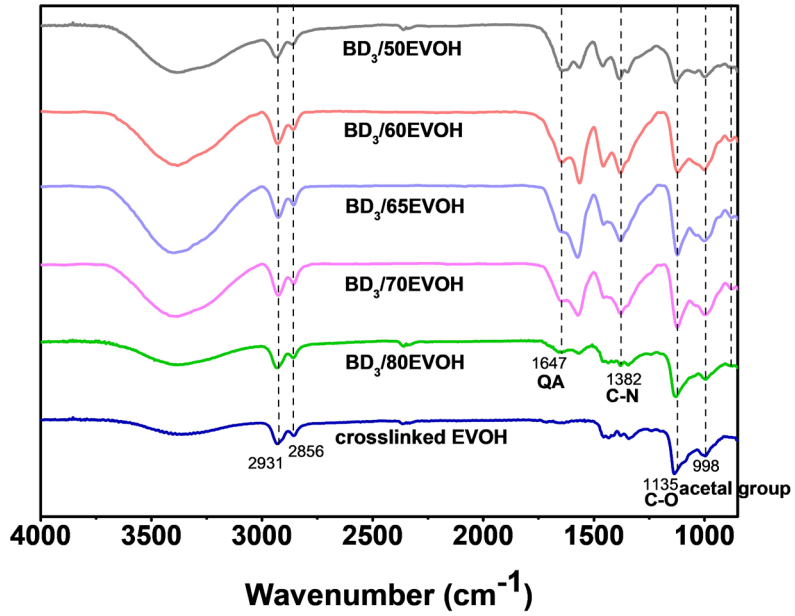
Figure 2-23. FT-IR spectra for crosslinked EVOH and BD₃/xEVOH
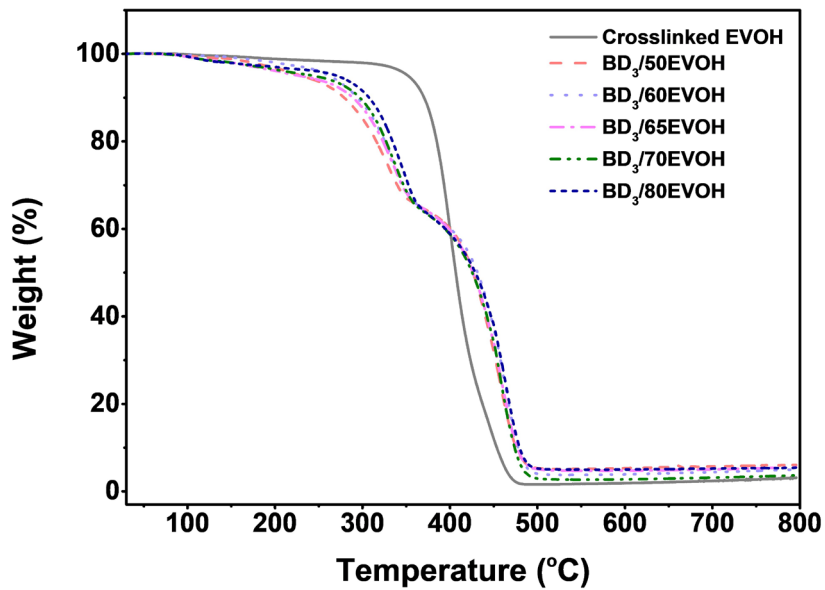
Figure 2-24. TGA curve for crosslinked EVOH and BD₃/xEVOH
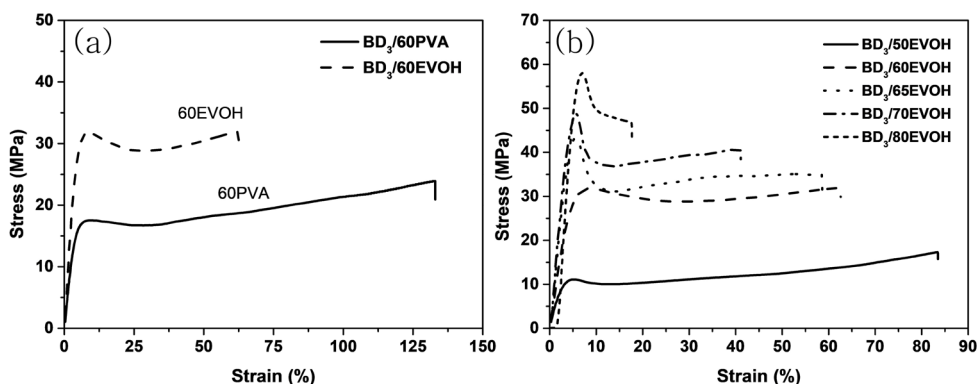
Figure 2-25. Strain-stress curves for (a) $BD_3/60PVA$ and $BD_3/60EVOH$ (b) $BD_3/xEVOH$

      The mechanical properties were also evaluated, as the mechanical strength of the membrane is related to its durability. As PVA has low tensile strength and high elongation at break value[8], we chose EVOH over PVA as the ion-solvating materials to impart high mechanical strength. Figure 2-25(a) compares the mechanical strength of $BD_3/60PVA$ and $BD_3/60EVOH$. As expected, $BD_3/60PVA$ showed higher elongation at break values but lower tensile strength than that of $BD_3/60EVOH$. This is due to the inclusion of ethylene units in the EVOH backbone, which functions to increase the membrane film rigidity[9]. As shown in Figure 2-25(b), the tensile strength of $BD_3/xEVOH$ membranes ranged from 17.3 to 46.7 MPa, whereas the elongation values were in the range of 17.5%-83.4%. The tensile strength of the $BD_3/xEVOH$ membranes increased upon the increasing of EVOH content and $BD_3/80EVOH$ exhibited the highest tensile strength of 46.7MPa, which was close to that of neat EVOH. As expected, BD3/50EVOH has the poorest mechanical properties than $BD_3/60-80EVOH$, but this was only a relative comparison and $BD_3/50EVOH$ has strong enough tensile strength for use in AEMWE applications.

Hydration properties of BD$_3$/xEVOH
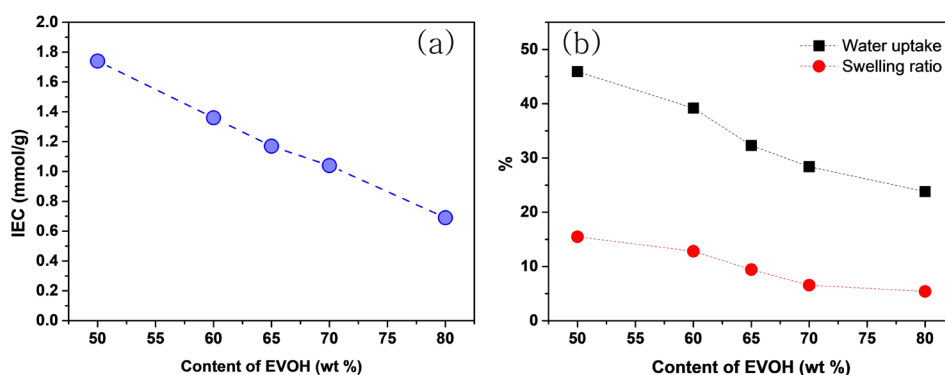
Figure 2-26. (a) IEC (b) water uptake and swelling ratio of BD$_3$/xEVOH

Figure 2-26(a) shows the IEC of the membranes. As the EVOH content increased, the IEC decreased because the content of the cationic network was reduced, and BD$_3$/50EVOH showed the highest IEC value of 1.74 mmeq/g. As higher IECs represent a higher number of ion exchangeable ammonium groups per repeating unit, correspondingly, the higher the IEC, the higher the water uptake, swelling ratio, and KOH uptake value was obtained.(Figure 2-26(b)) As shown in Table 2-2, BD$_3$/50EVOH had 45.9%, 15.49% and 50.2% values of water uptake, swelling ratio, and KOH uptake, respectively. As ionic conductivity is by all accounts, the decisive factor that influences the performance of membranes for AEMWEs, we measured the ionic conductivity of membranes.

Table 2-2. Hydration properties of membranes

Sample	IEC[a] (mmeq g^{-1})	Water uptake (%)[b]	Swelling ratio (%)[c]	KOH uptake (%)[d]	Ionic conductivity (mS cm^{-1})[e]	
					25 °C	70 °C
FAA-3	2.01	41.6	13.5	80.2 ± 0.8	23.4	59.6
crosslinked PVA	-	19.3 ± 1.1	0.7 ± 0.7	19.3 ± 0.1	-	-
crosslinked EVOH	-	8.4 ± 0.1	4.2 ± 0.5	7.3 ± 1.3	-	-
BD$_3$/50EVOH	1.74	45.9	15.49	50.2	101.2	161.0
BD$_3$/60EVOH	1.36	39.2	12.82	40.5	64.4	120.1
BD$_3$/65EVOH	1.17	32.3	9.43	36.3	52.9	89.5
BD$_3$/70EVOH	1.04	28.4	6.56	29.3	47.8	70.1
BD$_3$/80EVOH	0.69	23.8	5.41	18.3	40.1	62.8

Hydroxide conductivity

Figure 2-27 shows the hydroxide conductivity of IPN membranes and FAA-3 anion exchange membrane (non-ion-solvating wholly ammonium polymer) which is commercially available. In general, the higher the IEC, the higher the ionic conductivity[10]. However, the ionic conductivity of FAA was lower than that of BD_3/xEVOH, although the IEC was higher. This was attributed to the hydroxide group in EVOH can also transfer OH- through the Grotthuss mechanism but hydroxide group in EVOH can't be reflected in the IEC value because it's not a cationic group[11]. BD_3/50EVOH exhibited the highest ion conductivities at all temperatures with values of 101.2 mS/cm and 161 mS/cm at 25℃ and 70℃, respectively.
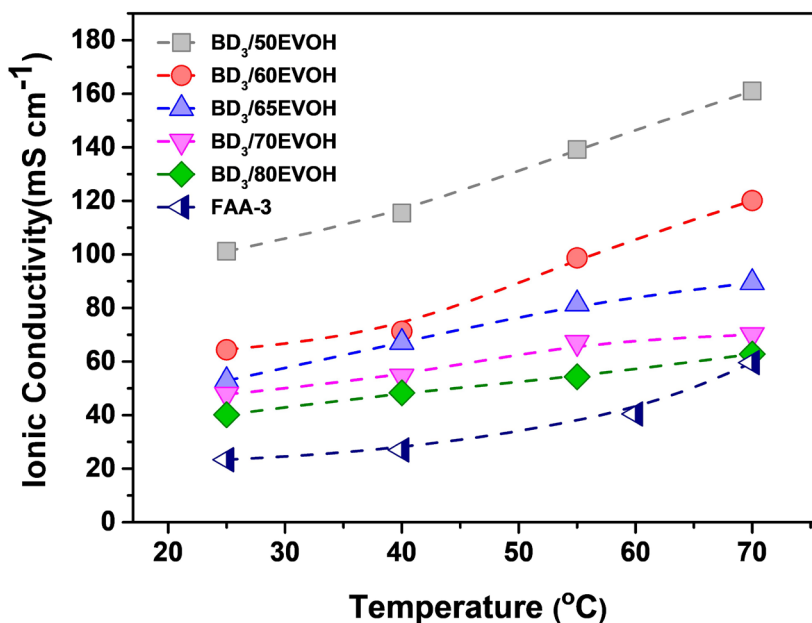
Figure 2-27. Hydroxide conductivity of BD_3/xEVOH and FAA-3 at different temperature

Alkaline stability

To evaluate the alkaline stability of the anion exchange membrane, the membrane was immersed in 1M KOH at 70℃, and the IEC and ionic conductivity were measured for each immersion time as shown in Figure 2-28 (a),(b). When the FAA-3 membrane was subjected to this test, the IEC precipitously dropped from 1.8 mmeq/g to 0.8 mmeq/g after 300 hrs, and accordingly, the ionic conductivity also decreased significantly from 59.6 mS/cm to 4.17 mS/cm. This loss in both IEC and conductivity could be explained by cation degradation. By comparison, the alkaline stability tests of the BD_3/xEVOH membranes showed a high retention degree of initial IEC value and ionic conductivity even after 310 hrs.
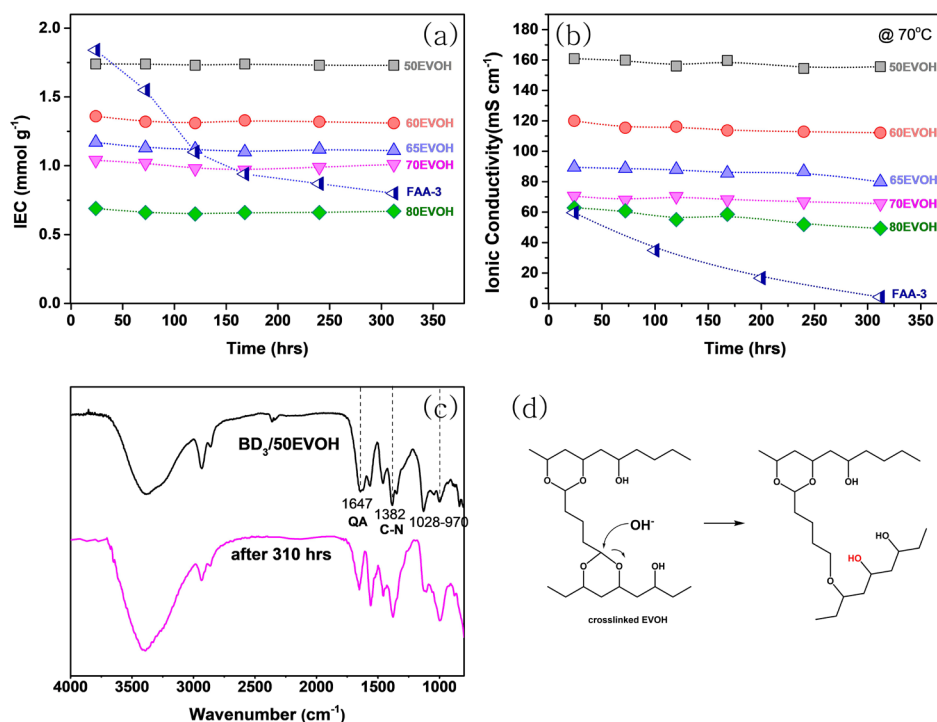
Figure 2-28. Alkaline stability of BD_3/xEVOH and FAA-3 in 1M KOH at 70℃ for 300h (a) IEC (b) ionic conductivity retention (c) FT-IR spectra for BD3/50EVOH after immersing in 1M KOH at 70℃ for 300h (d) major degradation mechanism

Two main reasons for this difference in alkaline stability may exist. First, there are few sites where the hydroxide group can attack the quaternary ammonium group and all of the β hydrogens of quaternary ammonium are in the five membered ring and are sterically hindered.[12] Moreover, the ion-solvating polymer also functions as a buffer layer holding both KOH of hydroxide ions for conduction but shields it from the ammonium backbone, preventing premature cation degradation.

Figure 2-28(c) gives FT-IR spectra of BD_3/50EVOH membrane before and after immersed in 1M KOH at 70℃ for 310 h. The most notable change is the increase of 1028-970 cm^{-1} peaks, indicating increase in primary or secondary alcohol. Considering that all peaks related to quaternary ammonium are maintained, it is assumed that a small amount of acetal group in crosslinked EVOH is decomposed by hydroxide ions and mechanism is shown in Figure 2-28(d). In fact, as shown in Fig. 5, the ionic conductivity and IEC of BD_3/50EVOH were maintained even after 310 h, confirming that the quaternary ammonium group of the ring structure was not damaged.

AEMWEs performance

The applicability of the BD$_3$/xEVOH membranes in AEMWEs was confirmed through the incorporation of the BD$_3$/xEVOH-based membranes into AEMWE MEAs. Cell temperature was held constant at 70℃ with supplying 1M KOH electrolyte. All BD$_3$/xEVOH membranes were tested and their cell performance was compared. It is noteworthy that for the catalyst layer ionomer, we utilized a highly quaternized polystyrene ionomer in all MEA tests.

Figure 2-29(a) shows the LSV curves for all the BD$_3$/xEVOH membranes and FAA-3. Trends in higher performance were shown for membranes containing higher contents of ammonium network polymers, due to higher IEC, and thus ionic conductivity.[13] For example, the BD$_3$/50EVOH membrane showed good performance of 1.57 A/cm^2 at 2.0 V. Through increasing the content of EVOH in the membrane, lower current densities with 1.45 A/cm^2 (x=60), 1.05 A/cm^2 (x=65), 0.22 A/cm^2 (x=70), 0.13 A/cm^2 (x=80) at 2.0 V were shown, respectively.

The ohmic resistances of BD$_3$/EVOH membrane series that mainly originated (Figure 2-29(b)) from the magnitude of the resistance of AEMs are comprehensively compared since AEMWE was tested under identical conditions with the same consisting anode and cathode. As a result, the trend of ionic conductivity matches with the polarization curve.
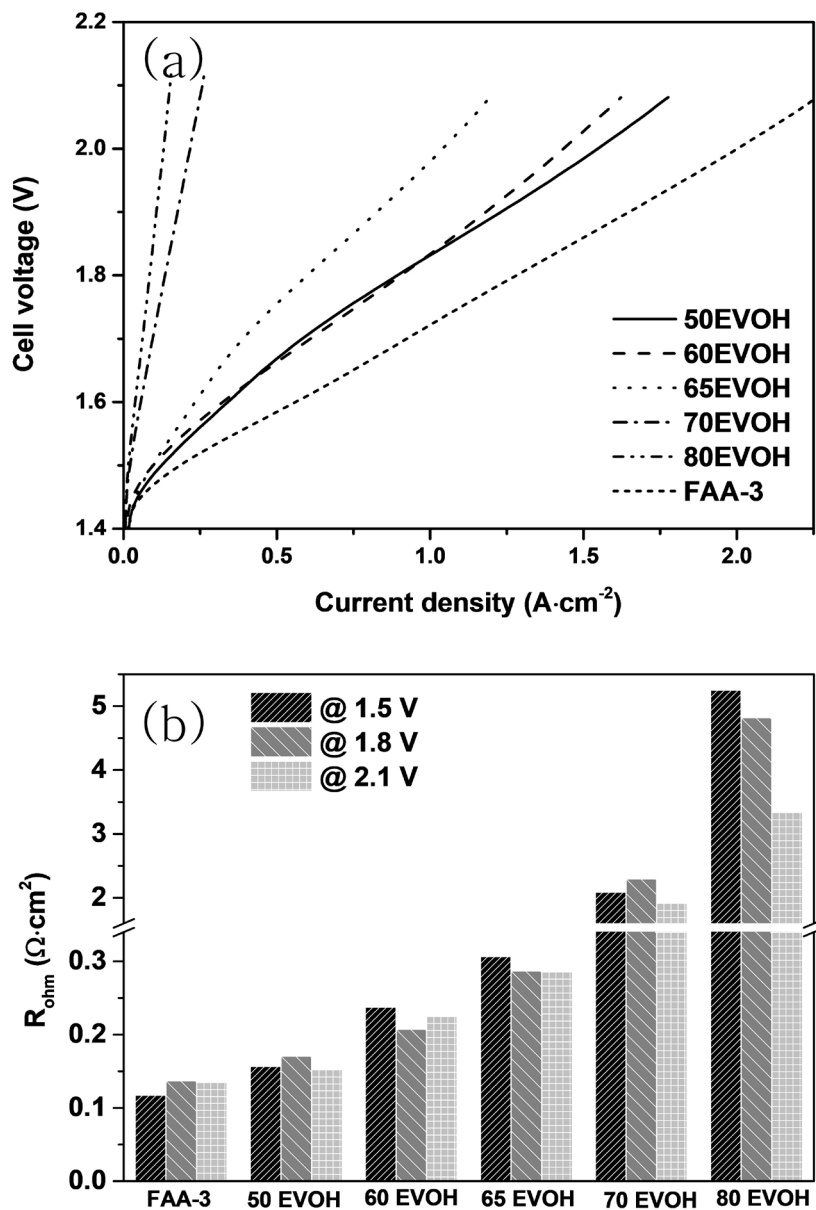
Figure 2-29. (a) Linear sweep voltammetry(LSV) curves of BD₃/50EVOH and FAA-3, (b) ohmic resistance of each membrane's electrochemical impedance spectroscopy(EIS) nyquist plot.

In comparing the AEMWE performance with a fully ammonium anion exchange membrane, FAA-3 membrane only shows slightly higher performance than BD_3/50EVOH membrane. FAA-3 is a complete anion exchange membrane, so it shows slightly better performance due to its higher IEC. On the other hand, BD_3/xEVOH is a combination of anion exchange membrane and ion solvating membrane. Therefore, BD_3/xEVOH exhibited lower performance due to reduced IEC[14] but was compensated by better mechanical strength and alkaline stability from the ion-solvating material.

Effect of KOH concentration for AEMWEs performance
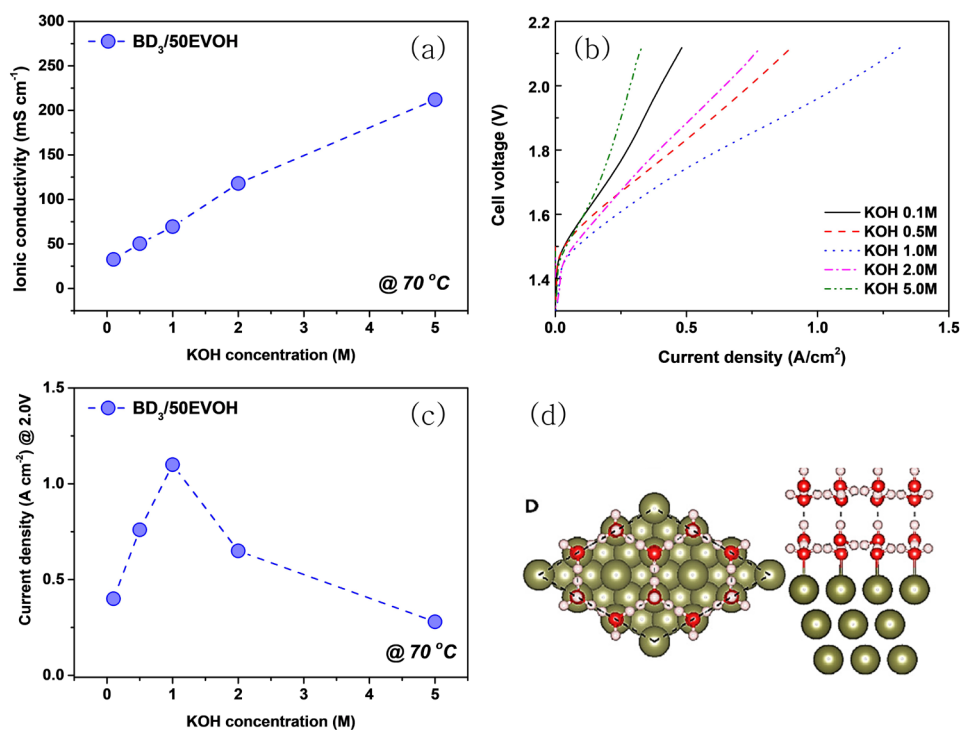
Figure 2-30. Effect of supporting KOH electrolyte concentration (a) ionic conductivity (b) LSV curve (c) current density at 2.0V of BD_3/50EVOH (d) tetrahedral coordination of water at the electrode surface[15]

The working temperature and KOH concentration of an AEMWEs is generally around 60−80℃ and 1M KOH solution[17], so it is interest to measure the conductivity in the KOH solution as a function of temperature and KOH concentration. Figure 2−30(a) gives hydroxide conductivity of BD3/50EVOH membrane in KOH solution. As the temperature increased in 1M KOH, the ionic conductivity of BD3/50EVOH increased and was 69.4 mS/cm at 70℃. The conductivity also increased as the KOH concentration[17] increased from 0.1 M to 5 M and reached 212 mS/cm at 5M KOH at 70℃.

The effect of supporting KOH electrolyte concentration was also investigated as the concentration of electrolyte determines both performance and durability, and the optimal condition of different membranes may exist. In Figure 2−30(b) and (c), we found that the 1M KOH solution shows the peak performance rather than 2M and 5M KOH solutions. This was attributed to the fact that an increase in KOH concentration results in a decrease in AEM ohmic resistance and an increase in OER and HER reaction kinetics, which is directly related to improved performance[18]. Typically, it is expected that AEMWE performance would result in the best performance when conducted with a higher concentration of KOH (e.g., 5M KOH), as this concentrated solution exhibits the largest ionic conductivities irrespective of temperature change[19]. As KOH concentration goes higher, the following viscosity increase may detrimentally affect its reaction kinetics[20] and eventually leads to performance decay due to hydroxide ion−water bond interaction change. Recently, Guha et al. reported that KOH concentration significantly affects the molecular structure of water, the relationship between water structure and alkaline water electrolysis was studied by theoretical and spectroscopic investigations[15]. In their study, they revealed that the molecular structure of water gradually transformed to tetrahedrally coordinated as the alkalinity was increased from 0.1 M to 6.0 M. (Figure 2−30(d)) In particular, DFT calculation verified that the tetrahedrally coordinated water

possessed the highest water dissociation energy, and it showed detrimental effects on HER activity in high alkaline conditions, but no effects on OER activity. These theoretical and experimental results are in line with our data trends in AEMWE performance, indicative of stemming from collective phenomena occurring in AEM as well as both cathode and anode.

AEMWEs performance with non-PGM catalyst

As shown in Figure 2-31, non-PGM catalyst cobalt was also investigated with low loading, 0.7 mgCo/cm^2. Under 0.1M and 1M KOH conditions, the MEA fabricated with non-PGM catalyst cobalt and BD$_3$/50EVOH exhibits a current density of 0.5 A/cm^2 and 0.8 A/cm^2, respectively at 2.0 V and 70℃. Through this we were able to demonstrate good AEMWE performance under various electrolyte concentration, and even non-PGM OER catalyst conditions.
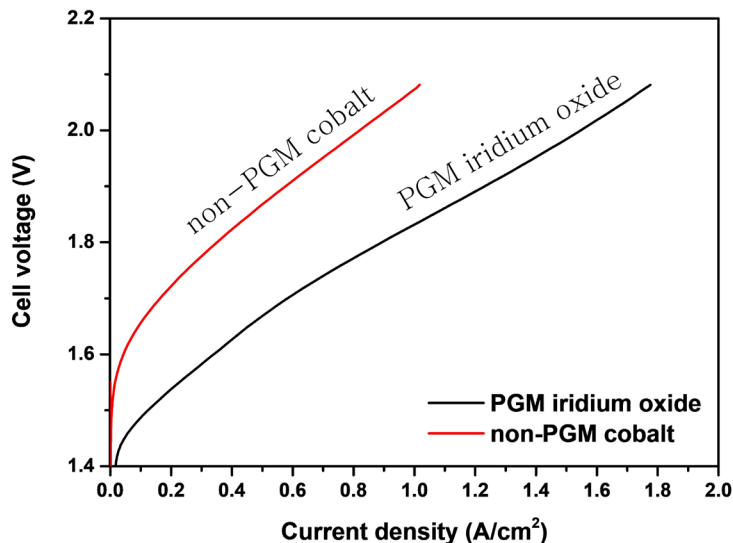
Figure 2-31. LSV curve with BD$_3$/50EVOH comparing to concentration of electrolyte with IrO$_2$, non-PGM cobalt catalyst on anode

AEMWEs durability test
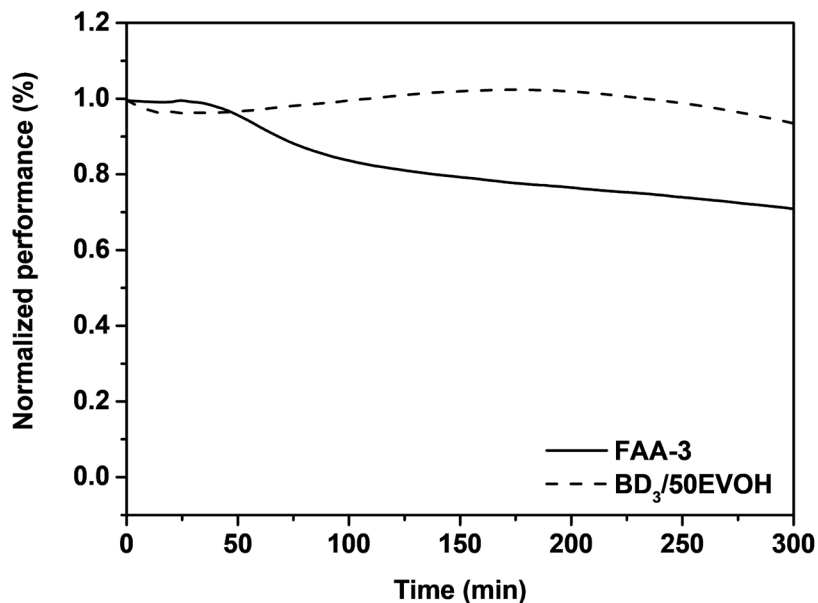
Figure 2-32. Single cell stability test of BD$_3$/xEVOH and FAA-3 at constant voltage of 1.6 V at 70 ℃.

In order to demonstrate the durability of our membranes, the BD$_3$/50EVOH membrane cell was set at a constant voltage 1.6 V at 70℃ and measured the initial current density loss as a function of time(Figure 2-32). For time constraints, durability tests were intentionally stopped after 300 min. The test showed that the BD$_3$/50EVOH membrane showed drastically improved durability compared to that of the commercial AEM, FAA-3, even under a short duration of 300 min. While the FAA-3 membrane kept the initial current for less than 50 min and degraded continuously over time,[21] the BD$_3$/50EVOH membrane maintains initial current density with little fluctuation of less than 3%. This result reflects the loss in both IEC and conductivity under accelerated alkaline stability tests. These AEMWE results showed that the development of both ion-solvating polymer and ion exchangeable properties can be synergistically integrated for the development of anion exchange membranes for AEMWE technology. Further optimization of

chemistries of the ionomer and ionomer−membrane interface are expected to improve performance and durability in future works.

2.3.4 Conclusion

An ion−solvating polymer, EVOH, incorporated with alkaline stable, cationic network polymers, were examined as anion exchange membranes for AEMWEs. EVOH, which has good mechanical strength, high alkali absorption, and film forming ability[23] was applied as a membrane material for AEMWE for the first time, and IPN anion exchange membrane based on poly(diallyalkylamine) was fabricated as a function of EVOH content. This IPN membrane with ether−free and N−spirocyclic quaternary ammonium cation structure was found to improve ionic conductivity, mechanical properties and alkaline stability.[24] As a result, ionic conductivity of BD₃/50EVOH (161 mS/cm at 70℃) was higher than with the commercial available FAA−3 membrane. In addition, high alkaline stability was confirmed as the ionic conductivity was maintained even after immersion in 1M KOH at 70℃ for 310 hours. BD₃/50EVOH membrane exhibited excellent AEMWE performance with the current density of 1.57 A/cm^2 at the potential of 2.0 V in 1 M KOH at 70 ℃, which indicated that the BD₃/EVOH membranes are a good candidate for AEMWEs.

2.3.5 References

[1] Gu, F., Dong, H., Li, Y., Sun, Z., & Yan, F., **2014**, *Macromolecules*, *47*(19), 6740-6747.

[2] Mohanty, A. D., & Bae, C., **2014**, *Journal of Materials Chemistry A*, *2*(41), 17314-17320.

[3] Yuan, J., Prescher, S., Sakaushi, K., & Antonietti, M., **2015**, *Journal of Materials Chemistry A*, *3*(14), 7229-7234.

[4] Gong, Y., Liao, X., Xu, J., Chen, D., & Zhang, H., **2016**, *international journal of hydrogen energy*, *41*(13), 5816-5823.

[5] Li, D., Park, E. J., Zhu, W., Shi, Q., Zhou, Y., Tian, H., ... & Kim, Y. S., **2020**, *Nature Energy*, *5*(5), 378-385.

[6] Kraglund, M. R., Carmo, M., Schiller, G., Ansar, S. A., Aili, D., Christensen, E., & Jensen, J. O., **2019**, *Energy & environmental science*, *12*(11), 3313-3318.

[7] Kraglund, M. R., Aili, D., Jankova, K., Christensen, E., Li, Q., & Jensen, J. O., **2016**, *Journal of The Electrochemical Society*, *163*(11), F3125.

[8] Lagaron, J. M., Powell, A. K., & Bonner, G., **2001**, *Polymer testing*, *20*(5), 569-577.

[9] Zhang, K., McDonald, M. B., Genina, I. E., & Hammond, P. T., **2018**, *Chemistry of Materials*, *30*(18), 6420-6430.

[10] Park, E. J., Arges, C. G., Xu, H., & Kim, Y. S., **2022**, *ACS Energy Letters*, *7*(10), 3447-3457.

[11] Wang, K., Wu, Q., Yan, X., Liu, J., Gao, L., Hu, L., ... & He, G., **2019**, Branched poly (ether ether ketone) based anion exchange membrane for H2/O2 fuel cell. *International Journal of Hydrogen Energy*, *44*(42), 23750-23761.

[12] Xue, J., Zhang, J., Liu, X., Huang, T., Jiang, H., Yin, Y., ... & Guiver, M. D., **2022**, *Electrochemical Energy Reviews*, 1-53.

[13] Overton, P., Li, W., Cao, X., & Holdcroft, S., **2020**, *Macromolecules*, *53*(23), 10548-10560.

[14] Fortin, P., Khoza, T., Cao, X., Martinsen, S. Y., Barnett, A. O., & Holdcroft, S., **2020**, *Journal of Power Sources*, *451*, 227814.

[15] Guha, A., Sahoo, M., Alam, K., Rao, D. K., Sen, P., & Narayanan, T. N., **2022**, *Iscience*, *25*(8), 104835.

[16] Li, D., Motz, A. R., Bae, C., Fujimoto, C., Yang, G., Zhang, F. Y., ... & Kim, Y. S., **2021**, *Energy & Environmental Science*, *14*(6), 3393−3419.

[17] Allebrod, F., Chatzichristodoulou, C., Mollerup, P. L., & Mogensen, M. B., **2012**, *International Journal of Hydrogen Energy*, *37*(21), 16505−16514.

[18] Li, D., Park, E. J., Zhu, W., Shi, Q., Zhou, Y., Tian, H., ... & Kim, Y. S., **2020**, *Nature Energy*, *5*(5), 378−385.

[19] Umoren, S. A., Solomon, M. M., Ali, S. A., & Dafalla, H. D., **2019**, *Materials Science and Engineering: C*, *100*, 897−914.

[20] Liu, X., Fan, X., Liu, B., Ding, J., Deng, Y., Han, X., ... & Hu, W., **2021**, *Advanced Materials*, *33*(31), 2006461.

[21] Park, J. E., Kang, S. Y., Oh, S. H., Kim, J. K., Lim, M. S., Ahn, C. Y., ... & Sung, Y. E., **2019**, *Electrochimica Acta*, *295*, 99−106.

[22] Bahcegul, E., Toraman, H. E., Erdemir, D., Akinalan, B., Ozkan, N., & Bakir, U., **2014**, *RSC advances*, *4*(64), 34117−34126.

[23] Zhang, Y., Chen, W., Yan, X., Zhang, F., Wang, X., Wu, X., ... & He, G., **2020**, *Journal of Membrane Science*, *598*, 117650.

Chapter 3. Polydiallylammonium hydroxide based AEMs and AEIs for AEMWEs

3.1 Introduction

In Chapter 2, IPN membranes were effective in increasing durability while increasing mechanical strength, but showed lower performance than commercially available AEMs due to low the IEC. Therefore, a fully cationic membranes are essential to enhance the performance of AEMWEs.

The most important properties of AEMs are excellent alkaline stability, proper water uptake, excellent mechanical strength and high ionic conductivity.[1] For good alkaline stability, it is good to have aryl−ether free and ring structure QA groups.[2] In addition, the IEC must be able to be adjusted to have proper water uptake and ionic conductivity.[3] Also crosslinking of the polymer backbone can be used to increase the mechanical strength.[4] Since these characteristics are in a trade−off relationship with each other, it is important to strike a good balance of each characteristic. In addition, the interfacial contact between the AEM and the electrode containing the AEI has a great effect on the performance. If the interfacial resistance between membrane and electrode is high, ion transfer or electrode transfer does not proceed quickly, resulting in reduced hydrogen production efficiency.[5] Another strategy to lower the interfacial resistance is to use soft AEMs and AEIs with high water uptake. Another method is to use AEMs and AEIs with similar structures.

Unlike AEMs, AEIs do not require high mechanical strength, but the basic characteristics are similar to those of AEMs. One important difference is that oxidation stability on the electrode catalyst. Benzene groups that can easily undergo oxidation to form phenols, which should be avoided according to previous studies.[6]

In this study, fully AEMs and AEIs were developed to

improve the performance of AEMWEs. To reduce the interfacial resistance between membrane and electrode, AEMs and AEIs with similar structures were developed through the same chemical reaction called diallylammonium cyclization. As a result of cyclopolymerization of diallylammonium, ring type QA groups of pyrrolidinium were formed, and alkaline stability was also expected to be good.[7] Chapter 3.2 describes the development, characteristics, and application of AEMWEs of poly(diallylammonium)hydroxide (PDDA) based AEMs, and chapter 3.3 describes research on PDAA based aliphatic AEIs. Finally, in chapter 3.4, PDAA−based AEMs and AEIs developed in chapter 3.2 and 3.3 are simultaneously applied to AEMWEs to examine the effects of high ionic conductivity, water uptake, and low interfacial resistance using a similar structure.

3.1.1 Synthesis of polydiallylammonium hydroxide

The synthesis of polydiallylammnoium (PDAA) halide proceeds by cyclopolymerization of diallylamine, and first reported in 1958, JACS, 80(14) 1986, 3615−3618. Since PDAA synthesis uses water−based radical polymerization, it is an eco−friendly synthesis method and easy to scale−up.

The cyclopolymerization of diallylamine occurs through the mechanism of initiation, intramolecular cyclization, and linear propagation, and the mechanism is shown in Figure 2−1(b). After cyclopolymerization of diallylamine monomer, five−membered pyrrolidinium rings are generated.[8] These pyrrolidinium based quaternary ammoniums have good alkaline stability[9], so it can be applied to the fabrication of AEM. Because cationic diallylammonium monomers undergo polymerization better than neutralized diallylamine[10], diallylamine monomer reacts in aqueous HCl to form ammonium forms.

One of the advantages of synthesizing PDAA using diallylamine is that can introduce various functional groups of the

QA group. Therefore, IEC, hydrophilicity and hydrophobicity can be easily controlled and crosslinking is also possible. Diallylamine's monomer modification, PDAA synthesis and crosslinking mechanism are shown in Figure 3-1.
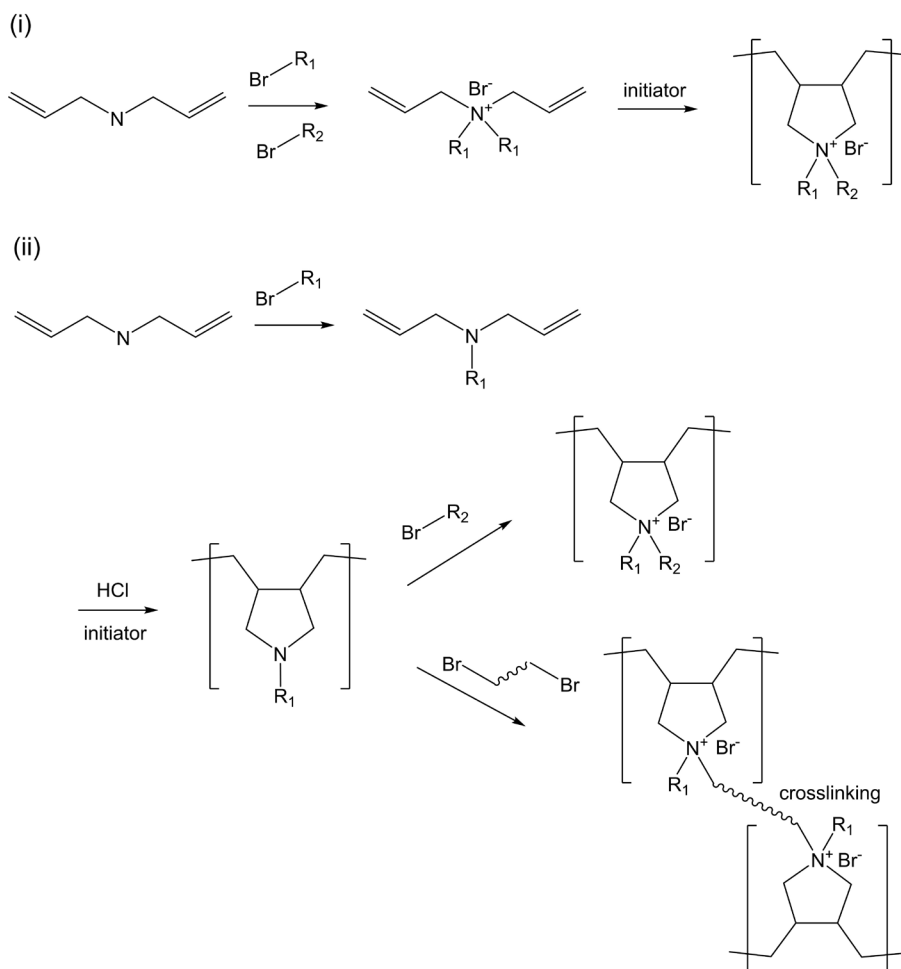
Figure 3-1. Diallylamine modification, PDAA synthesis and crosslinking mechanism

3.1.2 Superacid-catalyzed polyhydroxyalkylation reaction

In many past studies, polysulfones, polyethers, and polyphenylene, which are relatively easy to synthesize,[11−16] have been used to make AEMs. However, since these polymers contain aryl−ether bonds, alkaline stability is not guaranteed.

As a method for synthesizing aromatic polymers without aryl−ether bonds, there is superacid−catalyzed condensation of ketones and aromatic compounds, which is a hydroxyalkylation reaction.[17−20] As the intermediate alcohol reacts with another aromatic compound, a high molecular weight polymer with a linear para−substitution main chain is synthesized.[21] In addition, thermochemically and mechanically robust ether−free polymers are obtained as a result of the reaction, so it is suitable for use as AEMs.[22],[23] Corresponding mechanism is shown in Figure 3−2. In this mechanism, the carbonyl monomer is relatively unreactive, whereas the carbinol intermediate formed after the first reaction is more reactive. Therefore, if an excess of carbonyl monomer is added, a high molecular weight polymer can be obtained in a short time by a nonstoichiometric effect due to a large reactivity difference.[24]

There are three considerations for superacid mediated hydroxyalkylation to occur effectively. First is the acidity of the superacid affecting protonation energy of carbonyl components.[25] Superacid is a stronger acid than sulfuric acid and serves to stabilize other sensitive cations. In general, trifluoromethanesulfonic acid (CF_3SO_3H, TFSA) is used as a superacid, and TFSA itself is used as a catalyst and reaction solvent or used together with dichloromethane. Also, sometimes a mixed solution of trifluoroacetic acid and TFSA is used to reduce the acid strength. The second is the electrophilicity of carbonyl components, and the reactivity varies depending on the carbonyl functional group. If there are strong electron withdrawing groups (EWG) or strong electron donating groups (EDG) on both sides of the carbonyl group,

the carbonyl carbon has too much δ^+ or δ^- for the reaction to occur. In strong EWG, monoprotonation of the carbonyl group is difficult to occur, so the electrophilic aromatic substitution reaction does not proceed well. In strong EDG, monoprotonation structure of the carbonyl group is too stable, so next reaction doesn't occur well. [27],[28] Therefore, carbonyl with an EDG group on one side and an EWG on the other side is most often used. In the past, EWG's polymerization using a carbonyl compound with a CF_3 group has been studied[29],[30], but recently, a lot of research has been conducted on polymerization using a piperidone−based carbonyl monomer that does not contain fluorine.[31],[32]
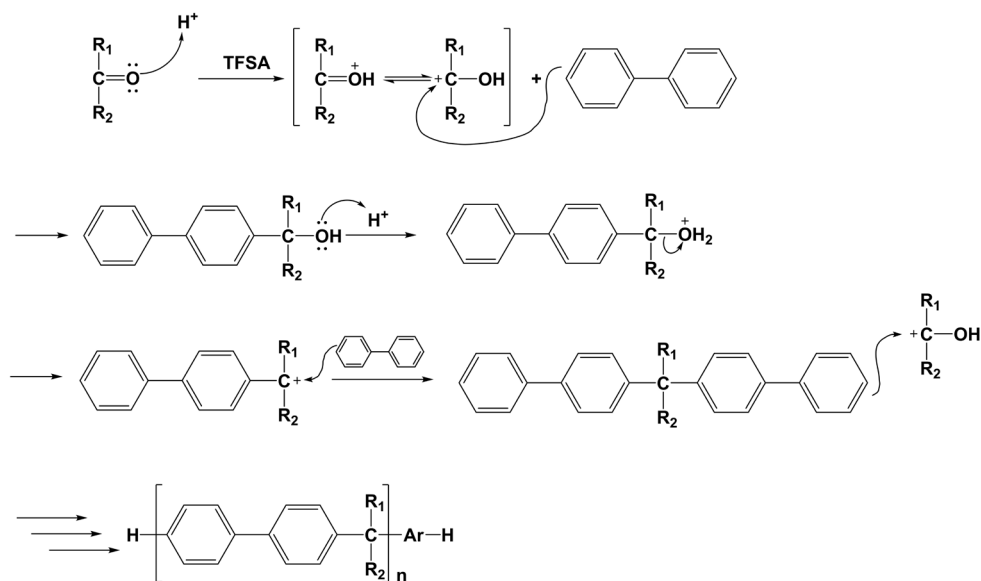
Figure 3−2. Superacid−catalyzed polyhydroxyalkylation reaction mechanism

3.1.3 References

[1] Lin, B., Qiu, L., Lu, J., & Yan, F., **2010**, *Chemistry of materials*, *22*(24), 6718-6725.

[2] Park, E. J., & Kim, Y. S., **2018**, *Journal of Materials Chemistry A*, *6*(32), 15456-15477.

[3] Disabb-Miller, M. L., Zha, Y., DeCarlo, A. J., Pawar, M., Tew, G. N., & Hickner, M. A., **2013**, *Macromolecules*, *46*(23), 9279-9287.

[4] Safranski, D. L., & Gall, K., **2008**, *Polymer*, *49*(20), 4446-4455.

[5] Pivovar, B. S., & Kim, Y. S., **2007**, *Journal of the Electrochemical Society*, *154*(8), B739.

[6] Motz, A. R., Li, D., Keane, A., Manriquez, L. D., Park, E. J., Maurya, S., ... & Kim, Y. S., **2021**, *Journal of Materials Chemistry A*, *9*(39), 22670-22683.

[7] Gu, F., Dong, H., Li, Y., Sun, Z., & Yan, F., **2014**, *Macromolecules*, *47*(19), 6740-6747.

[8] Umoren, S. A., Solomon, M. M., Ali, S. A., & Dafalla, H. D., **2019**, *Materials Science and Engineering: C*, *100*, 897-914.

[9] Sun, Z., Lin, B., & Yan, F., **2018**, *ChemSusChem*, *11*(1), 58-70.

[10] Tuzun, N. S., Aviyente, V., & Houk, K. N., **2003**, *The Journal of Organic Chemistry*, *68*(16), 6369-6374.

[11] Deberdeev, T. R., Akhmetshina, A. I., Karimova, L. K., Ignat'eva, E. K., Galikhmanov, N. R., Grishin, S. V., ... & Deberdeev, R. Y., **2020**, *Polymer Science, Series D*, *13*, 320-328.

[12] Martos, A. M., Sanchez, J. Y., Várez, A., & Levenfeld, B., **2015**, *Polymer Testing*, *45*, 185-193.

[13] Pandele, A. M., Serbanescu, O. S., & Voicu, S. I., **2020**, *Coatings*, *10*(7), 609.

[14] Yin, Y., Du, Q., Qin, Y., Zhou, Y., & Okamoto, K. I., **2011**, *Journal of Membrane Science*, *367*(1-2), 211-219.

[15] Zeng, Q., Wan, Z., Jiang, Y., & Fortner, J., **2022**, *Chemical Engineering Journal*, *431*, 134071.

[16] Saimani, S., Kumar, A., Dal-Cin, M. M., & Robertson, G., **2011**, *Journal of membrane science*, *374*(1-2), 102-109.

[17] Cai, Z. H., Gao, X. L., Gao, W. T., Choo, Y. S. L., Wang, J. J., Zhang, Q. G., ... & Liu, Q. L., **2022**, *ACS Applied Energy Materials*, *5*(8), 10165-10176.

[18] Hernandez, M. C. G., Zolotukhin, M. G., Fomine, S., Cedillo, G., Morales, S. L., Fro¨hlich, N., ... & Ruiz-Trevino, A., **2010**, *Macromolecules*, *43*(17), 6968-6979.

[19] Zolotukhin, M. G., Fomine, S., Lazo, L. M., Salcedo, R., Sansores, L. E., Cedillo, G. G., ... & Khalizov, A. F., **2005**, *Macromolecules*, *38*(14), 6005-6014.

[20] Cruz-Rosado, A., Romero-Hernández, J. E., Ríos-López, M., López-Morales, S., Cedillo, G., Ríos-Ruiz, L. M., ... & Vivaldo-Lima, E., **2022**, *Polymer*, *243*, 124616.

[21] Olah, G. A., Rasul, G., York, C., & Prakash, G. S., **1995**, *Journal of the American Chemical Society*, *117*(45), 11211-11214.

[22] Guzman-Gutierrez, M. T., Nieto, D. R., Fomine, S., Morales, S. L., Zolotukhin, M. G., Hernandez, M. C. G., ... & Wilks, E. S., **2011**, *Macromolecules*, *44*(2), 194-202.

[23] Pham, T. H., Olsson, J. S., & Jannasch, P., **2019**, *Journal of Materials Chemistry A*, *7*(26), 15895-15906.

[24] Hernández-Cruz, O., Zolotukhin, M. G., Fomine, S., Alexandrova, L., Aguilar-Lugo, C., Ruiz-Treviño, F. A., ... & Cadenas-Pliego, G., **2015,** *Macromolecules*, *48*(4), 1026-1037.

[25] Castillo, U. J., Zolotukhin, M. G., Fomina, L., Nieto, D. R., Garza, L. O., & Fomine, S., **2013**, *Journal of molecular modeling*, *19*, 793-801.

[26] Klumpp, D. A., Zhang, Y., Kindelin, P. J., & Lau, S., **2006**, *Tetrahedron*, *62*(25), 5915-5921.

[27] Lira, A. L., Zolotukhin, M. G., Fomina, L., & Fomine, S., **2007**, *Macromolecular theory and simulations*, *16*(3), 227-239.

[28] Olvera, L. I., Zolotukhin, M. G., Hernẚndez-Cruz, O., Fomine, S., Cẚrdenas, J., Gaviño-Ramírez, R. L., & Ruiz-Trevino, F. A., **2015**, *ACS Macro Letters*, *4*(5), 492-494.

[29] Olvera, L. I., Guzmán-Gutiérrez, M. T., Zolotukhin, M. G., Fomine, S., Cárdenas, J., Ruiz-Trevino, F. A., ... & Prokhorov, E., **2013**, *Macromolecules*, *46*(18), 7245-7256.

[30] Cai, Z. H., Gao, X. L., Gao, W. T., Choo, Y. S. L., Wang, J. J., Zhang, Q. G., ... & Liu, Q. L., **2022**, *ACS Applied Energy Materials*, *5*(8), 10165−10176.

[31] Li, Z., Yu, R., Liu, C., Zheng, J., Guo, J., Sherazi, T. A., ... & Zhang, S., **2021**, *Polymer*, *222*, 123639.

[32] Pham, T. H., Olsson, J. S., & Jannasch, P., **2019**, *Journal of Materials Chemistry A*, *7*(26), 15895−15906.

3.2 Polydiallylammonium hydroxide based AEMs

3.2.1 Introduction

The aromatic structures used to increase the mechanical strength of AEMs have high glass transition and stiff characteristics.[1] This results in the formation of a solid−solid interface between the membrane and the catalyst, resulting in slow mass and electron transfer. To solve this problem, Xu et al. produced a soft membrane with high water uptake.[2] Fabricated membrane showed a very high swelling ratio of 485% in the through−plane direction, indicating that it was hydrophilic. However, anion exchange materials with high water uptake could not be used by themselves because of their weak mechanical strength. Thus, they used a porous PTFE substrate as a support to increase the mechanical strength. As a result, although the mechanical strength could be increased, it had a low IEC of 1.86 mmol/g.

In this study, an aromatic backbone was used to impart appropriate mechanical strength,[3] and PDAA with a high IEC was attached as a cationic group to improve the stiffness and low water uptake of the aromatic polymer. The aromatic backbone and PDAA exist in a cross−linked structure, and diallyldimethylammonium chloride (DADMAC) was added to PDAA to increase water uptake, IEC and hydroxide conductivity. PDAA−based AEMs are fully anion exchange membranes, which can control IEC in a wide range of 2.32−3.39 mmol/g, and show the characteristics of soft membranes during water uptake. It is also expected to have good alkaline stability because it has ring−type pyrrolidinium QA groups. The concept of PDAA based AEMs is shown in Figure 3−3.
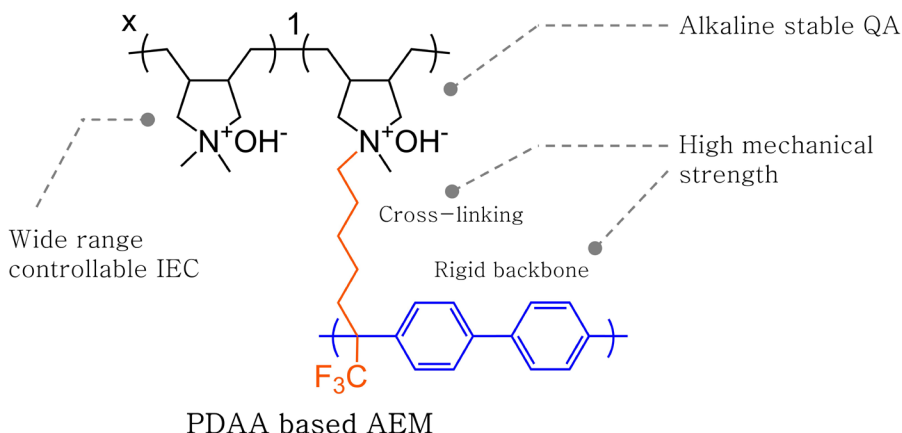
Figure 3-3. Concept of PDAA based AEMs

3.2.2 Experimental

Materials

For the membrane preparation, biphenyl (BP, >99%), diallylmethylamine (97%), diallyldimethylammonium chloride (DADMAC, >97%), butylated hydroxytoluene (BHT, 99%) and dimethyl sulfoxide-d6 (DMSO-d6, 99.9 atom% D) were supplied by Sigma Aldrich Chemical Co. Ltd and used as received. 7-Bromo-1,1,1-trifluoroheptan-2-one (95%) was supplied by Habotech and used as received. Potassium hydroxide (KOH, 93%), dichloromethane (DCM, 99%), trifluoromethane sulfonic acid (TFSA, triflic acid, 99%), N-methyl-2-pyrrolidone (NMP, 99%), n-hexane (98.5%), dimethyl sulfoxide (DMSO, 99.5%), 2,2'-azobis(2-methylpropionitrile) (AIBN, 99%), tetrahydrofuran (THF, 99.5%), and methyl alcohol (MeOH, 99.5%) were obtained from Daejung and used as received.

For membrane electrode assembly fabrication, platinum ruthenium (Pt-50 wt%, Ru-25 wt%, 047371.06) on high surface area advanced carbon support, and iridium(IV) oxide (99.99 wt%, 043396.06), cobalt nanopowder (99.8%, 46347) were received from Alfa Aesar.

Synthesis of BP-HBrF₃

TFSA was used as an acid catalyst for polyhydroxyalkylation reaction using BP and 7-bromo-1,1,1-trifluoroheptane-2-one. Dissolve biphenyl (1.34 g, 8.69 mmol) in 8.3 ml of DCM and dissolve 7-bromo-1,1,1-trifluoroheptane-2-one (2.37 g, 9.59 mmol). Place the round bottle in an ice-bath and slowly add 8.3 ml of TFSA. When the reaction is conducted for 23 h at room temperature while stirring, the reaction solution turns into a dark green color with high viscosity. Precipitate the viscous polymer fraction in excess methanol. The obtained polymer is once again dissolved in THF and precipitated in methanol to purify to obtain ivory BP-HBrF₃, followed by vacuum drying at 80℃.

Synthesis of BP-DAMA

A diallylmethylamine group was introduced into BP-HBrF₃ through the S_N2 reaction of an alkyl halide and a tertiary amine.[4] The synthesized BP-HBrF₃ (1g, 2.61 mmol) was dissolved in 7 ml of NMP, and BHT (0.009g, 0.04 mmol) was dissolved therein as a diallylmethyl amine polymerization inhibitor. After that, diallylmethylamine (0.58g, 5.22 mmol) was slowly added and reacted at 50℃ for 72h. After confirming that the substitution reaction was done by ^{1}H-NMR, the reaction solution is precipitated in n-hexane, washed several times, and vacuum dried at room temperature.

PDAA based AEMs fabrication

To prepare PDAA-based AEMs with IEC 3.39 mmol/g, BP-DAMA (1.39g, 2.82 mmol) was dissolved in 12.53g of DMSO. DADMAC (0.41 g, 2.53 mmol) was added to the solution followed by AIBN (0.007 g) as an initiator. After sufficiently mixing the solution, pour it into a mold and polycyclopolymerization in a 80℃ oven for 72 hours to obtain membranes. Similarly, PDAA based AEMs with other IECs can be manufactured in the same way as above by adjusting the content of DADMAC. The fabricated

membrane was immersed in 1M KOH for one day before use to exchange the counter ion into hydroxide form.

Characterization and measurements

^{1}H-NMR, and ^{19}F-NMR were measured at 25℃ using Varian Unity INOV. Fourier-transform infrared spectroscopy (FT-IR) spectra was obtained using PerkinElmer FT-IR system (Spectrum-GX) to analyze the structure of AEMs. The thermal stability of the PDAA based membranes were examined by using TA Instrument TGA 2950 with heating rate of 10 ℃/min under N_2 atmosphere. Mechanical property of the AEMs were characterized using universal tensile machine (Tinius Olsen H5K-T). Membrane samples (4cm*0.5cm) were prepared to measure the mechanical strength and tested at stretching speed of 10 mm/min. Field Emission Scanning Electron Microscopy (FE-SEM) images to verify morphology and shape of patterned Cu, was taken on an Inspect F50 (FEI, Korea).

Ion exchange capacity (IEC) value was determined by the back titration. OH- form membranes were immersed in 0.01 M HCl solution for 24 hrs. The HCl solution was titrated with 0.01 M KOH solution after adding three drops of phenolphthalein/EtOH indicator solution. The IEC (mmol/g) was calculated based on the following equation:

$$IEC = (V_{HCl}*C_{HCl} - V_{NaOH}*C_{NaOH})/W_{dry}$$

Where V_{HCl} and V_{NaOH} are volume of HCl and NaOH, respectively. C_{HCl} and C_{NaOH} are the concentration of HCl and NaOH, respectively. W_{dry} is the weight of the dried membranes.

The swelling ratio (SR) and water uptake (WU) were evaluated after immersing the membrane in water at room temperature for 24 hrs. After removing the membrane from the water, excess water on the surface was carefully wiped off and the weight and length was measured for comparison. After membrane was completely dried, the weight and length of the dried membrane

were also measured. As the result, SR and WU were calculated according to the following formula:

$SR = ((L_{wet} - L_{dry})/L_{dry})*100$

$WU = ((W_{wet} - W_{dry})/W_{dry})*100$

The KOH uptake rate is also tested in the same way. After the preparation of the membrane, the membrane was immersed in 1M KOH solution at room temperature for 24 hrs. The weight of the membrane was measured after removing the excess KOH solution on the surface of the membrane. After washing several times with water and drying, the weight of dried membrane was measured and compared. KOH uptake was calculated using the following equation.

$KOH\ uptake = ((m_{wet,KOH} - m_{dry})/m_{dry})*100$

The ohmic resistance of the AEMs were measured in water and 0.1M−5M KOH solution at different temperature by two−electrode electrochemical impedance spectroscopy (EIS, SI 1260, Solartron) over the frequency range from 10 Hz to 10 MHz with an amplitude of 20 mV. Before measurement, all OH^- form membranes were immersed in distilled water for at least 24 hrs to equilibrate in water. Hydroxide conductivity was calculated by the following equation:

$\sigma = L/(R \times W \times d)$

where L was the distance between two electrodes (cm), R was the measured ohmic resistance (Ω), W was the width of the membrane (cm) and d was the width of the membrane (cm).

MEA fabrication and electrolysis performance

PDAA AEM based MEAs (1cm^2 active area) were fabricated by the catalyst coated substrate (CCS) method. 50 wt% PtRu/C was used as anode and IrO_2, Co were used as cathode catalysts,

respectively. Catalyst inks were prepared by dispersing each catalyst powder over the TMA-70 ionomer which was synthesized, chemical structure and NMR spectra are shown in Figure 2-4(a) and (b). (4.65 wt% TMA-70 solution in n-propanol : aqueous 5:5 wt co-solution, the ionomer to carbon (I/C) weight ratio is 0.5, and for the OER catalyst layer the binder content was 10 wt%) in an aqueous solution of n-propanol and little amount of water, followed by ultrasonic treatment for more than 20 min with maintaining water temperature less than 35℃ to prevent catalyst agglomeration. The prepared catalyst inks were directly sprayed onto the gas diffusion layer (GDL) set on a 70℃ pre-heated hotplate. GDLs 39 BB (Fuel Cell Store), and Pt coated Ti paper (Giner) were used for the cathode and anode respectively. Cathode catalyst loading amount is 0.6 mgPt/cm^2, and anode catalyst loading amount is 2.0 mgIr/cm^2, 0.7 mgCo/cm^2. The fabricated CCS was dried at room temperature for more than 1 h to remove residual solvent in the catalyst layers. Prior to single cell application, the PDAA based membranes were sandwiched by the fabricated electrode without hot-pressing process. Polarization curves were obtained on Scribner electrolyzer cell with power supplied by Biologic potentiostat (SP-200) attached with power booster (HCV-3048) with electrolyte supplied with peristaltic pump.

3.2.3 Results and discussion

Synthesis of BP−HBrF$_3$ polymer

In the first step to synthesize PDAA−based AEMs, BP−HBrF$_3$ was synthesized. BP−HBrF3 was obtained by superacid−catalyzed hydroxyalkylation of biphenyl and 7−Bromo−1,1,1−trifluoroheptan−2−one,[5] and the reaction mechanism is shown in Figure 3−4(a). Figure 3−2(b) and (c) show the [1]H−NMR and [19]F−NMR spectra of synthesized BP−HBrF$_3$, respectively. In [1]H−NMR, an aromatic related peak appeared around 7.2~7.7 ppm,[6] and a bromoalkyl group was also confirmed. Since all F atoms in BP−HBrF$_3$ were placed in the same environment, they were detected as a single peak in [19]F−NMR.

The molecular weight of synthesized BP−HBrF$_3$ was confirmed by GPC, and related spectra is shown in Figure 3−5. A high molecular weight of 250,000 g/mol and PDI of 2.67 was obtained.

As shown in Figure 3−6(a), BP−HBrF$_3$ showed high thermal stability over 200℃. In the TGA curve, alkyl groups were first decomposed around 209℃, and degradation of the backbone started around 401℃. DSC measurement was performed to confirm the glass transition temperature (Tg) of BP−HBrF$_3$, and the DSC curve is shown in Figure 3−6(b). BP−HBrF$_3$ exhibited a high Tg of 182℃.

(a)

F₃C... Triflic acid / MC → BP-HBrF₃

BP
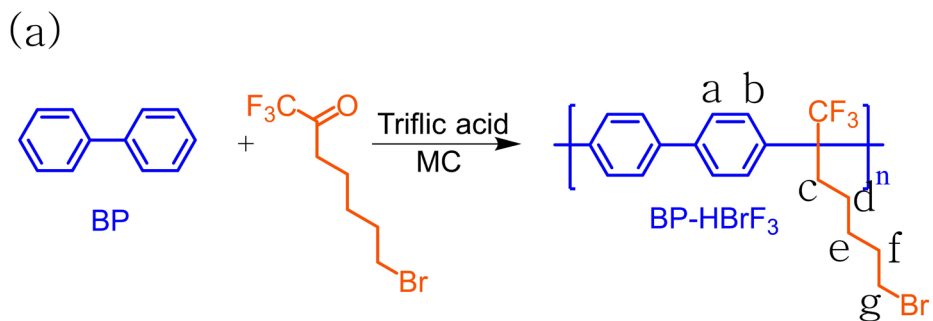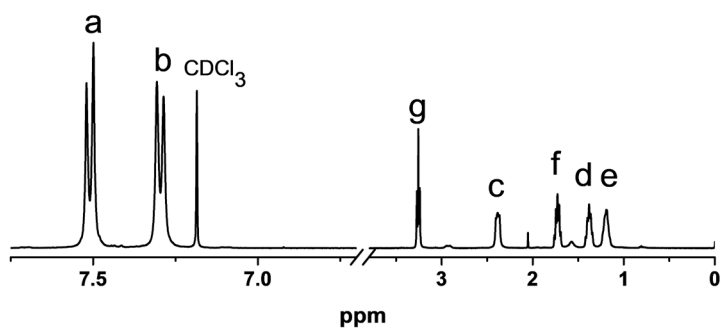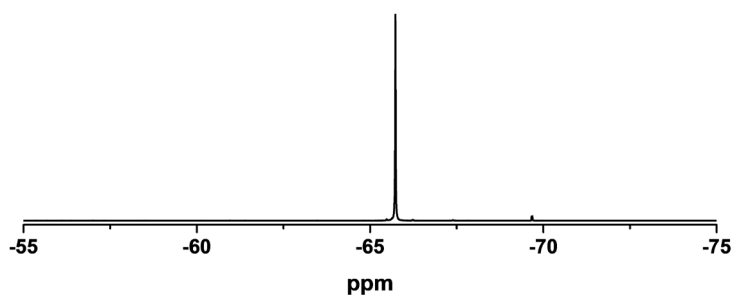
(b) <¹H−NMR>

(c) <¹⁹F−NMR>

Figure 3−4. (a) Synthesis mechanism of BP−HBrF₃ (b) ¹H−NMR (c) ¹⁹F−NMR spectra for BP−HBrF₃

Mw 250,000 / PDI 2.67
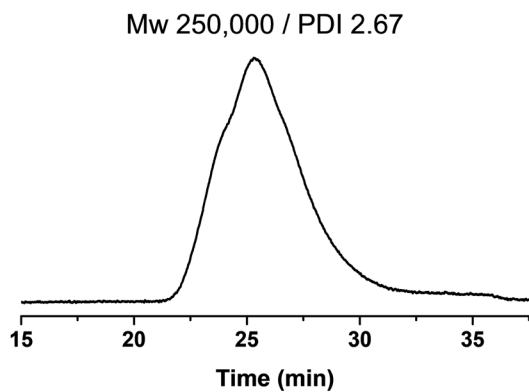
Figure 3−5. GPC spectra for BP−HBrF$_3$
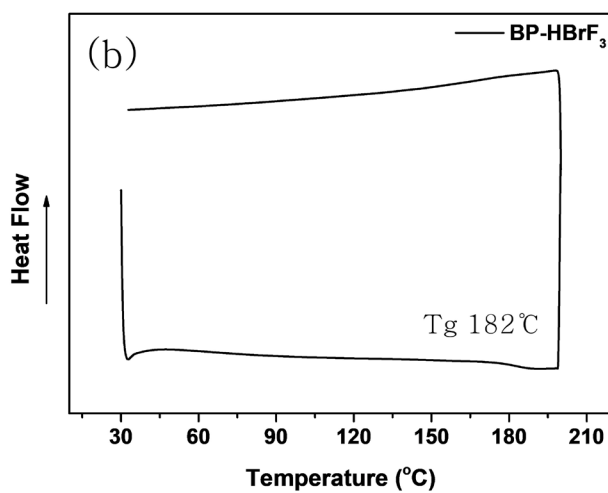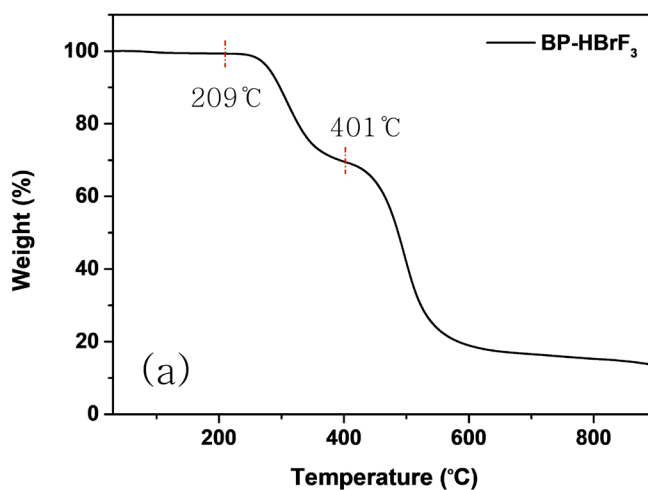
Figure 3−6. (a) TGA curve (b) DSC curve for BP−HBrF$_3$

Synthesis of BP-DAMA

The diallylmethylamine group was introduced into BP-HBrF$_3$ using the S$_N$2 reaction. In order to prevent the polymerization of diallylgroup, the reaction was carried out by adding BHT, a polymerization inhibitor.[7] Figure 3-7(a) shows the BP-DAMA synthesis mechanism and Figure 3-7(b) shows the ^{1}H-NMR results. Due to the introduction of the Diallylmethylamine group, allyl group-related peaks were detected at 5.5 to 6.2 ppm,[8] and a distinct methyl peak (h) was also confirmed. BP-DAMA shows good solubility in DMSO.

(a)
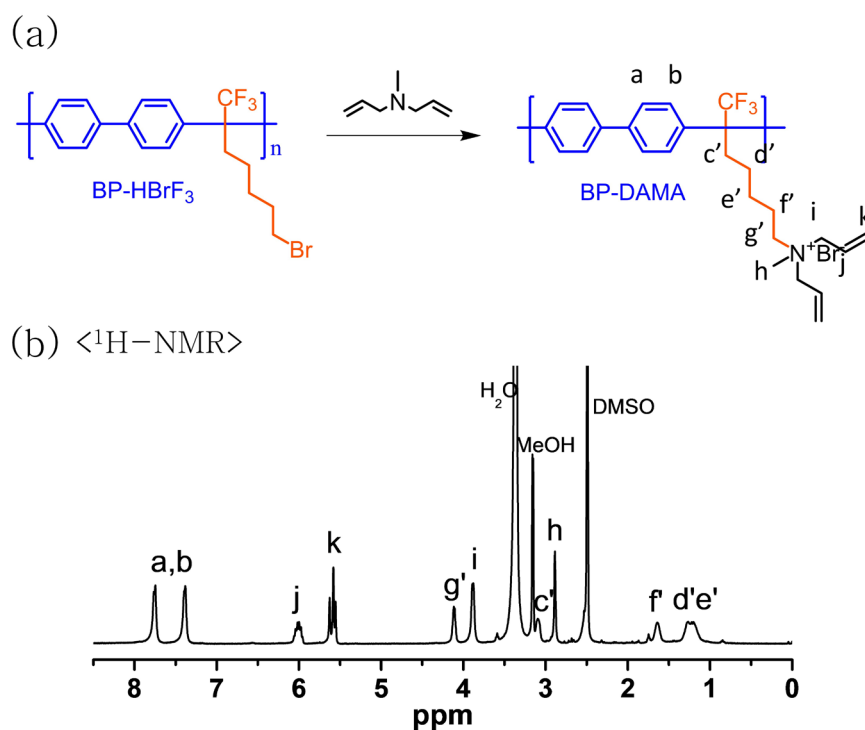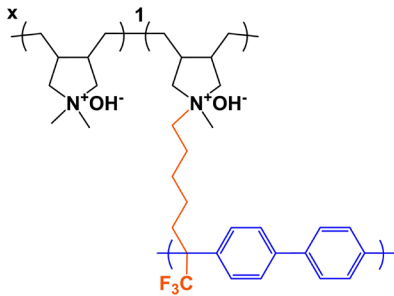
(b) <^{1}H-NMR>

Figure 3-7. (a) Synthesis mechanism of BP-DAMA (b) ^{1}H-NMR spectra for BP-DAMA

PDAA based AEMs fabrication and characterizations

The PDAA based membrane was fabricated by in-situ crosslinking and fabrication through cyclopolymerization of diallylammonium bromide groups in BP-DAMA using a radical initiator. The PDAA based membrane was named PDAA-BP (IEC), and the theoretical IEC was written in parentheses after the name. IEC can be increased by adding DADMAC when manufacturing membrane. The structure of PDAA-BP and the IEC according to the content of poly(DADMAC) groups are listed in Table 3-1.

Table 3-1. Theoretical IEC of PDDA based AEMs with different content of poly(diallyldimethylammonium) hydroxide groups

x	IEC (mmol/g)
0	2.32
0.25	2.61
0.75	3.19
0.9	3.39
1.0	3.48

If DADMAC is not added, minimum IEC of 2.32 mmol/g is obtained, and the IEC increases as the DADMAC content increases. Theoretically, it is possible to increase the IEC to infinity, but the introduction of too much poly(DADMAC) reduces the mechanical strength of the membrane. Therefore, in this study, AEMs with an IEC range of 2.32 to 3.39 mmol/g were fabricated and compared.
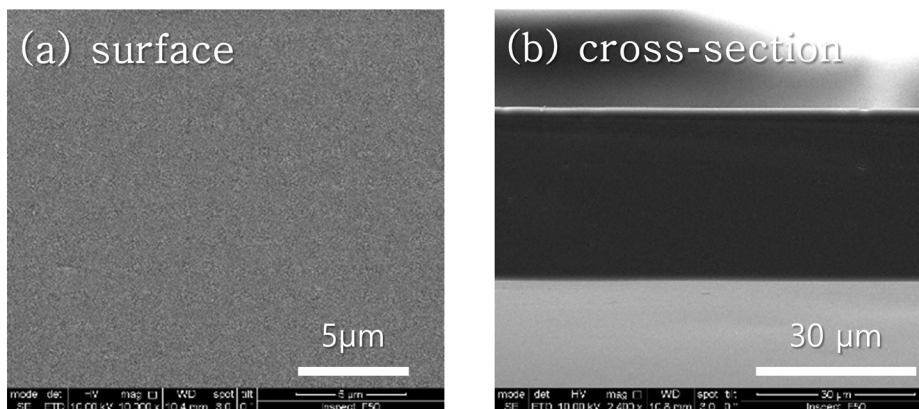
Figure 3-8. SEM images of PDDA-BP(3.39) (a) surface (b) cross-section

The PDAA-BP membrane was flexible upon water uptake and showed yellow color due to quaternary ammonium groups. As shown in Figure 3-8(a) and (b), PDAA-BP showed a dense structure both on the surface and in the cross section.

To be applied to AEMWEs, AEMs must show thermal stability above the operating temperature of 60~90℃.[9] Figure 3-9 shows the TGA curves of PDAA-BPs, all of which showed high thermal stability over 180℃. PDAA-BPs (2.32), (2.61), (3.19), and (3.48) showed T_{d5} of 194.2℃, 189.4℃, 219.0℃ and 194.2℃, respectively.
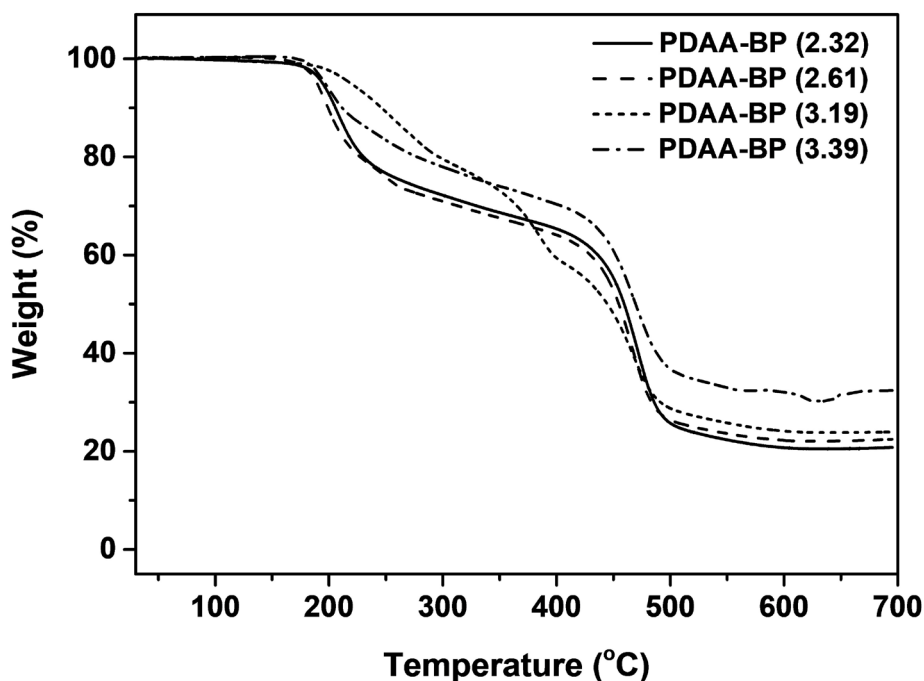
Figure 3-9. TGA curve for PDAA-BPs

Figure 3-10 shows the strain-stress curve of PDAA-BPs under water uptake. PDAA-BP with IEC 2.32 mmol/g without DADMAC showed the highest tensile strength of 13.2 MPa. As the content of poly(DADMAC), which has a high swelling property, increased, the strain value increased and the tensile strength value decreased as the IEC increased. Despite the presence of a rigid biphenyl backbone and crosslinking site, the mechanical strength under wetting conditions was measured to be relatively low.[10] This is considered to be due to the high water uptake characteristics of the PDDA groups. Although the tensile strength value itself is low, it was confirmed that PDAA-BPs operated stably during the actual AEMWEs performance test and had suitable mechanical strength for application to AEMWEs.
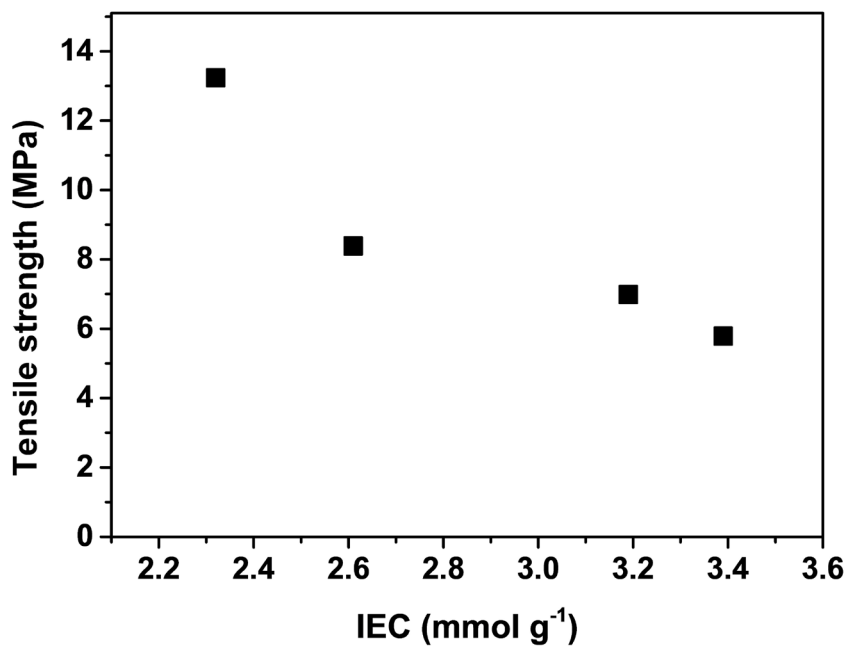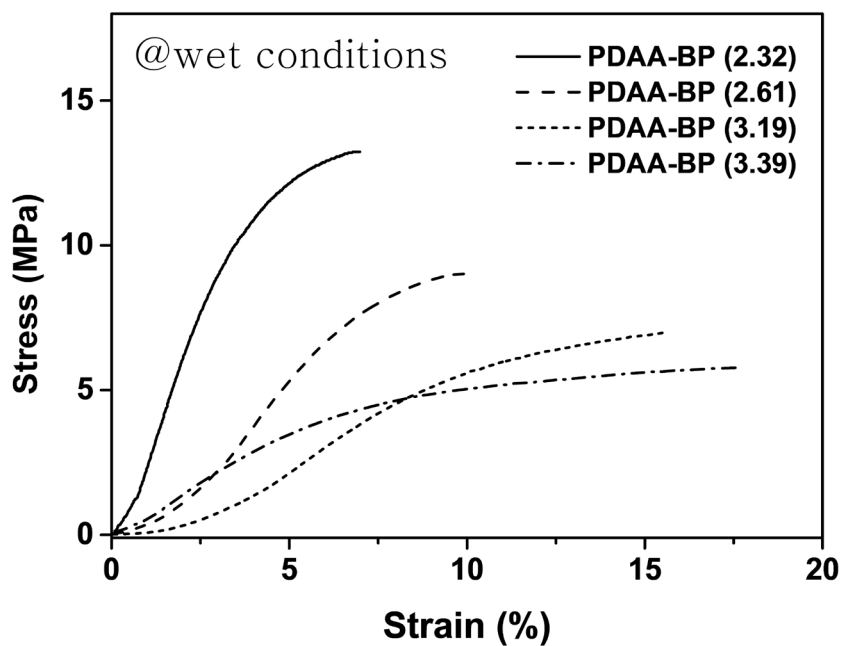
Figure 3-10. Strain-stress curve for PDAA-BPs under wet conditions

Hydration properties of PDAA-BPs

Table 3-2 lists the hydration properties of PDAA-BPs: IEC, water uptake, swelling ratio, KOH uptake and ionic conductivity. The experimental IEC of PDAA-BPs was measured by acid-base titration, and it was similar to the theoretical IEC.

Figure 3-11(a) shows a graph of water uptake and swelling ratio according to IEC. As expected, the water uptake and swelling ratio increased as the IEC increased.[11] In particular, PDAA-BP (3.39) had a high water uptake of 92.1% and the highest swelling ratio of 24.2%. Accordingly, KOH uptake also showed the same tendency as water uptake (Figure 3-11(b)).

Figure 3-11(c) shows the hydroxide conductivity of PDAA-BPs at the temperature of 25℃~80℃. All were measured at 100% RH, and as the temperature increased, the transport speed of hydroxide ions increased, resulting in high hydroxide conductivity.[12] Figure 3-11(d) compares the hydroxide conductivity according to IEC under the condition of 80℃ and 100% RH. Ion transport occurred better as IEC increased, and PDAA-BP (3.39) showed the highest and excellent hydroxide conductivity of 152.4 mS/cm. PDAA-BP (2.32), (2.61), and (3.19) had hydroxide conductivity of 90.35 mS/cm, 111.92 mS/cm, and 132.4 mS/cm at 80℃, respectively.

Table 3-2. Hydration properties of PDAA-BPs

Sample	IEC[a] (mmeq g^{-1})	Water uptake (%)[b]	Swelling ratio (%)[c]	KOH uptake (%)[d]	Ionic conductivity (mS cm^{-1})[e] 25 ℃	80 ℃
PDAA-BP (2.32)		20.8 (±5.05)	9.5 (±1.12)	52.6 (±4.61)	27.55 (±8.31)	90.35 (±12.9)
PDAA-BP (2.61)		38.4 (±3.87)	14.0 (±2.81)	64.8 (±8.20)	38.42 (±6.05)	111.92 (±8.69)
PDAA-BP (3.19)		62.3 (±4.64)	22.2 (±1.45)	106.7 (±6.78)	50.36 (±5.51)	132.4 (±7.35)
PDAA-BP (3.39)		92.1 (±6.11)	24.2 (±0.96)	137.4 (±9.56)	56.2 (±5.11)	152.4 (±14.7)

[a]Measured by acid-base titration, [b,c,d]Measured at 25 ℃, [e]Measured at 100% RH
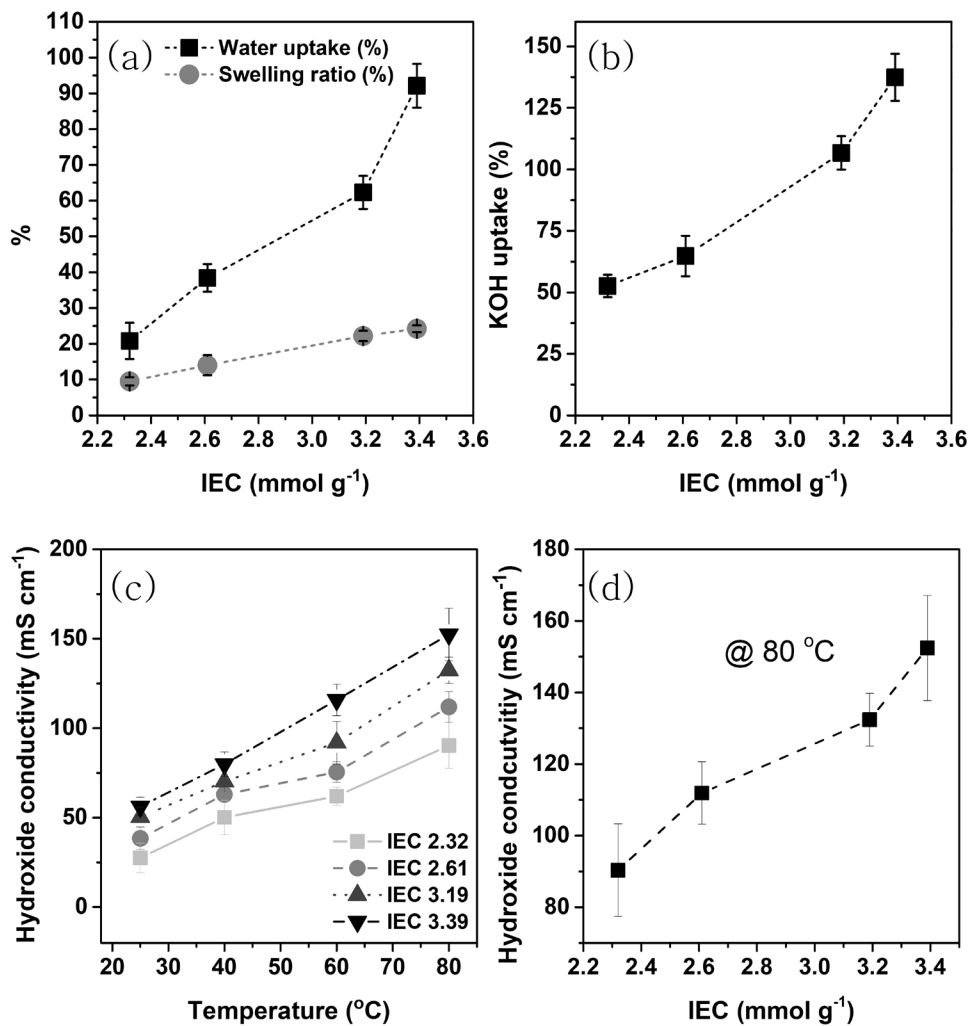
Figure 3-11. (a) Water and swelling ratio (b) KOH uptake (c) hydroxide conductivity at different temperature (d) hydroxide conductivity at 80℃ of PDAA-BPs

Alkaline stability test
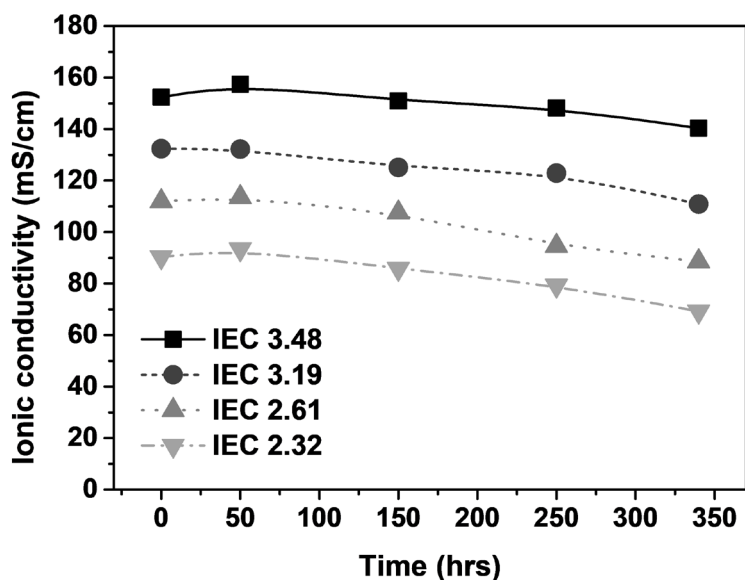
Figure 3-12. Ionic conductivity of BP-DAMAs after alkaline stability test in 1M KOH at 80 ℃

For the alkaline stability test of PDAA-BPs, the membrane was immersed in 1M KOH at 80 ℃ for 350 hrs, and the hydroxide conductivity was checked according to the immersion time. As shown in the Figure 3-12, there was a slight decrease in hydroxide conductivity after 350 hrs of immersion, but almost a similar level of initial conductivity. In particular, PDAA-BP of IEC 3.48 mmol/g showed a high hydroxide conductivity of 140.4 mS/cm even after 350 hours, showing excellent alkaline stability, confirming the alkaline stability effect of pyrrolidinium based quaternary ammonium.[13]

Figure 3-13(a) shows the comparison of FT-IR spectra before and after alkaline test of PDAA-BP(3.39) in 1M KOH at 80℃ for 500 hrs.
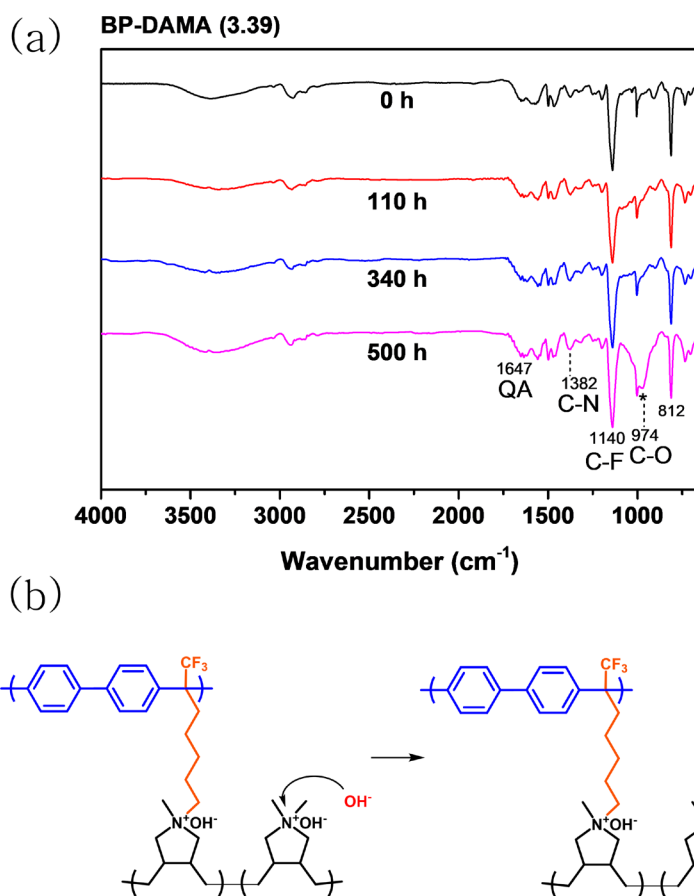
Figure 3-13 (a) comparison of FT-IR spectra before and after alkaline test of PDAA-BP(3.39) in 1M KOH at 80℃ for 500 hrs (b) PDAA-BP degradation mechanism under alkaline condition

The ATR-FTIR spectrum of PDAA-BP(3.39) is characterized by bands located at 1647 cm^{-1}, 1382 cm^{-1}, and 1140 cm^{-1} assigned to stretching vibration of quaternary ammonium groups, the C-N stretching, and the stretching of C-F, respectively.[14-16] After immersing in 1M KOH at 80 ℃ for 500 hrs, a new peak appeared at 974 cm^{-1}, which means that C-O was produced[17] due to degradation of pyrrolidinium. Accordingly, the PDAA-BP degradation mechanism is shown in Figure 3-13(b).
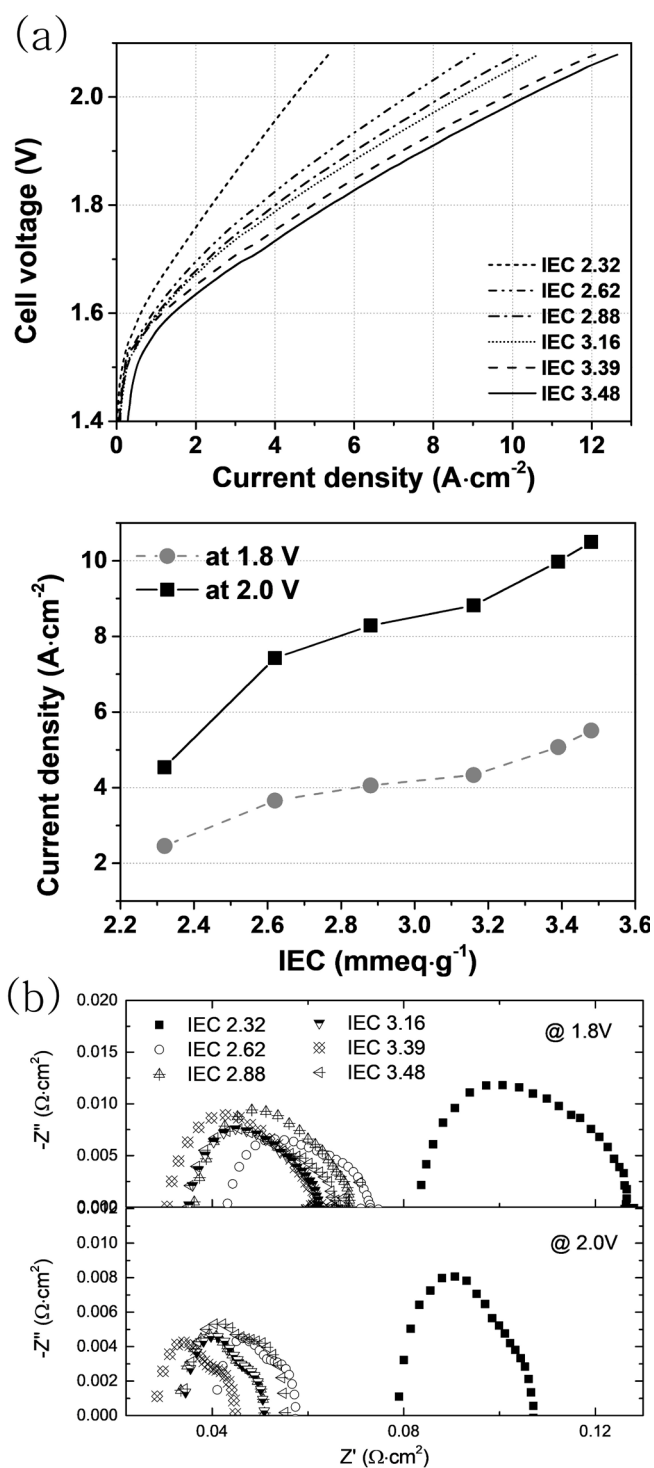
Figure 3-14. (a) LSV curve of BP-DAMAs (b) ohmic resistance of PDAA-BPs EIS nyquist plot

AEMWEs performance

　　Figure 3-14(a) shows the AEMWEs LSV curve of PDAA-BPs. AEMWEs test was measured in 1M KOH electrolyte at 80 ℃ using TMA-70 ionomer. As can be seen from the LSV curve, as the IEC increased, the current density proportional to the hydrogen production efficiency increased,[18] which also corresponded to the hydroxide conductivity result. The PDAA-BP (2.32) without any DADMAC added showed current density of 2.46 A/cm^2 at 1.8V and 4.54 A/cm^2 at 2.0V. PDAA-BP (3.39) with the highest IEC showed excellent performances of 5.07 A/cm^2 and 9.98 A/cm^2 at 1.8V and 2.0V, respectively. This is due to the high water uptake characteristics of the PDAA-based membrane, which is not rigid but smooth and slightly sticky during water uptake, which lowers the contact resistance between the electrode and the membrane, enabling fast mass transport. Figure 3-14(b) shows the ohmic resistance of PDAA-BPs EIS Nyquist plot. The larger the IEC, the lower the ohmic resistance.

3.2.4 Conclusion

　　In this study, PDDA based AEMs were developed for AEMWEs. The fabricated PDDA-BPs have a backbone of biphenyl group and quaternary ammonium groups of pyrrolidinium with good alkaline stability. The IEC of PDDA-BPs can be adjusted in a wide range of 2.32 to 3.39 mmol/g by controlling the content of poly(DADMAC) and has a dense structure. It showed good thermal stability over 180℃, and PDDA-BP(3.39) had a high hydroxide conductivity of 152.4 mS/cm at 80℃. In the AEMWEs performance test, PDAA-BP(3.39) with the highest IEC showed excellent performances of 5.07 A/cm^2 and 9.98 A/cm^2 at 1.8V and 2.0V, respectively. PDAA-BPs showed excellent hydrogen productivity by reducing the interfacial resistance between electrode and membrane and high ionic conductivity.

3.2.5 References

[1] Kundu, P. P., & Larock, R. C., **2005**, *Biomacromolecules*, *6*(2), 797-806.

[2] Xu, Z., Wan, L., Liao, Y., Wang, P., Liu, K., & Wang, B., **2021**, *Journal of Materials Chemistry A*, *9*(41), 23485-23496.

[3] Meador, M. A. B., Malow, E. J., Silva, R., Wright, S., Quade, D., Vivod, S. L., ... & Cakmak, M., **2012**, *ACS applied materials & interfaces*, *4*(2), 536-544.

[4] Pronin, S. V., Reiher, C. A., & Shenvi, R. A., **2013**, *Nature*, *501*(7466), 195-199.

[5] Romero-Hernández, J. E., Cruz-Rosado, A., Zolotukhin, M. G., & Vivaldo-Lima, E., **2017**, *Macromolecular Theory and Simulations*, *26*(5), 1700031.

[6] Guzman-Gutierrez, M. T., Nieto, D. R., Fomine, S., Morales, S. L., Zolotukhin, M. G., Hernandez, M. C. G., ... & Wilks, E. S., **2011**, *Macromolecules*, *44*(2), 194-202.

[7] Cook, W. D., Chen, F., Pattison, D. W., Hopson, P., & Beaujon, M., **2007**, *Polymer International*, *56*(12), 1572-1579.

[8] Yoshida, E., & Kuwayama, S., **2009**, *Colloid and Polymer Science*, *287*, 789-793.

[9] Kang, S. Y., Park, J. E., Jang, G. Y., Kim, O. H., Kwon, O. J., Cho, Y. H., & Sung, Y. E., **2022**, *International Journal of Hydrogen Energy*, *47*(15), 9115-9126.

[10] Mohanty, A. K., Song, Y. E., Jung, B., Kim, J. R., Kim, N., & Paik, H. J., **2020**, *International Journal of Hydrogen Energy*, *45*(51), 27346-27358.

[11] Huang, G., Mandal, M., Hassan, N. U., Groenhout, K., Dobbs, A., Mustain, W. E., & Kohl, P. A. , **2020**, *Journal of the Electrochemical Society*, *167*(16), 164514.

[12] Li, Z., Wang, W., Chen, Y., Xiong, C., He, G., Cao, Y., ... & Jiang, Z., **2016**, *Journal of Materials Chemistry A*, *4*(6), 2340-2348.

[13] Khan, M. I., Li, X., Fernandez-Garcia, J., Lashari, M. H., ur Rehman, A., Elboughdiri, N., ... & Ghernaout, D., **2021**, *ACS omega*, *6*(12), 7994-8001.

[14] Zhang, W., Cheng, W., Tufa, R. A., Liu, C., Aili, D., Chanda, D., ... & Ma, J., **2021**, *Membranes*, *11*(10), 771.

[15] Dhakshnamoorthy, M., Vikram, S., & Vasanthakumari, R., **2012**, *Int. J. Sci. Eng. Res*, *3*, 2229−2234.

[16] Shen, T., Zhang, Y., Kirillov, A. M., Cai, H., Huang, K., Liu, W., & Tang, Y., **2016**, *Chemical Communications*, *52*(7), 1447−1450.

[17] Lin, Q., Lu, Y., Ren, W., & Zhang, Y., **2015**, *RSC advances*, *5*(109), 90031−90040.

[18] Cheng, S., & Logan, B. E., **2011**, *Bioresource technology*, *102*(3), 3571−3574.

3.3 Benzene-free fully aliphatic PDAA based AEIs

3.3.1 Introduction

A high level of durability must be reached for commercialization of AEMWEs.[1] AEMs and AEIs are the main factors that determine the performance of AEMWEs and at the same time determine their durability.[2] Therefore, following AEMs, more studies are being conducted to improve the durability of AEIs within AEMWEs, recently.[3],[4]

Due to the alkaline electrolyte condition of AEMWEs, the alkaline stability of AEMWEs is a very important issue.[5-7] Ionomers with aryl-ether free and ring-type quaternary ammonium groups are expected to excellent durability under alkaline environments. Since AEIs are present on the electrode catalyst, oxidative degradation should be additionally considered.[8] Phenyl groups in the ionomers are adsorbed on the OER catalyst surface, followed by electrochemical oxidation to form phenol.[9] Related mechanism is shown in Figure 1-1(c) of Chapter 1. The formation of a phenolic compound of ionomers on the electrode surface was detected only after 100 hrs of AEMWEs operation, confirming that the oxidation reaction rate of the phenyl groups was very fast. Since the formed phenol is acidic, the local pH decreases through neutralizing the quaternary ammonium groups of ionomers. Accordingly, the OER activity is adversely affected, and eventually the durability of AEMWEs is reduced.

In this study, benzene-free ionomers with good alkaline stability were developed. Poly(diallylammonium) hydroxide (PDAA) based ionomers were synthesized using diallylammonium cyclopolymerization,[10] and are expected to have excellent alkaline stability because they contain pyrrolidinium type quaternary ammonium. Because PDAA has a small repeating unit molecular weight and can easily control the quaternary ammonium functional group, IEC control is possible over a wide range. In addition, it is

possible to control hydrophilicity and hydrophobicity by adjusting the chain length and IEC, and the reaction scale-up is relatively easy. Since PDAA-based ionomers have excellent alcohol solubility, preparing ionomer solutions is easy for loading on electrodes.

In general, performance increases as the IEC of ionomers increases. In Kim et al.'s study, the IEC of the ionomer was adjusted from 2.2 mmol/g to 3.3 mmol/g.[11] As a result of AEMWEs performance in pure water at 85 $^{\circ}$C the current density of the ionomer with 2.2 mmol/g IEC at 1.8V was 405 mA/cm^2, and the TMA-70 with the highest IEC showed a significant increase in performance to 1360 mA/cm^2. However, the effect on ionomers higher than IEC 3.3 mmol/g could not be confirmed because the adjusted IEC range was narrow. Since PDAA-based AEIs can control IEC in a wide range of 2.66 to 4.14 mmol/g, the IEC effect of ionomers can be confirmed in a wider range. Therefore, IEC and other secondary factors affecting the performance of AEMWEs are to be identified.

3.3.2 IEC control of ionomers

Alkyl groups of various chain lengths have been introduced to control the IEC of PDAA−based AEIs. PDAA−based AEIs were synthesized in two main ways, and the mechanism is shown in Figure 3−15. In the first method, poly(diallylmethyl)amine was synthesized through cyclization of commercially available diallylmethylamine and synthesized by introducing 1−bromoalkane. In the second method, a desired alkyl group is first introduced through monomer modification of diallylamine, and then poly(diallylalkyl)amine is synthesized through cyclization. Alkyl groups were introduced to poly(diallylalkyl)amine using the S_N2 reaction to generate quaternary ammonium groups. PDAA−based AEIs were named PDAA−X,Y, where x and y represent the number of carbons in R1 and R2 chains, respectively.

Table 3−3. IEC values according to the length of R1 and R2 groups of PDAA based AEIs

IEC (mmol/g)													
2.66		3.12		3.36		3.53		3.71		3.91		4.14	
R_1	R_2	R_1	R_2	R_1	R_2	R_1	R_2	R_1	R_2	R_1	R_2	R_1	R_2
1	F_9	1	13	1	12	1	11	1	10	1	9	1	8
		2	12	2	11	2	10	2	9	2	8	2	7
		3	11	3	10	3	9	3	8	3	7	3	6
		4	10	4	9	4	8	4	7	4	6	4	5
		5	9	5	8	5	7	5	6	5	5		
		6	8	6	7	6	6						
		7	7										

IEC effect

confirmation of secondary factors affecting performance

IEC can be adjusted according to the chain length and type of alkyl groups, and the IEC values according to the length of R1 and R2 groups are listed in Table 3-3. Interestingly, it is possible to design different lengths of R1 and R2 with the same IEC. Therefore, when R1 and R2 have similar lengths, and when R1 and R2 have different lengths, the water uptake characteristics and the performance of AEMWEs can be compared. In the first experiment, in order to first confirm the effect of IEC, R1 was fixed as a methyl group, the chain length of R2 was adjusted, and the performance was compared. In the second experiment, we compared the changes in water uptake, hydrophilicity, and hydrophobicity according to the change in chain length of R1 and R2, and finally confirmed the secondary factors affecting the performance of AEMWEs.
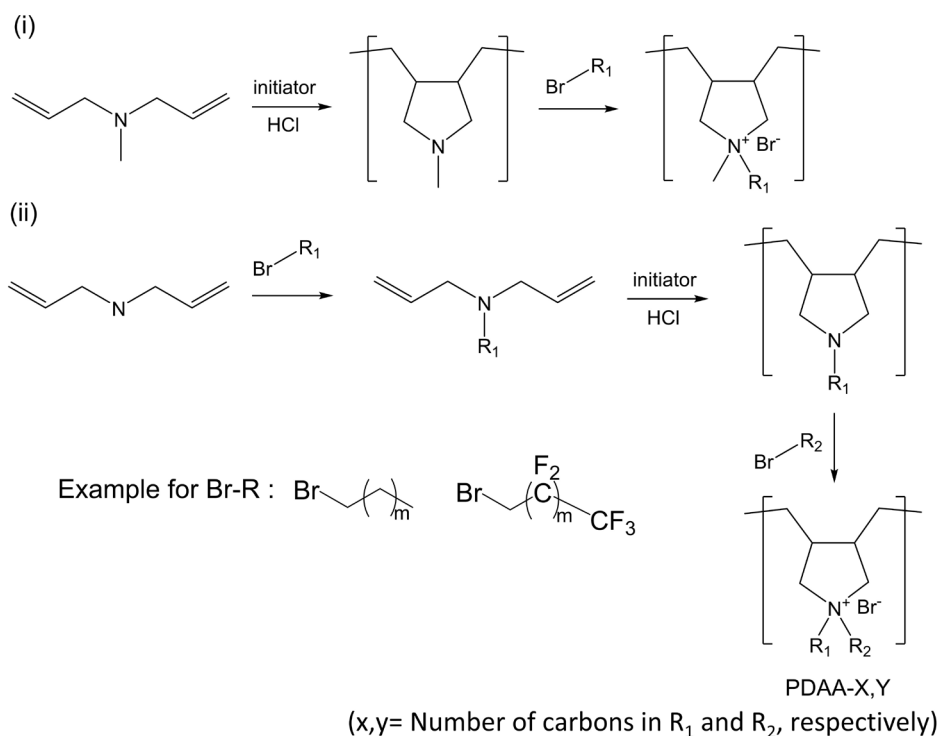
Figure 3-15. Synthesis of PDAA-based AEIs

3.3.3 Experimental

Materials

For synthesis of PDAA based AEIs, Diallylamine (99%), 1H,1H,2H,2H-nonafluorohexyl iodide (96%), iodomethane (99%), 1-bromopropane (99%), 1-bromobutane (99%), 1-bromopentane (98%), 1-bromohexane (98%), 1-bromoheptane (99%), 1-bromooctane (99%), 1-bromononane (98%), 1-bromodecane (98%), 1-bromoundecane (98%), 1-bromododecane (97%), 1-bromotridecane (98%), pyrrolidine (99%), N-methyl pyrrolidine (97%), 2,2 '-azobis(2-methylpropionamidine) dihydrochloride (AAPH, 97%) and triethylamine (99%) were supplied by Sigma Aldrich Chemical Co. Ltd. Dimethyl sulfoxide (DMSO, 99.5%), potassium carbonate anhydrous (K_2CO_3, 99.5%), dichloromethane (DCM, 99%), magnesium sulfate anhydrous ($MgSO_4$, 99%), hydrochloric acid (HCl, 37wt%), tetrahydrofuran (THF, 99.5%), acetonitrile (ACN, 99.5%), ethyl acetate (EA, 99%) and n-hexane (96%) were obtained from Daejung.

For membrane electrode assembly fabrication, platinum ruthenium (Pt-50wt%, Ru-25wt%, Alfa 047371.06) on high surface area advanced carbon support, and iridium(IV) oxide (99.99 wt%, Alfa 043396.06), cobalt nanopowder(99.8%, 46347) were received from Alfa Aesar. The commercial Pention membrane obtained from Sigma Aldrich Chemical Co. Ltd. has a thickness of 45-55 μm.

Synthesis of diallylalkylamine

The synthesis method of diallylhexylamine is as follows. Diallylamine (27g, 0.278 mol) was dissolved in DMSO (81g) and stirred at 70℃. After adding K_2CO_3 (34.8g) to the diallylamine/DMSO solution and stirring for 10 minutes, 1-bromohexane (41.35 g, 0.252 mol) was slowly drop-wise. After about 15 hrs at 70℃ under Ar environment, lower the temperature to room temperature and add DCM (30g). Then solution was

extracted with DI water more than 3 times. The DCM solution part was treated with MgSO$_4$, and the product in liquid form was obtained through filter and rotary evaporation. Likewise, other types of diallylalkylamines can be synthesized in the same way as above.

Synthesis of poly(diallylmethylammonium) bromide

A typical example was the synthesis of poly(diallylhexylamine). Diallylhexylamine (17.8g, 97.9 mmol) was put in a 100ml round bottle and condenser was installed. The round bottle was placed in an ice bath, 37 wt% HCl (7.2ml, 108.8mmol) was added and degassed with N$_2$ gas for 10 minutes.[12] Afterwards, the temperature of the solution was increased to 100℃, and 2,2'-Azobis(2-methylpropionamidine) dihydrochloride (AAPH, 2.66 g) was added at intervals of 3 minutes as an initiator. As an exothermic reaction, the reaction temperature briefly increased to 110℃. After 24hrs at 100℃, the reaction temperature was lowered to room temperature. The reaction mixture was purified by dialyzed against distilled water for 3 hours and freeze-dried. The freeze-dried sample was treated with triethylamine, washed several times with water until the pH is neutral, and then freeze-dried again to obtain poly(diallylhexylamine). In the same way as above, poly(diallylalkylamine) can be synthesized using other diallylalkylamine.

Synthesis of poly(diallylalkylammonium) bromide

Poly(diallylalkylammonium) bromide was synthesized by introducing alkyl groups into poly(diallylakylamine). A typical example was the synthesis of poly(diallyldihexylammonium) bromide. TEA-treated poly(diallylhexylamine) (0.5 g, 2.76 mmol) was dissolved in 2.75 g of THF. 1-bromohexane (0.55g, 3.31 mmol) was slowly dropped into the reaction solution and reacted with stirring at 60℃ for 3 days. THF was evaporated and purified several times with water. Then, poly(diallydihexylammonium) bromide is obtained through vacuum drying at 80℃. Similarly,

several types of poly(diallyldialkylammonium)bromide were synthesized using different types of poly(diallylakylamine) and 1-bromoalkane.

Synthesis of pyrrolidinium based monomer

A pyrrolidinium based monomer was synthesized to confirm the alkaline stability. First, the synthesis method using N-methylpyrrolidine monomer was explained. N-methylpyrrolidine (15g, 176.16 mmol) was dissolved in acetonitrile (300 ml) and 36.52 g of K_2CO_3 was added to the acetonitrile solution, followed by iodomethane over 10 minutes. After installing the condenser and refluxing for 48h, the reaction solution was cooled down to room temperature. The reaction solution was washed three times with an EA:n-hexane=1:1 solution and vacuum dried to obtain 1,1-dimehylpyrrolidin-1-ium iodide. In the same way, various pyrrolidinium based monomers were synthesized using N-methylpyrrolidine or pyrrolidine and 1-bromoalkane.

Characterization and measurements

^{1}H-NMR was measured at 25℃ using Varian Unity INOV to analyze the structure of AEIs. The thermal stability of the PDAA based AIEs were examined by using TA Instrument TGA 2950 with heating rate of 10 ℃/min under N_2 atmosphere. Differential scanning calorimetry was carried out with a TA Instrument DSC Q20-1426 using a heating rate of 10 ℃/ min under N_2 atmosphere. Note that second scans were only shown. The surface contact angles were measured by contact angle analyzer.

The water contact angles of the AEIs coated electrode with PtRu/C catalyst. The contact angle was measured immediately after water fell on the electrode surface. Time for complete absorption by the electrode was also measured.

PDAA-based AEIs were difficult to manufacture membranes, so water uptake was measured by coating them on vials. After weighing the vial, AEIs dissolved in THF were added to the vial. When dried at 80℃, the inner surface of the vial is coated with AEIs.

The coated AEIs were weighed (W_{dry}), filled with water, immersed for 24 hrs, then drained off, and the water absorbed weight (W_{wet}) was measured. As the result, water uptake was calculated according to the following formula.

Water uptake = $((W_{wet}-W_{dry})/W_{dry}) *100$

An alkaline stability test was conducted using a pyrrolidinium based monomer that dissolves well in the solvent and can observe neat peaks in ^1H-NMR. 1M KOH and 5M KOH solutions were prepared from a solution of deuterium oxide and methanol-d6:deuterium oxide=3:1 (MD31). 2% NMR solutions of each PDAA-based AEIs were prepared, and the degree of degradation over time at 80℃ in KOH solution was confirmed by ^1H-NMR.

MEA fabrication and electrolysis performance

PDAA-based AEIs ($1cm^2$ active area) were fabricated by the catalyst coated substrate (CCS) method. 50 wt% PtRu/C was used as anode and IrO_2, Co were used as cathode catalysts, respectively. Catalyst inks were prepared by dispersing each catalyst powder over the PDAA-based AIEs which was synthesized. (5 wt% PDAA-based AEI solution in n-propanol : aqueous 5:5 wt co-solution, the ionomer to carbon (I/C) weight ratio is 0.5, and for the OER catalyst layer the binder content was 10 wt%) in an aqueous solution of n-propanol and little amount of water, followed by ultrasonic treatment for more than 20 min with maintaining water temperature less than 35℃ to prevent catalyst agglomeration. The prepared catalyst inks were directly sprayed onto the gas diffusion layer (GDL) set on a 70℃ pre-heated hotplate. GDLs 39 BB (Fuel Cell Store), and Pt coated Ti paper (Giner) were used for the cathode and anode respectively. Cathode catalyst loading amount is 0.6 mg_{Pt}/cm^2, and anode catalyst loading amount is 2.0 mg_{Ir}/cm^2, 0.7 mg_{Co}/cm^2. The fabricated CCS was dried at room temperature for more than 1 h to remove residual solvent in the catalyst layers. Prior to single cell application, the PDAA based membranes were sandwiched by the fabricated electrode without hot-pressing

process. Polarization curves were obtained on Scribner electrolyzer cell with power supplied by Biologic potentiostat (SP-200) attached with power booster (HCV-3048) with electrolyte supplied with peristaltic pump.

3.3.4 Results and discussion

Synthesis of diallylalkylamine

To synthesize PDAA-X,Y with various IECs, diallylamine was modified as a monomer. Tertiary amine was synthesized by SN2 reaction using 1-bromoalkane to diallylamine, and the corresponding mechanism is shown in Figure 3-16. It was confirmed that the intensity of the alkyl groups peaks (f ~ j) increased as the alkyl chain lengthened, and allyl group peaks (a, b) were observed at 5.2 ppm and 5.9 ppm.

Cyclopolymerization of diallylalkylamine and characteristics

The cyclopolymerization of diallylalkylamine occurs through the mechanism of initiation, intramolecular cyclization, and linear propagation,[13] and the mechanism is shown in Chapter 2 Figure 2-1(b). After cyclopolymerization of diallylamine monomer, five-membered pyrrolidinium rings are generated.[14] These pyrrolidinium based quaternary ammoniums have good alkaline stability[15], so it can be applied to the fabrication of AEMs. Because cationic diallylammonium monomers undergo polymerization better than neutralized diallylamine[16], diallylamine monomer reacts in aqueous HCl to form ammonium forms. AAPH, an aqueous initiator, was used and poly(diallylalkylamine) was synthesized by reaction at 100℃ for 24 hours.

The synthesis mechanism is shown in Figure 3−17(a). In order to finally synthesize the synthesized PDAA−X,Y ionomers, an alkyl group was additionally introduced to poly(diallylalkylamine) to produce quaternary ammonium. Figure 3−17(b) shows the ^{1}H− NMR spectra of PDAA−1,Y with R1 fixed as a methyl group. Figure 3−18 shows the ^{1}H−NMR spectra of PDAA−X,Y where R1 and R2 are not methyl groups.
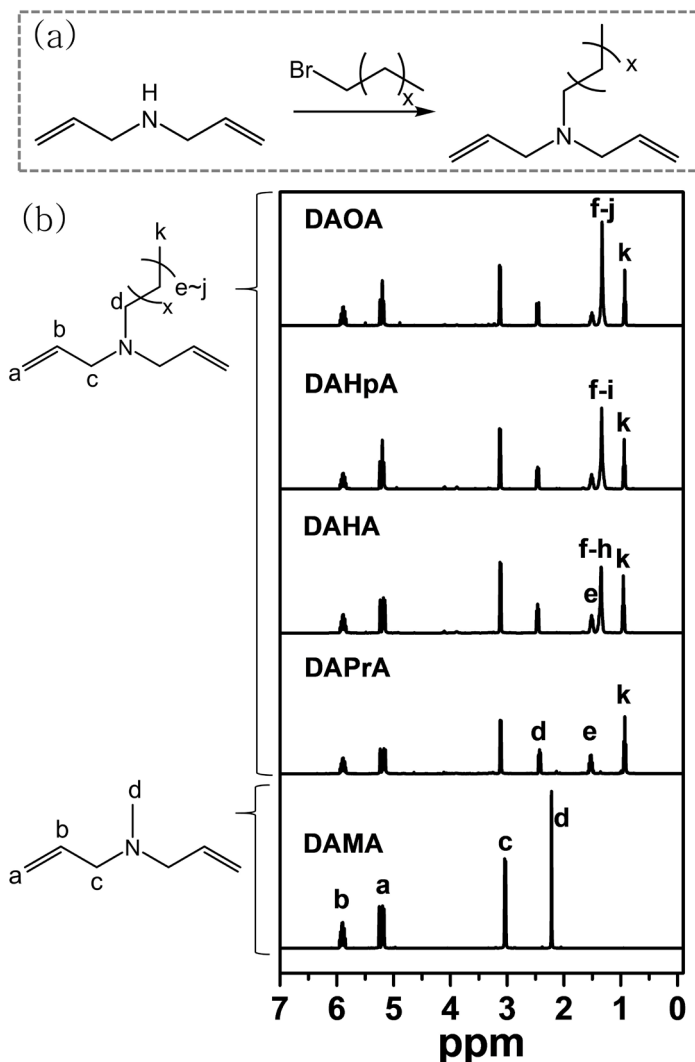
Figure 3−16. Synthesis of diallylamine (a) mechanism (b) ^{1}H−NMR spectra for diallylamine
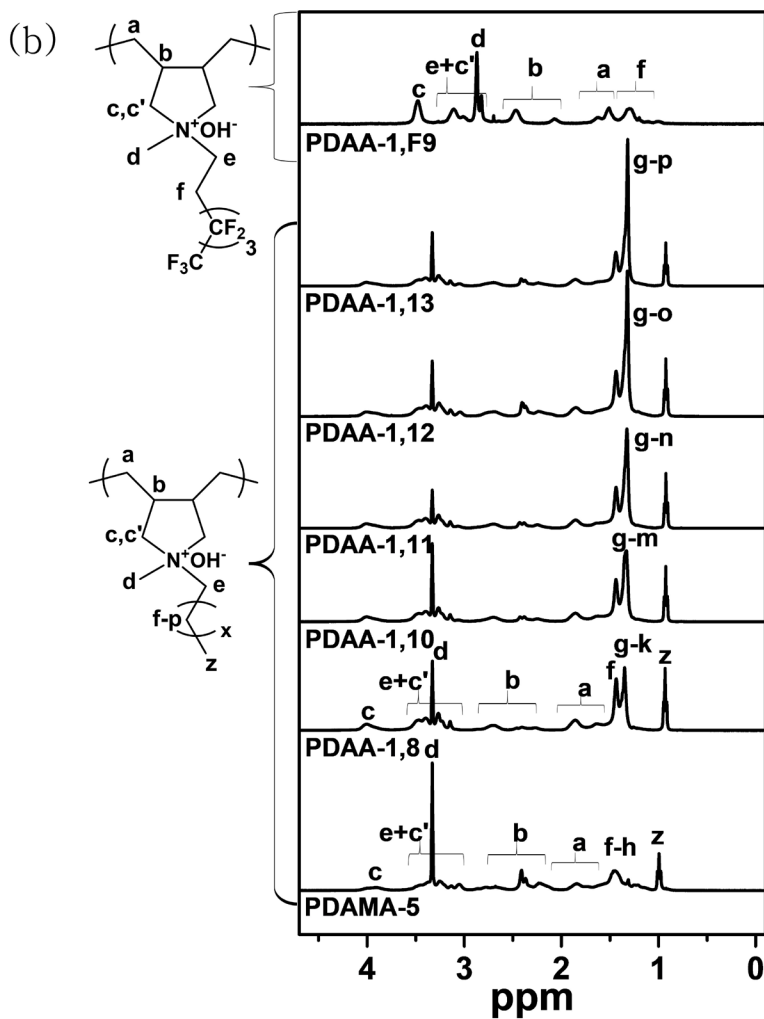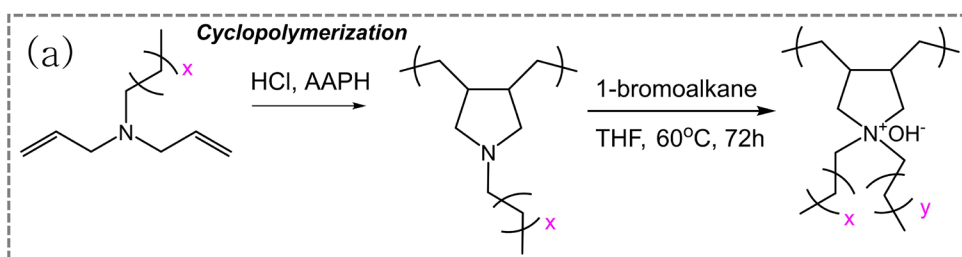
Figure 3-17. (a) Mechanism of cyclopolymerization and quaternization for PDAA-based AEIs, (b) ^{1}H-NMR spectra for PDAA-1,Y AEIs
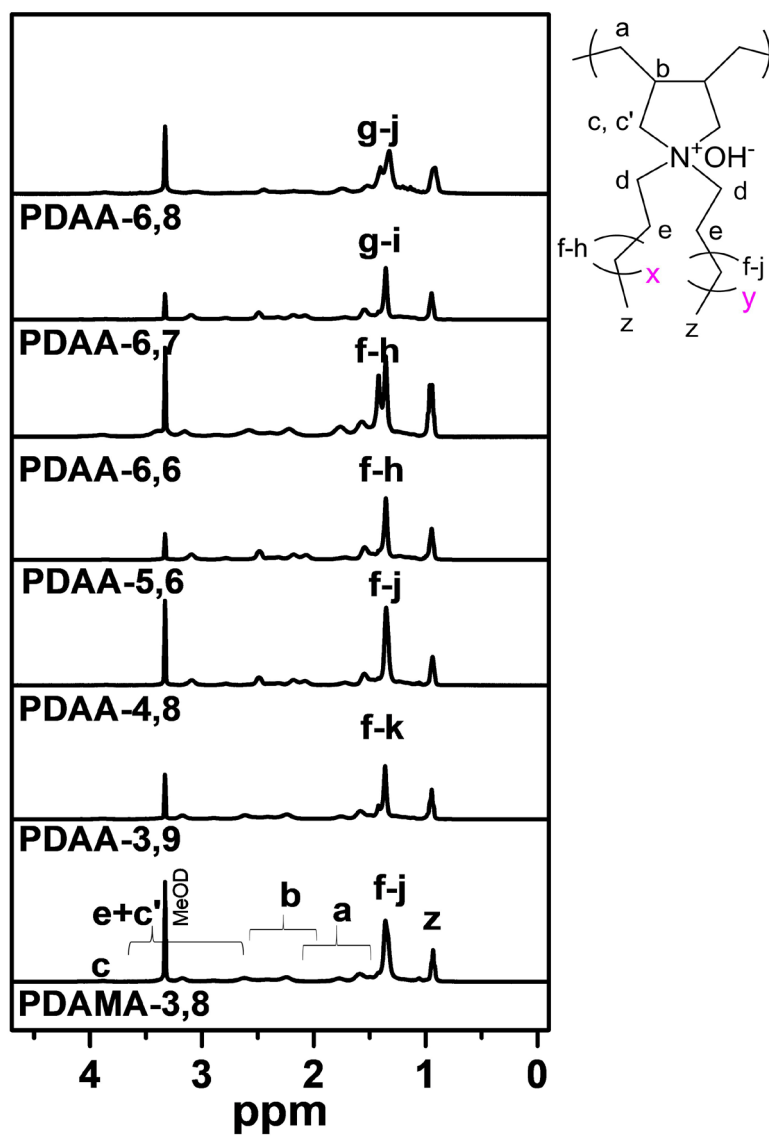
Figure 3−18. ^{1}H−NMR spectra for PDAA−X,Y AEIs

DSC measurement was performed to confirm the glass transition temperature (Tg) of PDAA−X,Y, and Figure 3−19 shows the DSC curve of PDAA−X,Y. As shown in Figure 3−19(a), PDAA−1,Y exhibited a Tg of 67~81℃ and has a Tg similar to the operating temperature of AEMWEs, so mass transport is expected to occur well due to its soft characteristics. PDAA−X,Y having relatively similar chain lengths of R1 and R2 showed either weak Tg or no Tg.

The operating temperature of AEMWEs is 60~90℃, and AEIs should have high thermal stability. TGA was measured to see the thermal stability of PDAA−X,Y, and Figure 3−20 shows the TGA curves of PDAA−X,Y. Figure 3−20(a) is the TGA curves of PDAA−1,Y in which the R1 group is substituted with methyl. All PDAA−1,Y showed excellent thermal stability over 200℃, and PDAA−6,Y in Figure 3−20(b) also showed good thermal stability over 180℃. PDAA−X,Y, in which R1 has more carbon atoms than the methyl group and the chain length of R1 and R2 is relatively large, showed relatively low thermal stability (Figure 3−20(c)). However, it has sufficient thermal stability to be used.
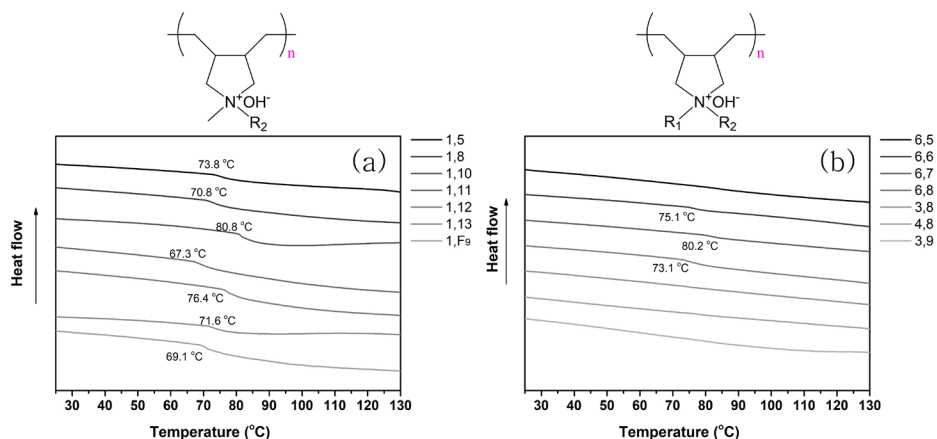
Figure 3−19. DSC curves for PDAA based AEIs (a) PDAA−1,Y (b) PDAA−X,Y
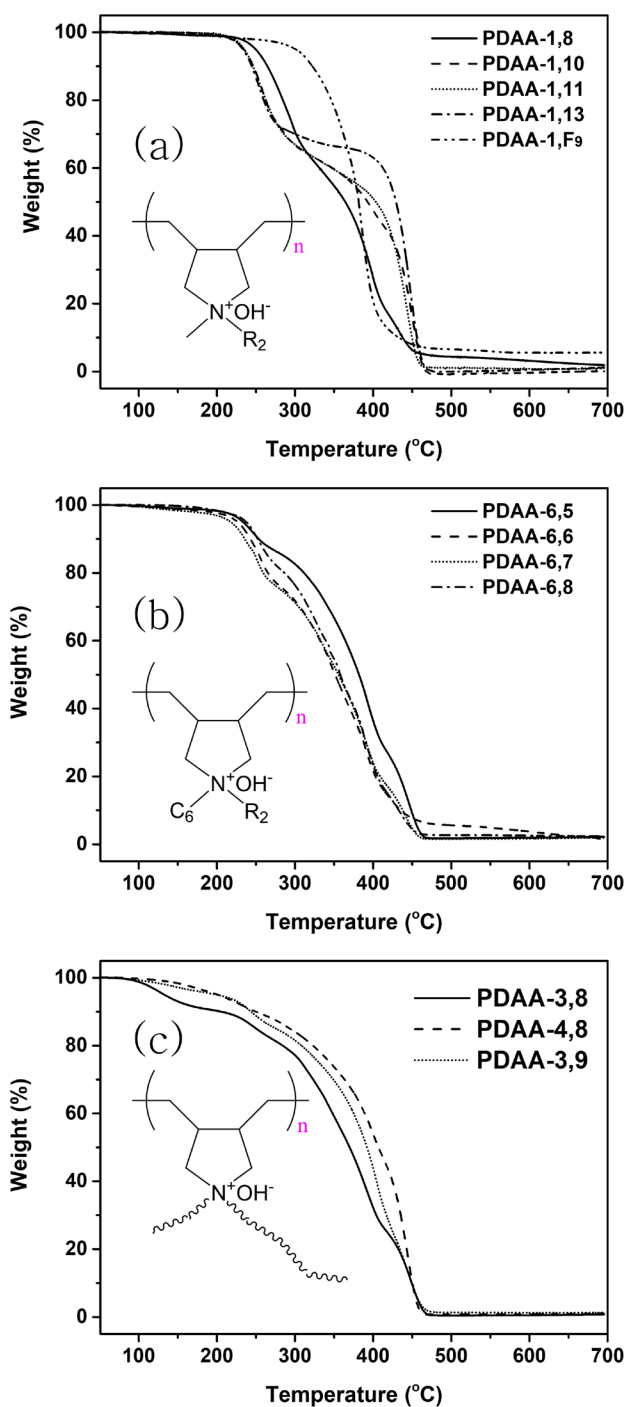
Figure 3-20. TGA curves for PDAA based AEIs (a) PDAA-1,Y (b) PDAA-6,Y, (c) PDAA-XY

Anion exchange membrane water electrolysis performance
－ IEC effect of AEIs

　　　To confirm the IEC effect of AEIs, PDAA-1,Y with an IEC range of 2.66 to 4.14 mmol/g was synthesized by fixing the R1 functional group to a methyl group and adjusting the R2 chain group. Figure 3-21(a) shows the AEMWEs LSV curve of PDAA-1,Y. AEMWEs test was measured in 1M KOH electrolyte at 80℃ using Pention AEMs. As can be seen from the LSV curve, all except PDDA-1,8 and PDDA-1,F9 showed higher performance than TMA-70. Current density according to IEC of PDAA-1,Y and TMA-70 are listed in Table 3-4. TMA-70 has a current density of 5.37 A/cm^2 at 2.0V, but PDAA-1,11 has increased performance to a current density of 6.43 A/cm^2 at 2.0V. Figure 3-21(b) shows the graph of current density according to IEC of AEIs at 2.0V. The current density increased as the IEC increased, and then decreased as the IEC further increased based on PDAA-1,11 having an IEC of 3.53. Therefore, there is an optimized IEC for high performance, not that the performance increases as the IEC increases.

Table 3-4. current density according to IEC of PDAA-1,Y and TMA-70 at 1.8V and 2.0V

Sample		IEC (mmeq/g)	current density (A/cm^2)	
			@1.8V	@2.0V
TMA-70		3.30	2.72	5.67
P D A A	1.F9	2.66	2.92	5.56
	1,13	3.12	3.43	6.15
	1,11	3.53	3.48	6.43
	1,10	3.71	3.34	6.25
	1,8	4.14	2.76	5.34
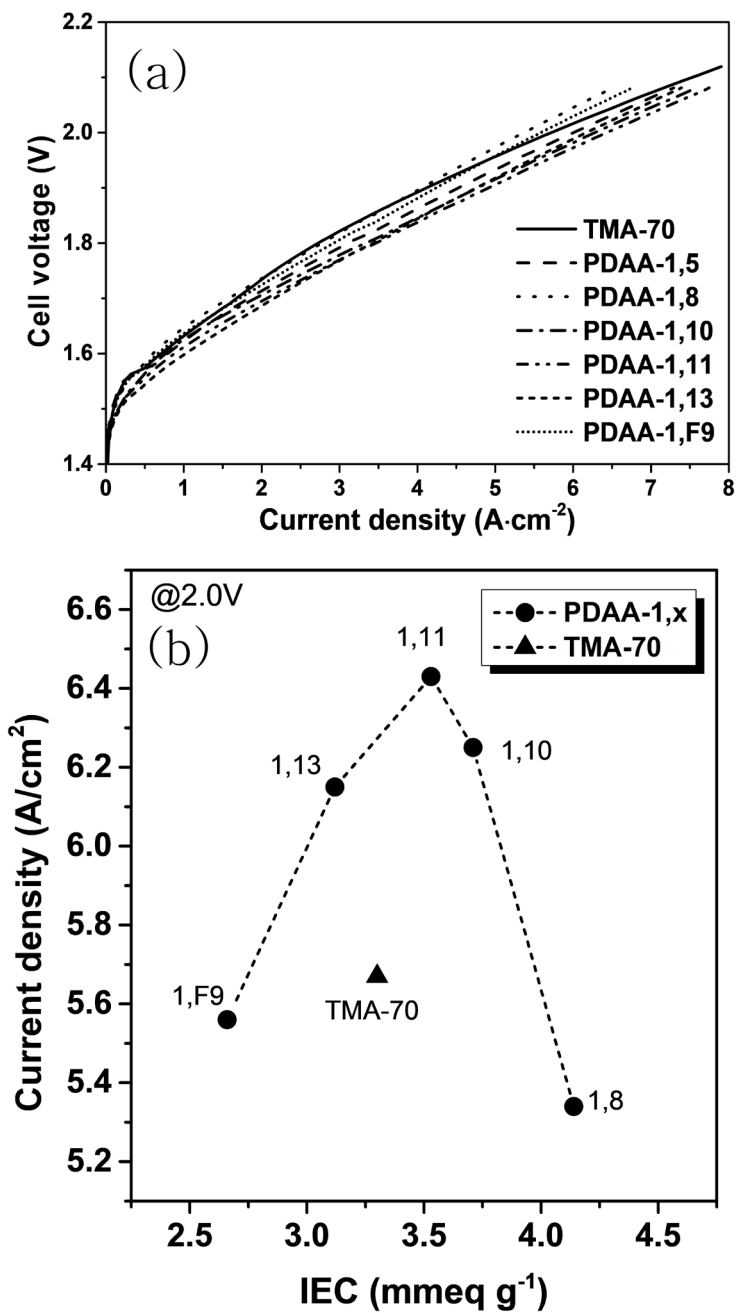
Figure 3-21. (a) LSV curves for PDAA-1,Y and TMA-70 (b) current density according to IEC of AEIs

- Secondary factors of AEIs affecting AEMWEs performance

In order to find out other factors of AEIs affecting performance in addition to the IEC effect, AEMWEs tests were conducted by varying the chain lengths of R1 and R2. There were many candidates, but it was difficult to evaluate all of them, so the PDAA-6,8, PDAA-6,7, PDAA-6,6, PDAA-4, 8, PDAA-3,9, PDAA-5,6 and PDAA-3,8 were selected.

Figure 3-22 shows the LSV curves of PDAA-X,Y. All PDAA-X,Y showed higher performance than TMA-70, and the current density at 1.8V and 2.0V is listed in Table 3-5. Among the PDAA-X,Y series, PDAA-3,8 showed the highest performance of 4.62 A/cm^2 at 1.8V and 8.23 A/cm^2 at 2.0V, and showed 1.45 times better performance than TMA-70 at 2.0V. Figure 3-23 shows the current density at 2.0V according to IEC of PDAA-X,Y. First of all, the surprising thing is that despite the same IEC, quite different performance results were obtained depending on the alkyl groups of R1 and R2. For example, PDAA-1,10, PDAA-5,6, and PDAA-3,8 all have the same IEC of 3.7 mmol/g. However, different current densities of 6.25 A/cm^2, 7.08 A/cm^2, and 8.23 A/cm^2 were obtained at 2.0V, respectively. This suggests that there is another effect on the performance of AEMWEs as well as IECs, and related additional experiments will be discussed later.

Another point to note is that when connecting PDAA-X,Y having one same chain group, all of them showed the highest performance in the range of IEC 3.3 to 3.7 mmol/g. PDAA-1,11 with IEC 3.53 mmol/g for PDAA-1,Y, PDAA-6,7 with IEC 3.36 mmol/g for PDAA-6,Y, and PDAA-3,8 with IEC 3.71 mmol/g for PDAA-8,X reached the highest peak of current density. This confirmed the IEC effect once more, and the optimized IEC range was in the range of 3.3 to 3.7 mmol/g.
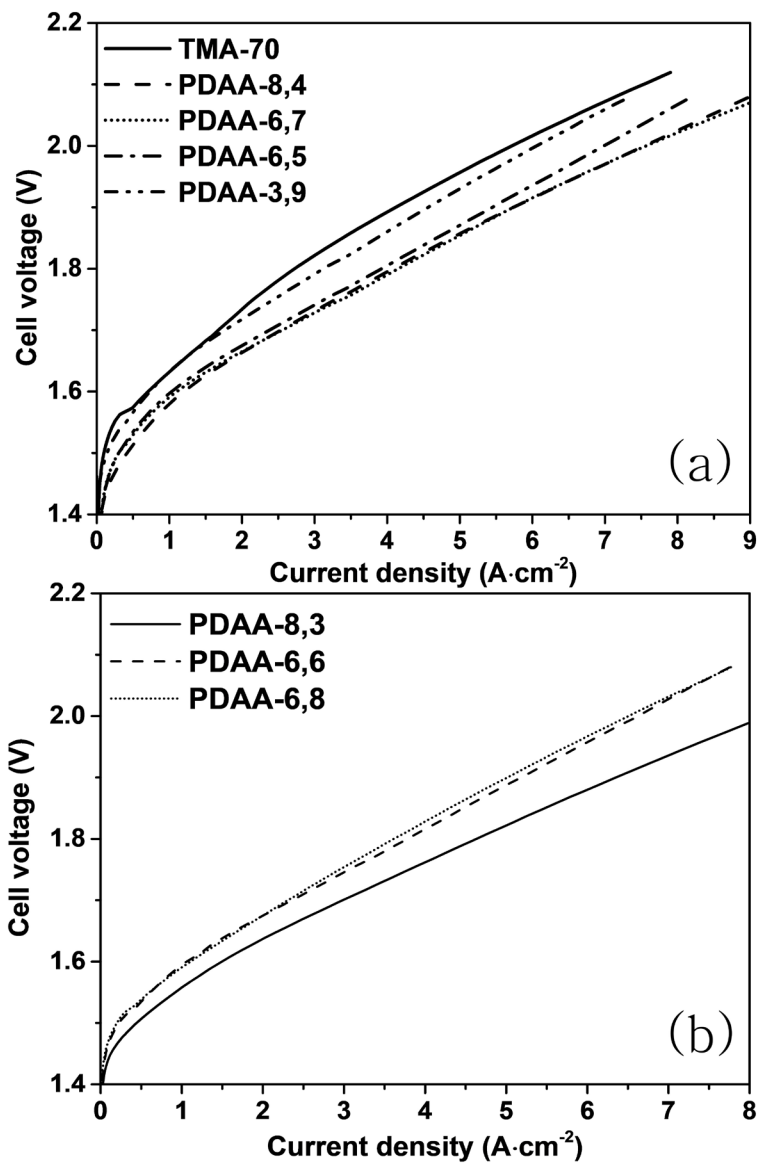
Figure 3-22. LSV curves for PDAA-X,Y

Table 3-5. Current density according to IEC of PDAA-X,Y and TMA-70 at 1.8V and 2.0V

Sample		IEC (mmeq/g)	current density (A/cm^2)	
			@1.8V	@2.0V
TMA-70		3.30	2.72	5.67
P D A A	6,8	3.12	3.60	6.49
	6,7	3.36	4.25	7.69
	6,6	3.53	3.77	6.53
	4,8	3.53	4.19	7.68
	3,9	3.53	3.23	6.18
	5,6	3.71	4.01	7.08
	3,8	3.71	4.62	8.23

Figure 3-23. PDAA-X,Y current density according to IEC

PDAA-xy

1,F9	1,13	1,11	1,10
0˚	138.2˚	151.9˚	129.6˚

1,8	3,9	6,8	4,8
0˚	94.7˚	148.9˚	144.0˚

3,8	6,7	6,6	5,6
155.4˚	143.9˚	140.8˚	128.3˚
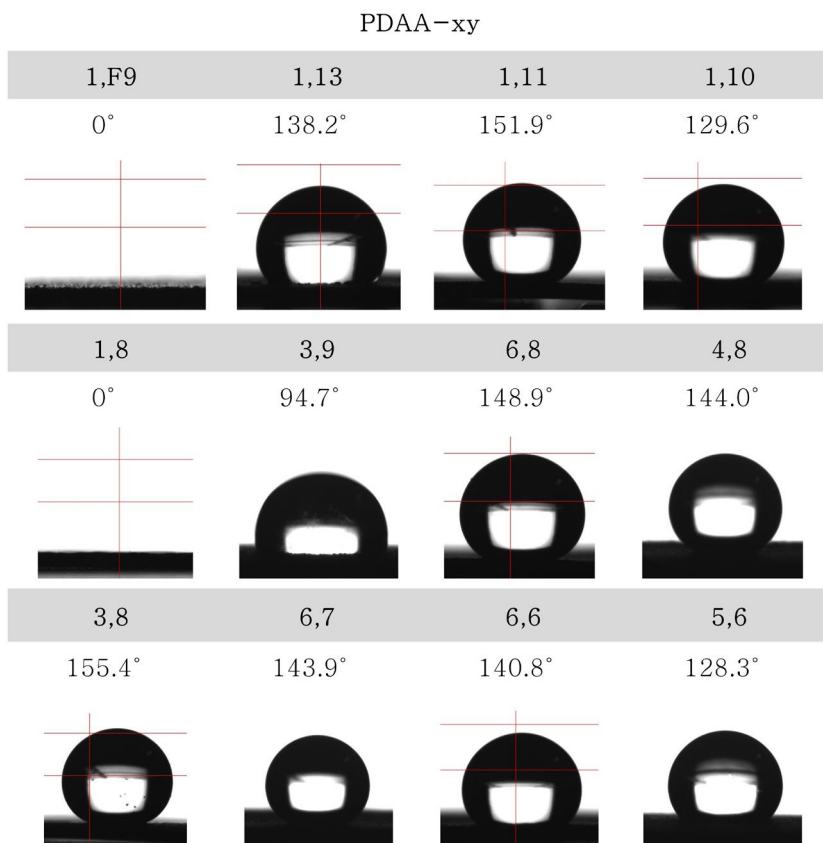
Figure 3-24. Contact angle of PDAA-XY

In order to compare the hydration properties according to the PDAA-X,Y chains, the water contact angles of AEIs and PtRu/C catalyst-coated electrodes were compared. The contact angle was measured immediately after water fell on the electrode surface and time for complete absorption by the electrode was also measured. Figure 3-24 shows the water contact angle of all PDAA-X,Y. PDAA-1,F9 and PDDA-1,8 showed a contact angle of 0˚ due to large hydrophilicity, and PDAA-3,8 showed the largest contact angle of 155.4˚.
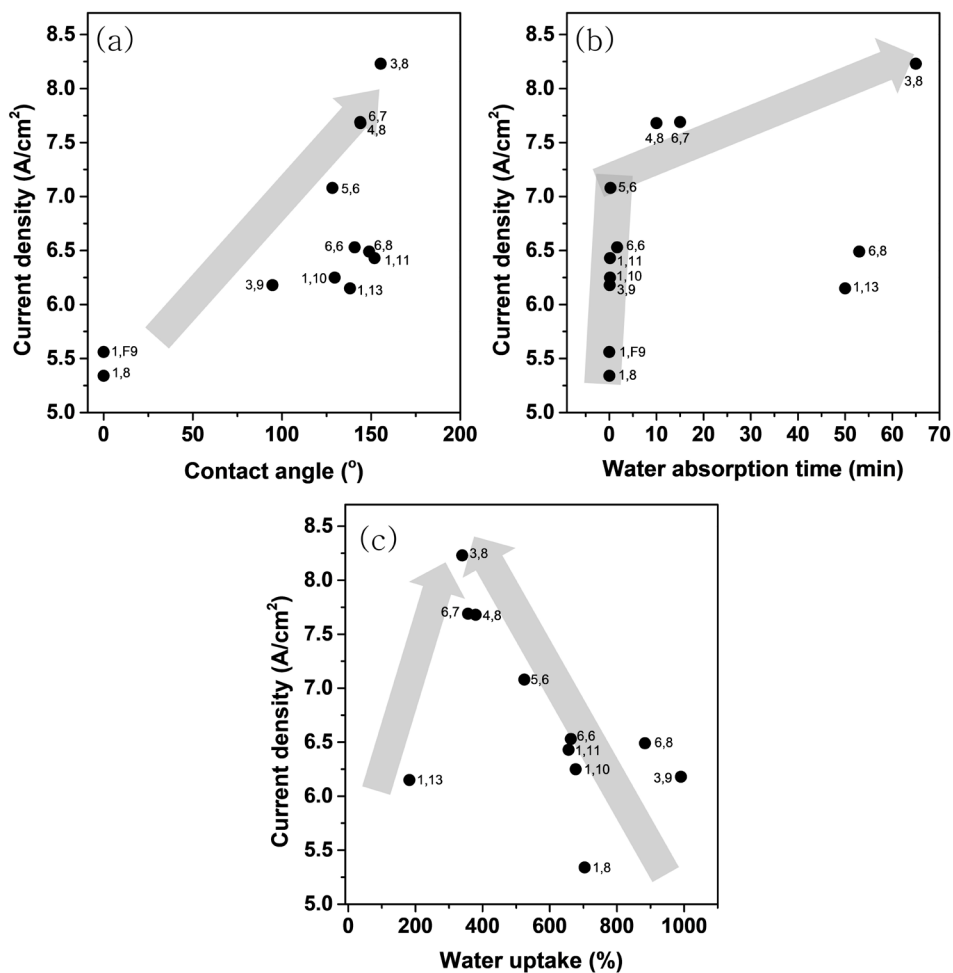
Figure 3-25. (a) Current density according to contact angle (b) current density according to water absorption time (c) current density according to water uptake of PDAA-X,Y

　　　Figure 3-25(a) shows current density according to contact angle. The higher the contact angle of the AEIs-coated HER cathode, the higher the current density. Figure 3-25(b) shows current density according to water absorption time. In general, PDAA-X,Y with a large water contact angle took longer to completely absorb water into the electrode due to its hydrophobic nature. It is believed that the performance increased because the hydrophobic H₂ gas generated from the cathode did not remain on the electrode surface, but met the hydrophobic surface and was

quickly discharged to the outside.

Figure 3-25(c) shows current density according to water uptake of PDDA-X,Y. Interestingly, the current density increased as the water uptake of PDAA-X,Y increased, but the current density decreased when the water uptake exceeded a certain level. PDAA-3,8, PDAA-6,7, and PDAA-4,8, which showed the highest performance, all had water uptake between 300 and 400%, and PDAA-3,8 had a water uptake of 339.5%. Therefore, in addition to IEC, degree of hydrophobicity and water uptake of AEIs are new factors affecting the performance of AEMWEs. In summary, the best performance was obtained when the IEC was 3.3 mmol/g or more, the hydrophobicity was high, and the water uptake was 300 to 400%.

Alkaline stability

In AEMWEs, the alkaline stability of AEIs is a critical factor. The PDAA-X,Y polymer itself was placed in an alkaline environment to analyze how much degradation was caused by ^{1}H-NMR, but the peaks were measured too broadly, making accurate analysis difficult. Therefore, the alkaline stability according to the chain length was compared by ^{1}H-NMR through the synthesis of pyrrolidinium based monomers having pentagonal rings. The synthesis mechanism is shown in Figure 3-26, pyrrolidine and N-methylpyrrolidine were used. Figure 3-27 shows the 1H-NMR spectra for Py-X,Y. The c' peak of Py-1,1, Py-1,3, and Py-1,6 was observed around 3ppm, and as the alkyl groups lengthened, the CH_2 groups present in the middle of the chain was observed at around 1.2~1.35 ppm.
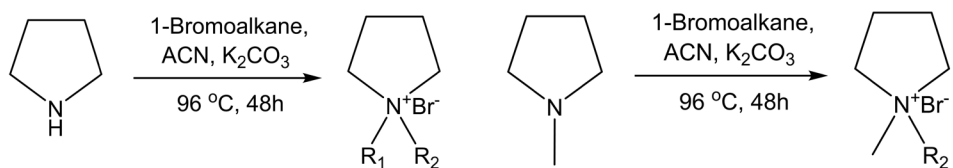
Figure 3-26. Synthesis mechanism of pyrrolidinium based monomers
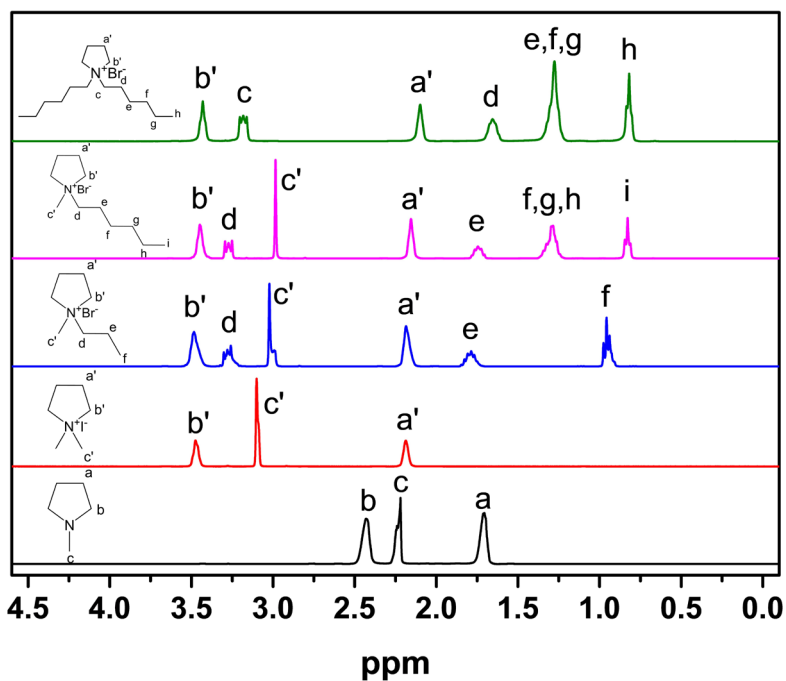
Figure 3-27. ^{1}H-NMR spectra (d-solvent : deuterium oxide) for Py-X,Y
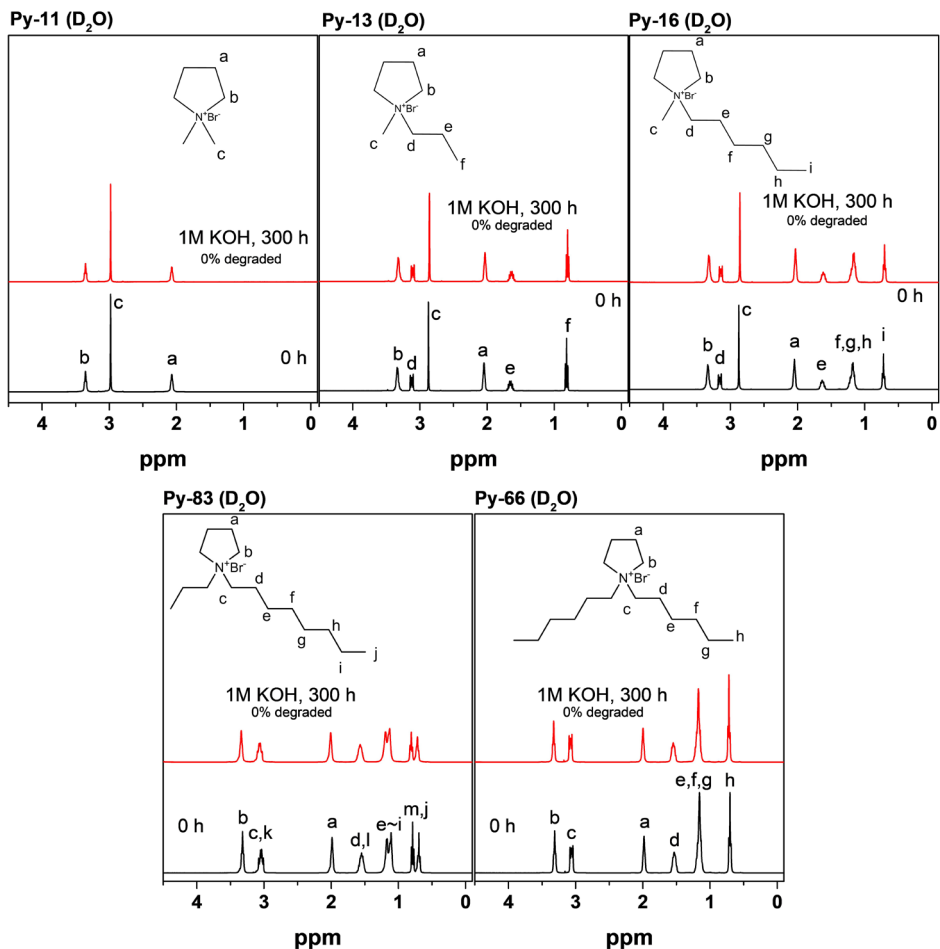
Figure 3-28. ¹H-NMR spectra (d-solvent : deuterium oxide) for Py-X,Y before and after 300 hours treatment in 80℃ alkaline solution

Figure 3-28 shows the ¹H-NMR spectra (d-solvent:deuterium oxide) for Py-X,Y before and after 300 hours treatment in 1M KOH at 80℃. 1M KOH solution at 80℃ is the actual operating temperature of AEMWEs, and degradation did not occur for all Py-X,Y even after 300 hrs. In 5M KOH in D₂O, it was not measured due to the solubility problem of Py-X,Y.

Figure 3-29 shows ^{1}H-NMR (d-solvent: Methanol-d3:D$_2$O=3:1 co-solvent) for Py-X,Y before and after 300 hours treatment in 1M and 5M KOH solution at 80℃. Since methanol dissolves Py-X,Y well while accelerating the hydroxide attack,[17] it was used for the alkaline stability test of Py-X,Y according to the chain length. The degradation degree was determined through the change in integral ratio of ^{1}H-NMR, and the degradation degree of Py-X,Y is summarized in Figure 3-30.
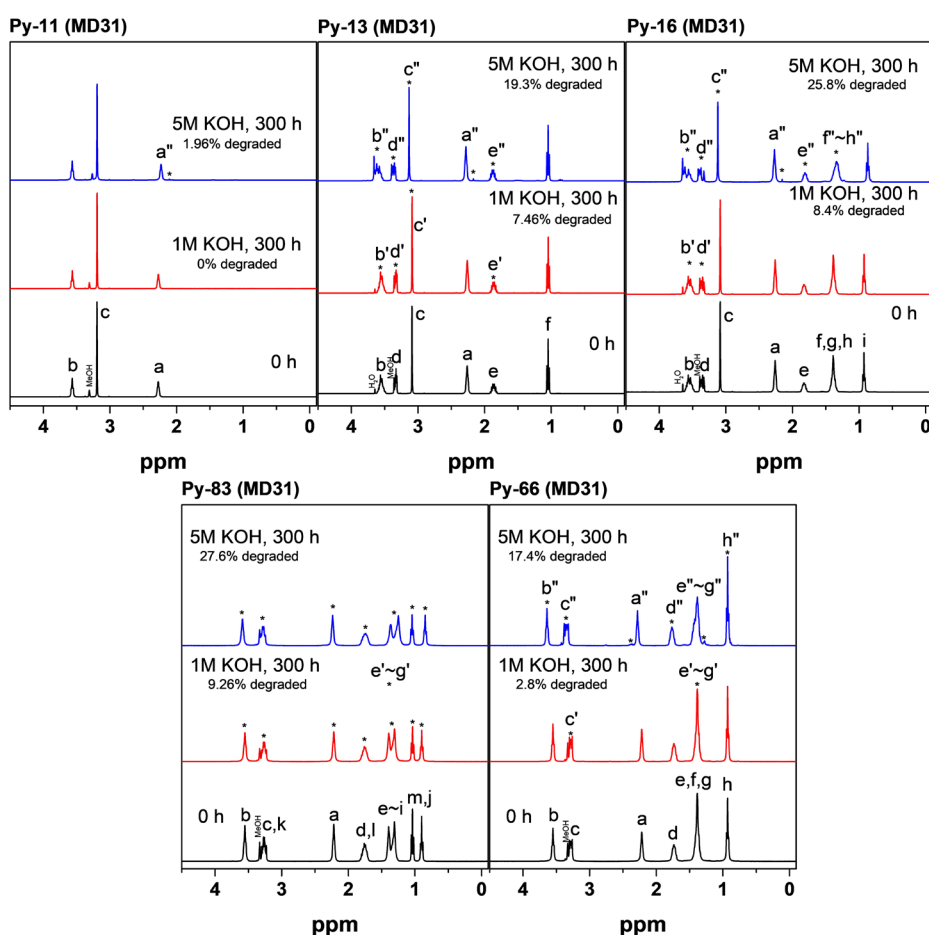
Figure 3-29. ^{1}H-NMR spectra (d-solvent : Methanol-d3 and D$_2$O co-solvent) for Py-X,Y before and after 300 hours treatment in 80℃ alkaline solution
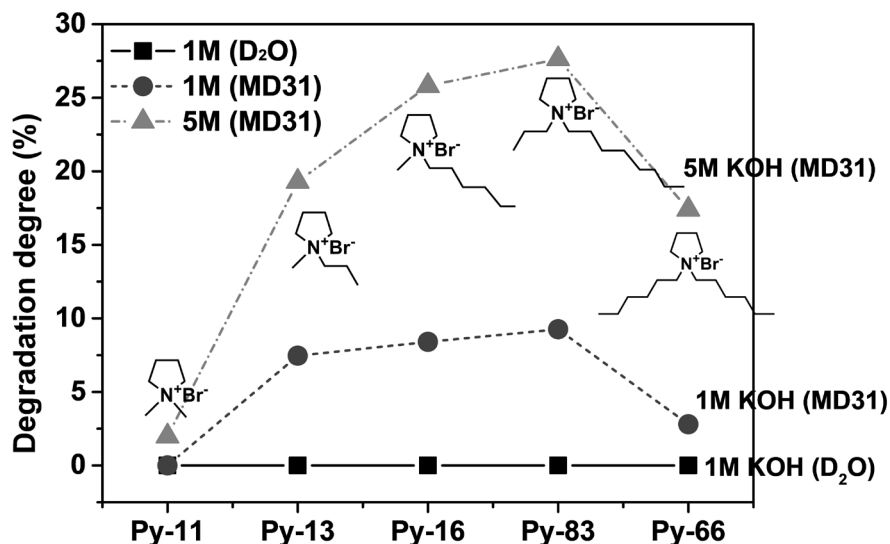
Figure 3-30. Degradation degree of Py-X,Y after 300 hours treatment with 1M KOH or 5M KOH at 80℃

In the case of methanol-d3:D₂O=3:1 co-solvent (MD31), the hydroxide attack was accelerated, so the degradation degree of the Py-X,Y series could be compared. Py-1,1, which has the shortest chain length, showed a degradation degree of 0% even in 1M KOH (MD31), and as the chain length increased, degradation occurred significantly from Py-1,1 to Py-3,8. This is because the number of sites subjected to hydroxide attack increases as the alkyl chain lengthens.[18] However, when the long chains were on both R1 and R2, the degradation degree was rather reduced. This is because the alkaline stability increased because the hydroxide was not easily accessible as the surroundings of the QA groups became bulky.[19-21] Therefore, the alkaline stability of PDAA-X,Y with long chains on both sides is considered to be good. Also, the degree of degradation was greater in 5M KOH solution rich in hydroxide than in 1M KOH solution.

3.3.5 Conclusion

In this study, ionomers with aryl−ether free and ring−type quaternary ammonium groups for AEMWEs were developed. By cyclopolymerization of diallylalkylamine, PDAA−X,Y ionomers with a wide range of IECs were synthesized, and all PDAA−X,Y showed high thermal stability. When applied to AEMWEs, the current density increased as the IEC of PDAA−X,Y increased, but the current density decreased after IEC 3.7 mmol/g. In addition, the greater the hydrophobicity of PDAA−X,Y, the faster the emission of generated H_2 gas and the higher current density was shown because the reaction site was not blocked with H_2 gas. PDAA−3,8, which satisfies all of these conditions, has an excellent current density of 8.23 A/cm^2 at 2.0V, and can be applied as commercial AEIs for AEMWEs in the future.

3.3.6 References

[1] Raja Sulaiman, R. R., Wong, W. Y., & Loh, K. S., **2022**, *International Journal of Energy Research*, *46*(3), 2241−2276.

[2] Cha, M. S., Park, J. E., Kim, S., Han, S. H., Shin, S. H., Yang, S. H., ... & Lee, J. Y., **2020**, *Energy & Environmental Science*, *13*(10), 3633−3645.

[3] Park, E. J., Arges, C. G., Xu, H., & Kim, Y. S., **2022**, *ACS Energy Letters*, *7*(10), 3447−3457.

[4] Leonard, D. P., Lehmann, M., Klein, J. M., Matanovic, I., Fujimoto, C., Saito, T., & Kim, Y. S., **2023**, *Advanced Energy Materials*, *13*(3), 2203488.

[5] Haj−Bsoul, S., Varcoe, J. R., & Dekel, D. R., **2022**, *Journal of Electroanalytical Chemistry*, *908*, 116112.

[6] Kang, S. Y., Park, J. E., Jang, G. Y., Kim, O. H., Kwon, O. J., Cho, Y. H., & Sung, Y. E., **2022**, *International Journal of Hydrogen Energy*, *47*(15), 9115−9126.

[7] Mandal, M., **2021**, *ChemElectroChem*, *8*(1), 36−45.

[8] Cossar, E., Murphy, F., & Baranova, E. A., **2022**, *Journal of Chemical Technology & Biotechnology*, *97*(7), 1611−1624.

[9] Li, D., Matanovic, I., Lee, A. S., Park, E. J., Fujimoto, C., Chung, H. T., & Kim, Y. S., **2019**, *ACS applied materials & interfaces*, *11*(10), 9696−9701.

[10] Ottenbrite, R. M., & Ryan Jr, W. S., **1980**, *Industrial & Engineering Chemistry Product Research and Development*, *19*(4), 528−532.

[11] Li, D., Park, E. J., Zhu, W., Shi, Q., Zhou, Y., Tian, H., ... & Kim, Y. S., **2020**, *Nature Energy*, *5*(5), 378−385.

[12] Sánchez−Delgado, R. A., da Rosa, R. G., & Ocando−Mavarez, E., **1996**, *Journal of Molecular Catalysis A: Chemical*, *108*(3), 125−129.

[13] Corfield, G. C., **1972**, *Chemical Society Reviews*, *1*(4), 523−552.

[14] Umoren, S. A., Solomon, M. M., Ali, S. A., & Dafalla, H. D.,

2019, *Materials Science and Engineering: C*, *100*, 897−914.

[15] Zhang, S., Zhu, X., & Jin, C., **2019**, *Journal of Materials Chemistry A*, *7*(12), 6883−6893.

[16] Tuzun, N. S., Aviyente, V., & Houk, K. N., **2003**, *The Journal of Organic Chemistry*, *68*(16), 6369−6374.

[17] Sun, Z., Pan, J., Guo, J., & Yan, F., **2018**, *Advanced Science*, *5*(8), 1800065.

[18] Sturgeon, M. R., Long, H., Park, A. M., & Pivovar, B. S., **2015**, *ECS Transactions*, *69*(17), 377.

[19] Park, J. S., Park, S. H., Yim, S. D., Yoon, Y. G., Lee, W. Y., & Kim, C. S., **2008**, *Journal of power sources*, *178*(2), 620−626.

[20] Cao, D., Yang, F., Sheng, W., Zhou, Y., Zhou, X., Lu, Y., ... & Li, Y., **2022**, *Journal of Membrane Science*, *641*, 119938.

[21] Shukla, G., & Shahi, V. K., **2018**, *ACS Applied Energy Materials*, *1*(3), 1175−1182.

Chapter 4. Protonated phosphonic acid ionomers and proton exchange membranes for HT-PEMFCs

4.1 Introduction

4.1.1 Protonated phosphonic acid polymer

In LT−PEMFCs, Nafion has been widely used as a PEM.[1−4] Nafion has high conductivity, excellent mechanical strength and chemical stability, but must be hydrated for ionic conductivity.[5],[6] As the humidity decreases, the conductivity of Nafion decreases rapidly.[7],[8] Therefore, the operating temperature of the PEMFC must be below 80 ℃ or high hydration of the membrane must be maintained. In other words, since water management is very important in Nafion−based LT−PEMFCs, LT−PEMFC stacks require proper heat management.[9],[10] To extract the heat, large radiators and heat exchangers are needed. In addition, Pt−based electrocatalysts show low resistance to fuel impurity such as CO at low temperatures.[11]

HT−PEMFC has the advantage of high CO tolerance, enhanced catalytic activity,[12−14] and system simplification.[15−18] HT−PEMFC uses a phosphoric acid−doped PBI (PA−PBI) membrane capable of proton conduction even at high temperatures and also in an anhydrous environment.[19−22] However, PA−PBI loses phosphoric acid during cell operation,[23],[24] which leads to a decrease in conductivity. Also, due to phosphate poisoning of Pt−based catalysts, HT−PEMFC shows a relatively lower power density than that of LT−PEMFC.

PTFE is widely used as a binder in PEMFC.[25] PTFE, which has excellent thermal stability, is hydrophobic and has good ORR kinetics because it has good oxygen solubility and diffusivity in PA.[26] However, since there is no proton conductivity and electron conductivity, as the content of PTFE increases, the reaction

pathway is hindered and the performance decreases. Excessive PA of the PA−PBI membrane crosses over to the catalyst layer, so ion transfer in the catalyst layer is possible to some extent, but poor results are shown in terms of phosphate poisoning of the Pt catalyst and mass transport.[27],[28] Another binder is PA−PBI. Although PA−PBI is capable of proton conduction under anhydrous conditions, the hydrophilicity hinders mass transport properties of PA−PBI. Phosphate poisoning of the Pt catalyst also occurs. Therefore, it is important to find the appropriate level of PA−PBI ionomer's advantages in ion transport and disadvantages such as hydrophilicity.

There have been studies on protonated phosphonic acid ionomers so that PEMFCs can operate in anhydrous conditions above 100 ℃.[29] Protonated phosphonic acid is composed of tetrafluorostyrene phosphonic acid and perfluorosulfonic acid (PFSA) polymer, and the concept is that proton transfer is possible even under anhydrous conditions as protons of PFSA with a low pKa are transferred to PWN. The protonated pentafluorophenylphosphonic acid (PFPA) has a pKa drop from 1.3 to −0.4, resulting in better proton dissociation. According to DFT calculations, the proton transfer from PFSA to PFPA is a spontaneous process with Gibbs free energy of −4.7 kJ/mol, although there is a small kinetic barrier. The functional group with a phosphonate group was prepared by blending PWN70 and Nafion. PWN70 was partially phosphonated, to form an ionomer. In ^{31}P−NMR, as the Nafion content increased, the peaks shifted as protonated phosphonic acid and hydrogen−bonded phosphonic acid were formed. In addition, a big problem with phosphonic acid is that can form anhydride at high temperature which leads to proton conductivity reduction. However, the anhydride of protonated phosphonic acid is not easily formed at 160 ℃ because it requires a large Gibbs energy. The protonated phosphonic acid under anhydrous conditions showed the best conductivity from the lowest temperature to the highest temperature, and also showed the best peak power density and durability in fuel cell performance.

Therefore, ionomers with protonated phosphonic acid has good performance and durability even in a high temperature/anhydrous environment, and humidifiers or radiators are not required, so the whole system can be simplified.

Focusing on previous study, in chapter 4－2, the effect of the dispersing solvent on the microstructure of protonated phosphonic ionomer capable of conducting ions even in anhydrous environment was examined. In chapter 4－3, the development and evaluation of proton exchange membranes containing protonated phosphonic acid are discussed.

4.1.2 References

[1] Budak, Y., & Devrim, Y., **2018**, *Energy Conversion and Management*, *160*, 486−494.

[2] Jannelli, E., Minutillo, M., & Perna, A., **2013**, *Applied Energy*, *108*, 82−91.

[3] Üregen, N., Pehlivanoğlu, K., Özdemir, Y., & Devrim, Y., **2017**, *International Journal of Hydrogen Energy*, *42*(4), 2636−2647.

[4] Özdemir, Y., Üregen, N., & Devrim, Y., **2017**, *International Journal of Hydrogen Energy*, *42*(4), 2648−2657.

[5] Slade, S., Campbell, S. A., Ralph, T. R., & Walsh, F. C., **2002**, *Journal of the Electrochemical Society*, *149*(12), A1556.

[6] Kuwertz, R., Kirstein, C., Turek, T., & Kunz, U., **2016**, *Journal of membrane science*, *500*, 225−235.

[7] Sone, Y., Ekdunge, P., & Simonsson, D., **1996**, *Journal of the Electrochemical Society*, *143*(4), 1254.

[8] Siroma, Z., Kakitsubo, R., Fujiwara, N., Ioroi, T., Yamazaki, S. I., & Yasuda, K., **2009**, *Journal of Power Sources*, *189*(2), 994−998.

[9] Bujlo, P., Cornelius, C., Barron, O., Dyantyi, N., Linkov, V., & Pasupathi, S., **2021**, *International Journal of Hydrogen Energy*, *46*(57), 29478−29487.

[10] Lotrič, A., Sekavčnik, M., & Hočevar, S., **2014**, *Journal of Power Sources*, *270*, 166−182.

[11] Budak, Y., & Devrim, Y., **2018**, *Energy Conversion and Management*, *160*, 486−494.

[12] Hu, Y., Jiang, Y., Jensen, J. O., Cleemann, L. N., & Li, Q., **2018**, *Journal of Power Sources*, *375*, 77−81.

[13] Chandan, A., Hattenberger, M., El−Kharouf, A., Du, S., Dhir, A., Self, V., ... & Bujalski, W., **2013**, *Journal of Power Sources*, *231*, 264−278.

[14] Zhai, Z. Y., Shen, Y. G., Jia, B., & Yin, Y., **2013**, *Advanced Materials Research*, 625, 239−242

[15] Rosli, R. E., Sulong, A. B., Daud, W. R. W., Zulkifley, M. A., Husaini, T., Rosli, M. I., ... & Haque, M. A., **2017**, *International*

Journal of Hydrogen Energy, *42*(14), 9293-9314.

[16] Liu, Y., Lehnert, W., Janßen, H., Samsun, R. C., & Stolten, D., **2016**, *Journal of power sources*, *311*, 91-102.

[17] Jannelli, E., Minutillo, M., & Perna, A., **2013**, *Applied Energy*, *108*, 82-91.

[18] Chandan, A., Hattenberger, M., El-Kharouf, A., Du, S., Dhir, A., Self, V., ... & Bujalski, W., **2013**, *Journal of Power Sources*, *231*, 264-278.

[19] Moradi, M., Moheb, A., Javanbakht, M., & Hooshyari, K., **2016**, *International Journal of Hydrogen Energy*, *41*(4), 2896-2910.

[20] Yang, J., Gao, L., Wang, J., Xu, Y., Liu, C., & He, R., **2017**, *Macromolecular Chemistry and Physics*, *218*(10), 1700009.

[21] Wang, P., Peng, J., Yin, B., Fu, X., Wang, L., Luo, J. L., & Peng, X., **2021**, *Journal of Materials Chemistry A*, *9*(46), 26345-26353.

[22] Li, X., Ma, H., Shen, Y., Hu, W., Jiang, Z., Liu, B., & Guiver, M. D., **2016**, *Journal of Power Sources*, *336*, 391-400.

[23] Lee, A. S., Choe, Y. K., Matanovic, I., & Kim, Y. S., **2019**, *Journal of Materials Chemistry A*, *7*(16), 9867-9876.

[24] Lim, K. H., Matanovic, I., Maurya, S., Kim, Y., De Castro, E. S., Jang, J. H., ... & Kim, Y. S., **2022**, *ACS Energy Letters*, *8*, 529-536.

[25] Kakaee, A. H., Molaeimanesh, G. R., & Garmaroudi, M. E., **2018**, *International Journal of Hydrogen Energy*, *43*(32), 15481-15491.

[26] Pang, H., Tian, K., Li, Y., Su, C., Duan, F., & Xu, Y., **2021**, *Separation and Purification Technology*, *274*, 118186.

[27] Wang, M., Lu, S., Wu, X., Veder, J. P., Johannessen, B., Thomsen, L., ... & Yang, S. Z., **2021**, *Applied Catalysis B: Environmental*, *284*, 119717.

[28] Cheng, Y., Zhang, J., Wu, X., Tang, C., Yang, S. Z., Su, P., ... & Liu, J., **2021**, *Nano Energy*, *80*, 105534.

[29] Lim, K. H., Lee, A. S., Atanasov, V., Kerres, J., Park, E. J., Adhikari, S., ... & Kim, Y. S., **2022**, *Nature Energy*, *7*(3), 248-259.

4.2 Dispersing agents impact performance of protonated ionomers

4.2.1 Introduction

The microstructure of ionomers plays a significant role in the performance of high−temperature polymer electrolyte membrane fuel cells (HT−PEMFCs). Here, we establish direct correlations between the properties of dispersing agents and the microstructure of a protonated phosphonic acid ionomer. Most importantly, the formation of the porous structure of a protonated phosphonic acid ionomer depends on the pKa of the liquid media. Namely, the acid−base interaction between the charged polymer and dispersing agents determines the porosity in the ionomer thin films. The HT−PEMFC performance increases with the level of porosity of the ionomer, as the pores enable fast reactant gas accessibility. This study concludes the importance of the pKa of ionomers' dispersing media for the HT−PEMFC performance.

Solvent−induced phase separation of non−charged polymers has been a crucial subject for the development of functional materials.[1] The most studied area is nonsolvent−induced phase separation for membrane−based separation processes.[2],[3] Another well−studied area is solvent vapor annealing of block copolymers for organic solar cells.[4],[5] For solvent−induced phase separation, the Flory−Huggins model employing solubility parameters correlates to the microstructure of the solution−cast polymers.[6],[7] Dispersing−agentinduced phase separation of charged polymers (ionomers) also plays a critical role in electrochemical devices' performance.8 Unlike solvent−induced phase separation, solubility parameters do not predict the phase separation behaviors[9−11] because most ionomers in liquid media are not a solution but a suspension. As such, the dielectric constant of the dispersing agent, ε, was proposed to describe the microstructure of ionomers[12],[13] but has yet to correlate well with the microstructure of the cast

ionomer films.[14],[15]

In our previous study, protonated phosphonic acid ionomers, made by blending poly(2,3,5,6−tetrafluorostyrene−4−phosphonic acid) (PWN)[16] with perfluorosulfonic acid (PFSA), were developed for high−temperature polymer electrolyte membrane fuel cells (HT−PEMFCs).[17] In the composite ionomers, a highly acidic proton from the PFSA is transferred to the phosphonic acid to enhance proton conduction. The ionomer processed with N−methylpyrrolidone (NMP) enables a high power density (∼800 mW cm^{-2}) of HT−PEMFCs at 160 °C under H_2/air conditions. The high performance with the non−aqueous dispersion caught our attention because most non−aqueous ionomer dispersions produced inferior cell performance compared to aqueous dispersions in the low−temperature PEMFCs.[18],[19] Here, we systematically investigate the dispersing−agent induced phase separation of the ionomer to understand the effect of dispersing agents on fuel cell performance. We first examine the phase separation behaviors of the ionomers cast from seven dispersing agents. Next, we discuss correlation parameters of the dispersing agents responsible for the phase separation and other physical properties of the cast films. Finally, we demonstrate the fuel cell performance of membrane electrode assemblies (MEAs) made from the dispersing agents and discuss the effects of dispersing agents.

4.2.2 Experimental

Materials
All solvents were used as received from J.T. Baker. Commercial 75% PtRu on high−surface−area carbon (HiSPEC 12100) and 60% Pt on high−surface−area carbon (Pajarito Powder) catalysts were obtained from Alfa Aesar and Pajarito Powder, respectively. Nafion membrane (Nafion NR−211, 25.4 μm thickness) and Nafion D2020 dispersion were purchased from Ion Power. Gas diffusion layer (W1S1009) was purchased from CeTech.

Synthesis of PWN

Polypentafluorostyrene, PFS (100 g, 515 mmol monomer units, Mw = 200 kDa, PDI = 3.4) was dispersed in dimethylacetamide, DMAc, (400 ml) at 140 $^{\circ}$C for 1 h. Tris(trimethylsilsyl)phosphite, TMSP (200 g, 670 mmol) was added and the reaction mixture was then heated to 160 $^{\circ}$C for 18 hrs. After the reaction was completed, the warm mixture was precipitated in 2 L water and collected via filtration. The resulting white powder was refluxed in water three times for 30 min each, exchanging water each time, followed by boiling in a 2 wt.% phosphoric acid solution. Washing with water until neutral and drying at 140 $^{\circ}$C under vacuum for 18 hrs, yielded the phosphonated polymer with 66% degree of phosphonation, PWN66 (Yield: 138g, 99%).

Preparation of dispersions

Nafion D2020 was diluted with isopropyl alcohol to 5 wt%. Nafion 211 films were converted to Na+ form by submerging them in boiling 1 wt% NaOH aqueous solution for 90 min. After washing copiously in deionized water, the Na^{+} form Nafion films were ripped into small pieces and directly dispersed at 5 wt% in DMSO, NMP, or EG at 100 $^{\circ}$C, 86 $^{\circ}$C, or 153 $^{\circ}$C, respectively and at 1 wt% in DMAc, DMF or NMF at 100 $^{\circ}$C, 100 $^{\circ}$C, or 110 $^{\circ}$C, respectively. For PWN dispersions, 5 wt% dispersions in DMSO, NMP, and EG and 1 wt% dispersions in DMAc, DMF, and NMF were prepared at 100 $^{\circ}$C. For the PWN, 1:1 Water/NPA dispersion, a pressurized reactor was used to prevent premature solvent evaporation and the dispersion temperature was 150 $^{\circ}$C.

Film sample preparation

Co-dispersions of PWN and Nafion was solvated at a 1:1 weight ratio at room temperature through magnetic stirring and mild sonication. The transparent co-dispersions were poured on a Teflon dish mold, and solvent evaporated at 80 $^{\circ}$C under high vacuum overnight. After confirmation of solvent evaporation, the

films were submerged in deionized water to delaminate them from the Teflon mold. Re-drying the membranes at 40 $^{\circ}$C gave free standing Nafion:PWN blend films. Because of a difficulty to detach the DMF- and DMAc-processed membranes from the Teflon dish mold, we added 20 % of water in the dispersion for free-standing DMF- and DMAc-cast ionomers. There was little difference in phase separation and mechanical property between the samples from the water inclusion. All of the fabricated blend membranes had film thickness of 40 μm ± 2 μm.

UV-vis

For the UV-vis measurement sample, dispersions of PWN and Nafion were drop-cast so that 5 mg of PWN and Nafion were placed on a glass plate with an area of 1.3 cm * 2 cm and the solvent was evaporated at 80 $^{\circ}$C. UV-vis measurement was conducted on a V-670 (JASCO INC., USA).

Microscopy

For microscopy experiments, 5 wt% dispersions of PWN-1.8 and Nafion were co-solvated at a 1:1 weight ratio at room temperature through magnetic stirring and mild sonication. The consequent co-dispersions were drop-casted onto either SEM or TEM grid and evaporated at 80 $^{\circ}$C over a period of 2 hours. SEM images were obtained on an Inspect F50 (FEI, Korea) instrument. TEM analyses were conducted on a Tecnai F20 G2 (FEI, Korea) instrument. In addition, EDX analysis was performed in STEM mode to confirm the dispersion of PWN and Nafion in the film.

Water or phosphoric acid uptake

Water or phosphoric uptake of ionomer films casted from different dispersing agents was measured by immersing the dried films in DI water for 3 h or in 85 % phosphoric acid for 5 h at room temperature. For phosphoric acid uptake, the phosphoric acid-doped films were dried at 60 $^{\circ}$C overnight to remove the water inside. The water or phosphoric acid uptake was calculated based

on the weight difference of each ionomer film.

Proton conductivity

The films casted from different solvents were immersed into 85% phosphoric acid solution for 48 h. Films were flipped after 24 h to wet the atmosphere facing surface with phosphoric acid. After phosphoric acid doping, films were cut into rectangle shape (1.5-inch*0.5-inch) and placed between two platinum-coated stainless-steel electrodes followed by clamping in PTFE window cell. The windows cell was put into oven at 120 ^{o}C for 30 min. The in-plane proton conductivity was measured between 180 ^{o}C to 80 ^{o}C by AC impedance spectroscopy in the frequency interval of $10^{-1} < f < 10^{5}$ Hz (Solartron 1260 gain phase analyzer).

Mechanical properties

The mechanical properties of films were analyzed in terms of stress-strain behavior using dynamic mechanical analyzer (TA instruments, Q800 DMA). The water saturated rectangular films were loaded in the testing chamber with preload force of 0.02 N to prevent any film slack. The tests were performed at ramp stress of 1 MPa min^{-1}.

MEA preparation

Electrodes were prepared in a gas diffusion electrode (GDE) type by hand painting the catalyst ink on the CeTech GDL (W1S1009). Catalyst ink consists of 1.5 wt.% PtRu/C catalyst or Pt/C catalyst for anode or cathode, 5.0 wt.% phosphonated ionomer and Nafion ionomer dispersion (5 wt.% in each dispersing agent, DMSO, NMP, EG, Water/NPA, DMF/water, NMF or DMAc) with 1:1 wt. ratio, and 93.5 wt.% additional dispersing agent for well-dispersed catalyst ink. The catalyst ink was sonicated in ultrasonic bath for an hour and then painted onto the GDL which was set on a vacuum hotplate (80 ^{o}C). After painting the catalyst ink, the GDE was left on the vacuum plate for another 10 min to remove all the residual dispersing agent inside. For clarifying the residual dispersing agent

effect with NMP, further NMP−removed GDEs were also prepared by additional rinsing with 0.5 M H_2SO_4 (60 °C for 1 h) or extended drying at higher temperature in vacuum oven (100 °C for 5 h). The target catalyst loadings of anode and cathode were 0.5 mg_{Pt} cm^{-2} and 0.8 mg_{Pt} cm^{-2}, respectively, and the loading was confirmed with X−ray fluorescence (XRF) spectroscopy. For HT−PEMFC membrane, DAPP−HTMA (38−45 μm thickness) was doped with phosphoric acid (PA, 85%) for 25 h at room temperature. The PA−doped DAPP−HTMA membrane was sandwiched with prepared anode and cathode after blotting the excess PA on its surface.

Fuel cell testing

HT−PEMFC performance was measured with a fuel cell station (Fuel Cell Technologies), after break−in the cell under constant voltage condition (from 0.7 to 0.4 V). Polarization curves and HFRs of each MEAs were recorded at a cell temperature of 160 °C and 10 psig back pressure under H_2/air atmosphere with 500/500 sccm flow rate, and no external humidification was applied during the tests. Accelerated stability test (AST) was also conducted by leaving the single cell under humidified N_2/N_2 gas with RH 50% and 500/500 sccm flowrate for 2 h. Before measuring the performance after 2 h of humidification, the cell was dried with dry H_2/O_2 gas for about an hour at constant voltage 0.6 V until the current density and HFR got stabilized. Electrochemical impedance spectroscopy was also conducted using Biologic SP−200. The spectra were recorded by sweeping frequencies from 1 MHz to 0.1 Hz at a voltage of 0.8 and 0.6 V and constant current density of 1.2 A cm^{-2}. The recorded experimental spectra were fitted to equivalent circuits including Ohmic resistance (R_{Ohm}) in series with two parallel constant phase elements, CPE_{ct}/R_{ct} for charge transfer resistance and CPE_{mt}/R_{mt} for mass transport resistance.

4.2.3 Results and discussion
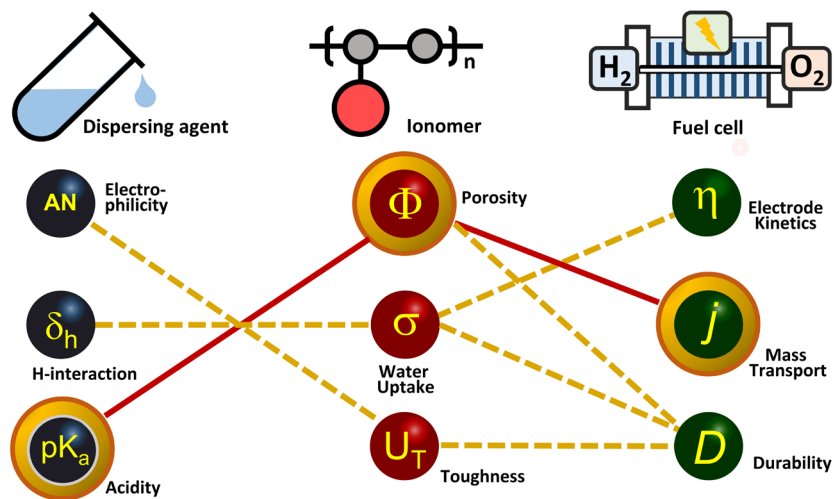
Figure 4-1. Relationship between the parameters of dispersing agents, the properties of the cast ionomers and fuel cell performance.

The dispersing-agent induced phase separation of the ionomer was investigated to understand the effect of dispersing agents on fuel cell performance. First, the phase separation behaviors of the ionomers cast were examined from seven dispersing agents. Next, correlation parameters of the dispersing agents responsible for the phase separation and other physical properties of the cast films were discussed. Finally, the fuel cell performance of MEAs mad from the dispersing agents was demonstrated and the effects of dispersing agents were discussed. Figure 4-1 shows the relationship between the parameters of dispersing agents, the properties of the cast ionomers and fuel cell performance.

Figure 4-2 shows the transmission electron microscopy (TEM), scanning transmission electron microscopy (STEM), and energy-dispersive X-ray (EDX) images of the dispersion cast Nafion and PWN. The two individual films do not show phase-separated morphology at low magnification (scale bar=500 nm). The STEM-EDX images show that the sulfur and phosphorus

elements are uniformly distributed in Nafion and PWN, respectively. High-magnification images (scale bar=20nm) show that the Nafion thin film has phase separation. The average domain size of the hydrophilic regions is 4 nm, in good agreement with other reports.[20],[21] No phase separation was observed for PWN from the high-magnification images.
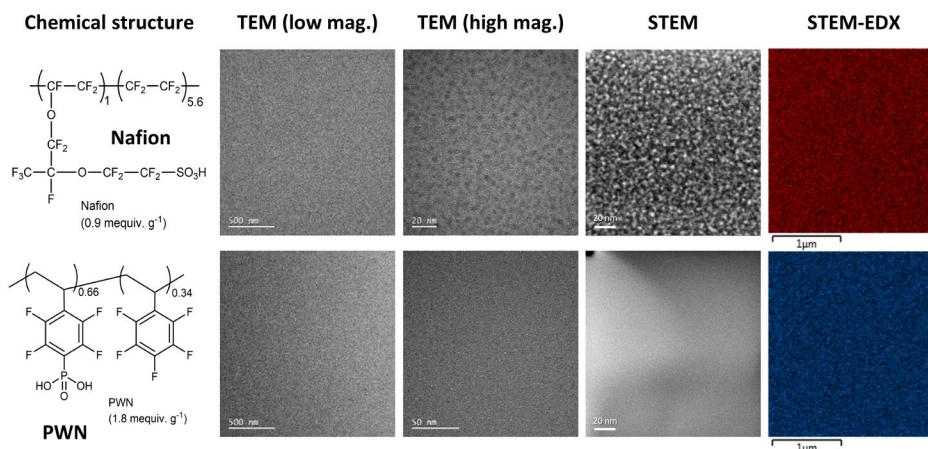
Figure 4-2. Chemical structure, microstructure and elemental analysis of dispersion-cast Nafion and PWN thin films. Nafion was cast at 80 °C from 5 wt% Water/NPA(1:1) dispersion at 80 °C. PWN was cast at 80 °C from 4 wt% DMSO. STEM-EDX: Sulfur: red; Phosphorus: blue.

Figure 4-3 shows the scanning electron microscopy (SEM) and STEM images of the protonated phosphonic acid ionomers cast from dimethyl sulfoxide (DMSO), water/1-propanol (water/NPA), ethylene glycol (EG), N-methyl formamide (NMF), dimethylformamide (DMF), dimethylacetamide (DMAc), and NMP and the average pore size and distribution.
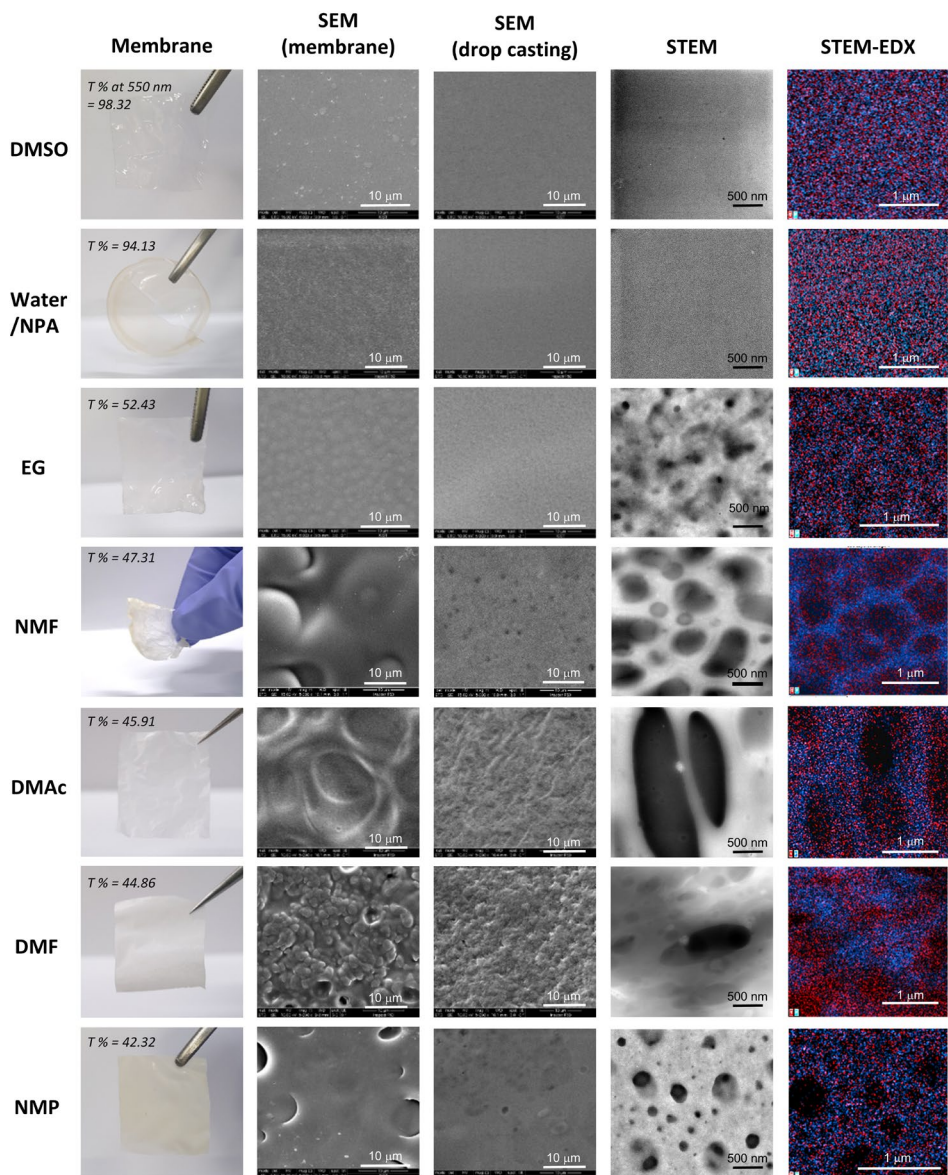
Figure 4‑3. Microstructure and elemental analysis of dispersion‑cast protonated phosphonic acid films (Naion:PWN weight ratio = 1:1). Visible transmittance (T %) at 550 nm was shown. STEM‑EDX: Sulfur: red; Phosphorus: blue.
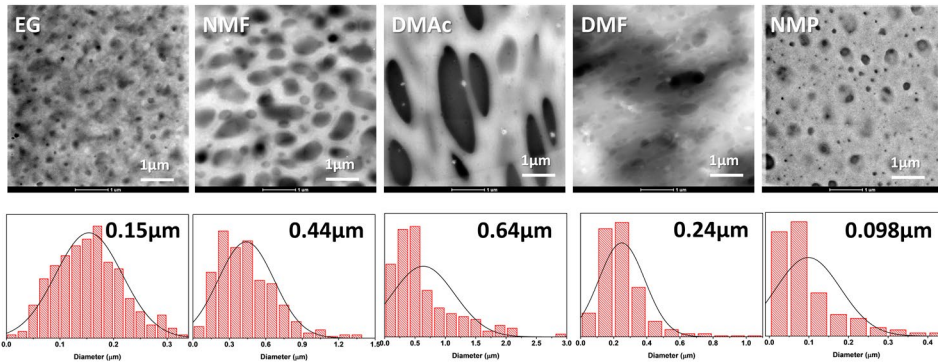
Figure 4-4. Pore size distribution of dispersion-cast protonated phosphonic acid films

Low-magnification STEM images are shown in Figure 4-4. As shown in Figure 4-5, the transparency of the cast membranes drastically changes, depending on the dispersing agents, as the visible transmittance of the membranes at 550 nm decreases in the order of DMSO > water/NPA > EG > NMF > DMAc > DMF > NMP.
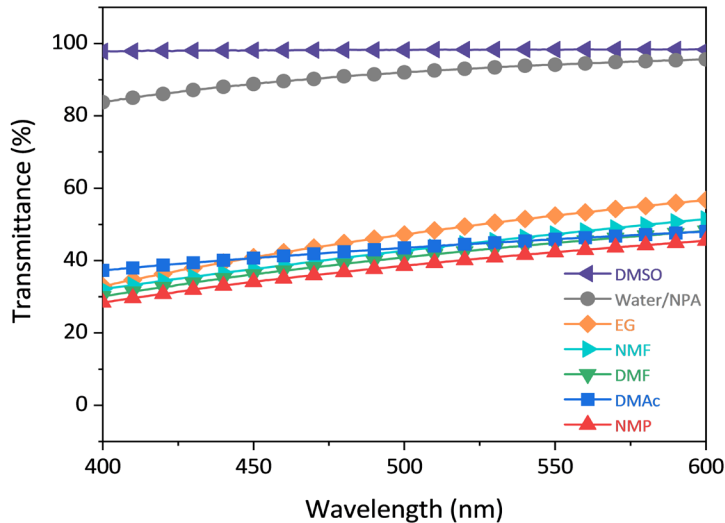
Figure 4-5. Uv-vis spectra of the dispersing cast films.

Table 4-1. Survey of Chemical Parameters for Dispersing Agents
That Correlate with Transmittance of Dispersion-Cast Films

Dispersing agent	T % @550 nm	Solubility parameter, δ (MPa$^{1/2}$)	Surface tension, σ (mN/m)	Dielectric constant, ε	pK$_a$, (protonated form)
DMSO	98.32	26.4	43.5	46.7	-2.48
Water	94.13	48.0	72.8	80.1	-0.7
EG	52.43	34.9	26.0	37.0	NA [a]
NMF	47.31	30.0	40.7	167.8	-0.3
DMAc	45.91	22.8	36.7	37.8	-0.19
DMF	44.86	24.7	37.0	36.7	-0.19
NMP	42.32	23.1	41.3	32.2	-0.17

[a] NA: Not available.

Table 4-1 lists the parameters of dispersing agents that may
correlate with the porous structure of the cast thin films. We found
no correlation between the visible transmittance of the membranes
and the solubility parameter, surface tension, or dielectric constant.
The lack of correlation with the solubility parameter and surface
tension is due to the distinctive transparency of the DMSO-cast
film, which has a solubility parameter (26.4 MPa$^{1/2}$) and surface
tension (43.5 mN m^{-1}) similar to those of other aprotic dispersing
agents. The correlation with dielectric constant is not any better,
because the NMF-cast film, with a significantly higher dielectric
constant, exhibits visible transmittance similar to those of cast films
from other dispersing agents. Other parameters of the dispersing
agents, such as the acceptor number,[28] Dimroth-Reichardt
parameters, dipole moment, Hansen Hbond parameter, and viscosity,
were not correlated well, either (Table 4-2).
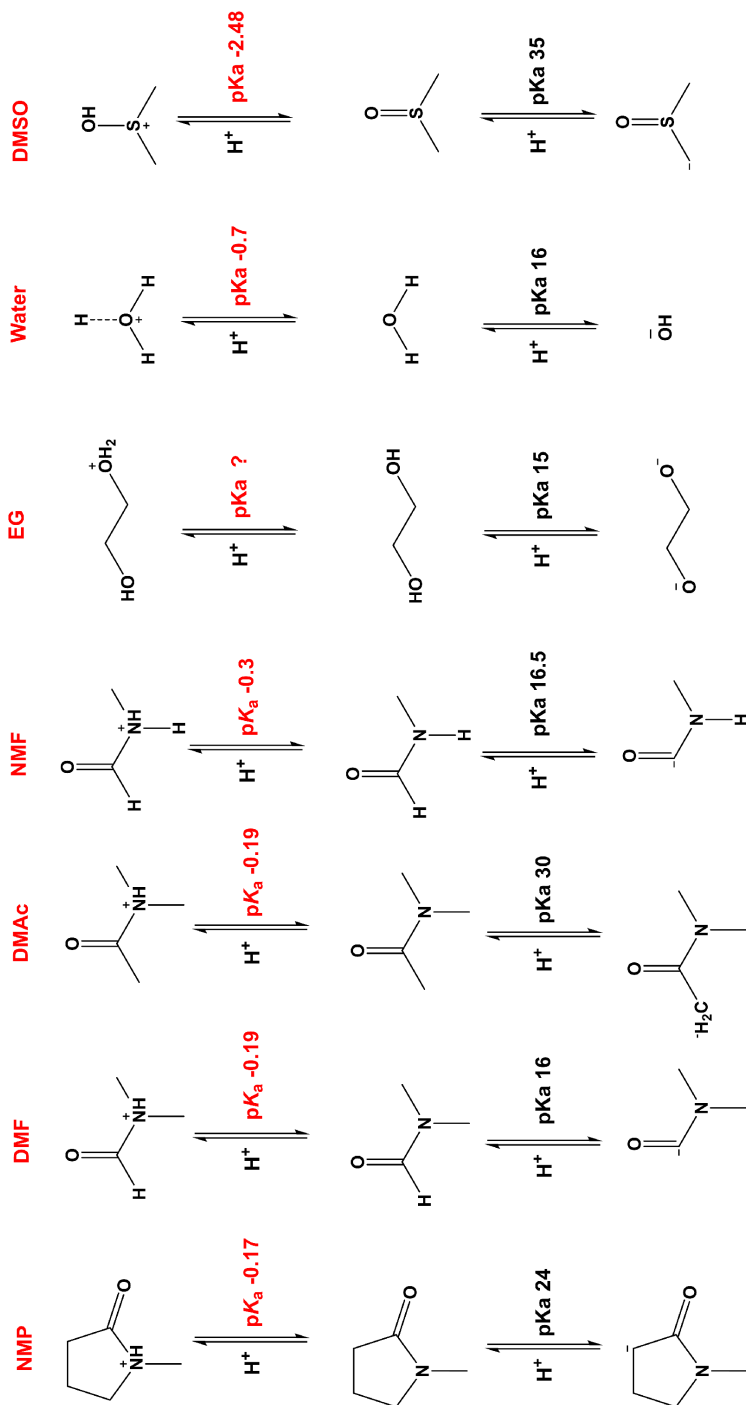
Figure 4-6. pKa of dispersing agents

The best parameter that correlates with the visible transmittance is the pKa of the dispersing agent (Table 4-1). In the mixture of PFSA and PWN in a dispersing agent, PFSA, being a super-acid (pKa ≈ -6), transfers its protons to the dispersing agent. Comparing these values with the pKa of PWN (pKa = 1.3),[16] the proton dissociation of PWN is suppressed, and PWN is, to a larger extent, in non-dissociated form. The lower pKa of DMSO (Figure S5) together with the high polymer concentrations will push the protons back to the polymer acids, thus keeping them to a more non-dissociated state, resulting in less-porous films.

Physical properties of the cast films relevant to fuel cell performance was evaluated. The water uptake of the cast films depends on the dispersing agents (Figure 4-7(a)), with the water/NPA-processed film exhibiting the highest water uptake (1250%), followed by the EG-processed film (444%). The membranes from aprotic dispersing agents had relatively low water uptake, ranging from 113 to 155%, correlating well with the Hansen H-bond parameter. The good correlation between membranes' water uptake and H-bonding interaction of the dispersing agents is because the H-bonding interaction can create segregated groups while suppressing polymer backbone entanglement. The segregate acid groups create hydrophilic domains with high phase contrast and more water uptake. Note that the dielectric constant fails to predict the water uptake of the dispersion cast films, as the NMF-cast film (ε =167.8) showed moderate swelling (235%). This result suggests that the aggregation of acid groups is driven primarily by the H-bonding interaction, not by the ion-pair interactions between the charged molecules.
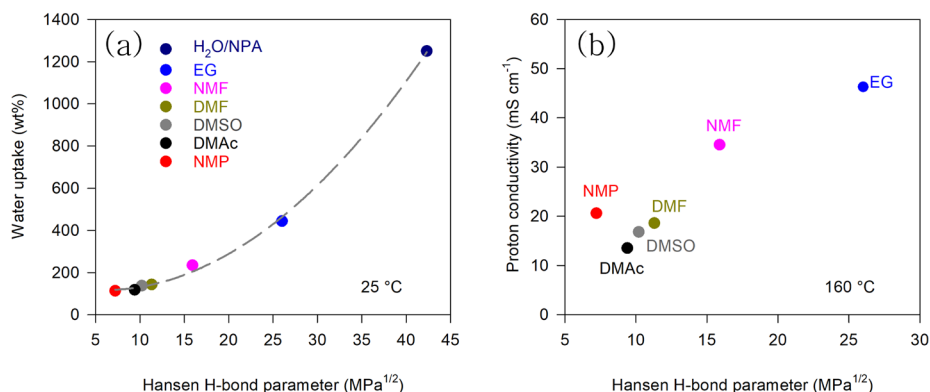
Figure 4-7. (a)Correlation between water uptake of the cast films and Hansen H-bond parameter. (b)Correlation between proton conductivity of phosphoric acid doped films and Hansen H-bond parameter

     Next, the proton conductivity of the dispersion cast ionomers was examined. The proton conductivity of the phosphoric acid-doped membranes was measured at 160°C under anhydrous phosphoric acid-doped membranes to mimic the fuel cell operating environments, in which redistributed phosphoric acid is present. The proton conductivity of the films increased with temperature (Figure 4-8). The dispersion-cast ionomers with high Hansen H-bond parameters (EG and NMF) exhibited a relatively higher conductivity (Figure 4-7(b)). A general trend was found that the proton conductivity increases with the hydrogen-bonding interactions of the dispersing agent, probably due to the higher phosphoric acid adsorption of the dispersing agents, having higher H-bonding interactions (Table 4-2).

Table 4-2. Correlation between the PA uptake of dispersion cast films and H-bond interaction of the dispersing agents.

Dispersing agent	H-bond parameter $(Mpa^{1/2})$	PA uptake (%)
EG	26	468.3
DMAc	10.2	109.7
NMP	7.2	107.1

148
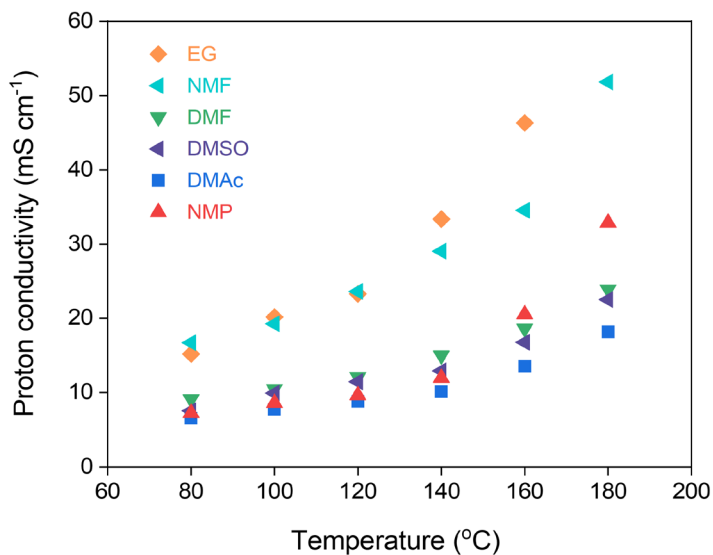
Figure 4-8. Proton conductivity of the phosphoric acid-doped protonated ionomer films as a function of temperature under anhydrous conditions.

The mechanical properties of the cast films were also investigated after soaking them in water. The membrane from DMSO, DMAc, and NMP showed the highest mechanical properties (Figure 4-9). The EG-cast film exhibited a lower mechanical strength but a higher elongation at the break due to the high water uptake. The DMF-cast film showed a trend opposite to that of the EG-cast membrane, i.e., higher mechanical strength but lower elongation at the break. The mechanical properties of water/NPA- and NMF-processed ionomers were the lowest. The poor mechanical properties of water/NPA- and NMF processed films are due to a low degree of polymer chain entanglement by strong repulsion between dispersed particles.[29] However, it should be noted that the porosity and water uptake of the cast films also affect the mechanical properties and that all solvents were fully dried (Figure 4-10). Consequently, no single parameter of the dispersing agents correlates with the mechanical properties of the cast films.
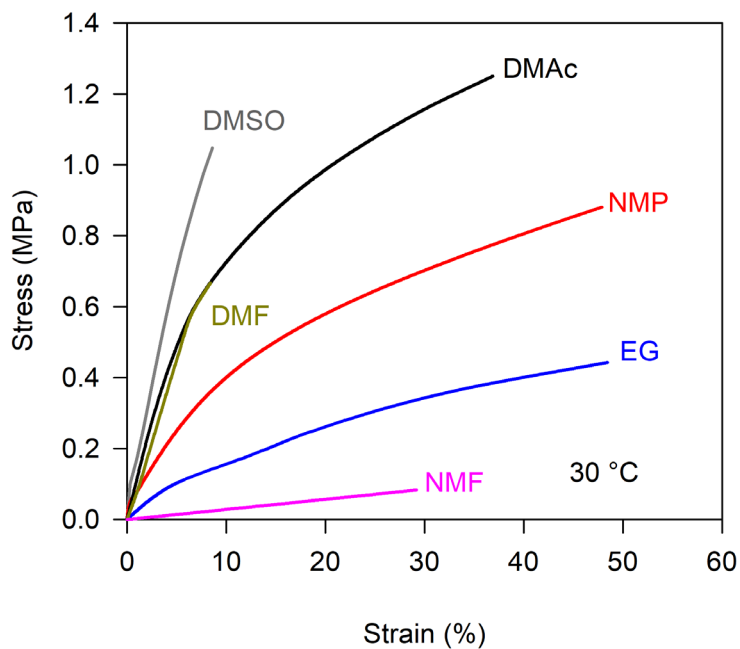
Figure 4-9. Stress-strain curves of the dispersion-cast films.
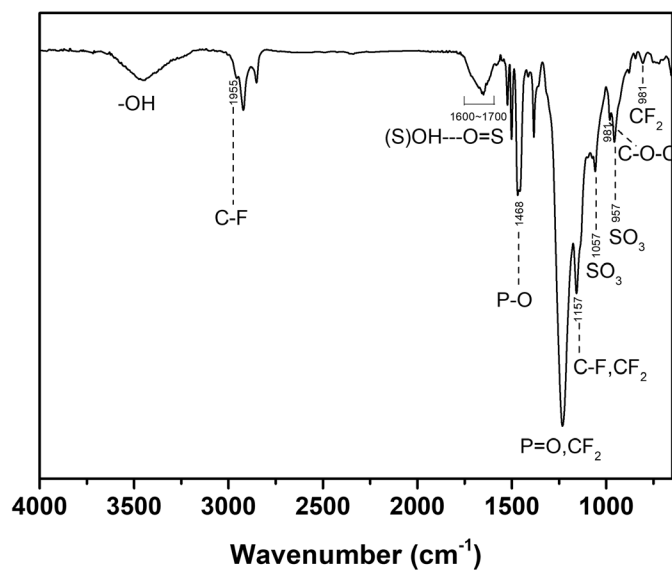
Figure 4-10. FT-IR spectrum of protonated phosphonic acid ionomer cast from NMP

Figure 4-11 (a),(b) compares the performance of HT-PEMFCs with the protonated phosphonated ionomer. The cell performance varied drastically, depending on the porous structure of the ionomer. The MEAs processed by NMP, DMAc, and DMF (high level of pores) exhibited the highest peak power density (PPD) (~700 mW cm^{-2}), while the MEAs processed by DMSO and water/NPA (no pores) showed the lowest PPD (~540 mW cm^{-2}). The MEAs processed by EG and NMF showed an intermediate PPD (~600 mW cm^{-2}). Figure 4-11(c) shows that the PPDs of the fuel cells are inversely proportional to the visible transmittance. Figure 4-11 (d),(e) shows the Nyquist plot and electrochemical impedance spectroscopy analysis (EIS) of the MEAs, respectively. The ohmic resistance (Rohm) for all MEAs was similar, indicating no substantial difference in the phosphoric acid content among all tested membranes. The charge transport resistance (Rct) of the water/NPA- and NMF processed MEA was high, suggesting that the electrode may not have an optimal three-phase interface. The mass transport resistance (Rmt) of the MEAs processed by NMP, DMAc, and DMF was low (0.11 Ω cm^2) compared to that of the MEAs processed by DMSO and water/NPA (>0.17 Ω cm^2). This result confirms that the porous structure of the ionomer thin film helps reactant gas accessibility to improve overall fuel cell performance. The proton conductivity difference of the dispersion-cast thin film has negligible impact, probably because the redistributed phosphoric acid provides enough conductivity. Also, ionomer thin films with higher phosphoric acid doping levels have a higher level of phosphoric acid poisoning,[30] which compensates for the higher performance by high conductivity.
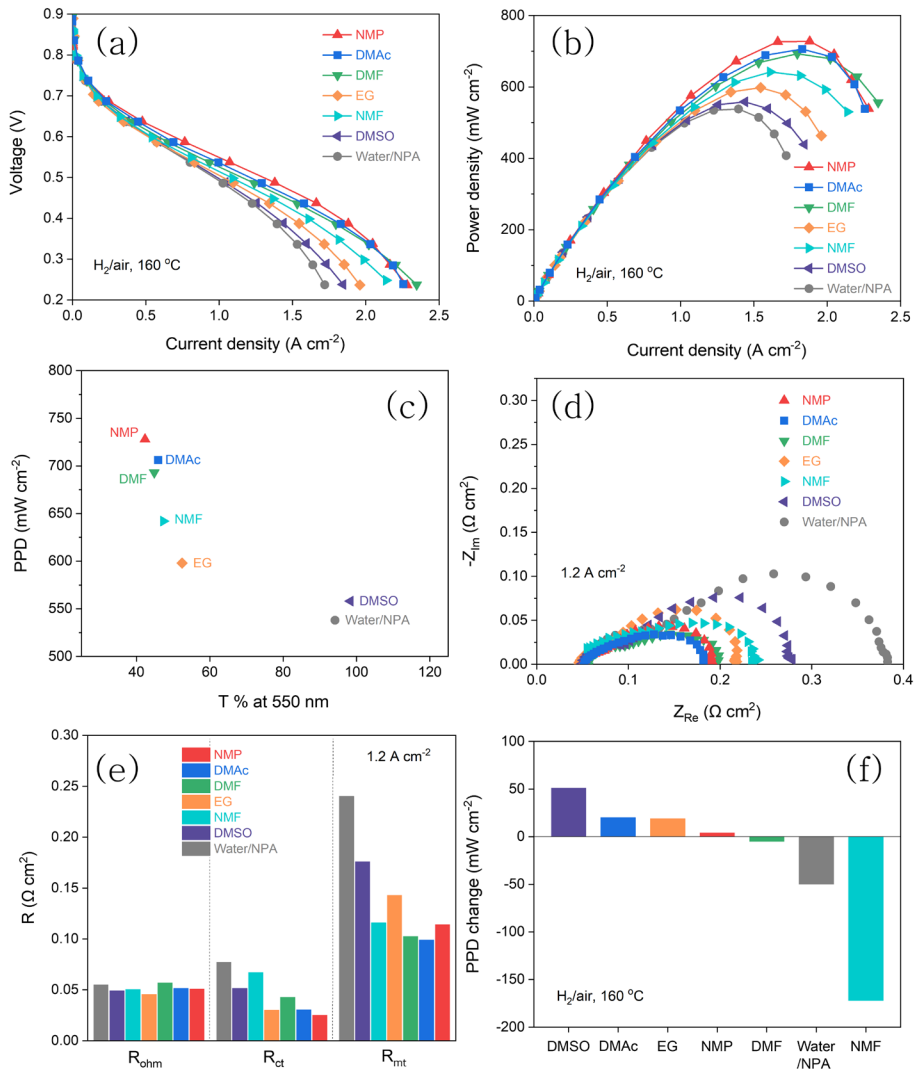
Figure 4-11. (a) Polarization curves and (b) power densities of MEAs processed from different dispersing agents. membrane, PA-doped quaternized poly(phenylene); anode/cathode ionomer, protonated phosphonic acid; anode, PtRu/C (0.6 mg$_{Pt}$ cm^{-2}); cathode, Pt/C (0.9 mg$_{Pt}$ cm^{-2}); humidification,0%; back-pressure,148kPa; anode/cathode flow rate, 500/500 sccm. (c) Correlation between PPD and ionomers' transmittance. (d) EIS of the electrodes at 1.2 A cm^{-2}. (e) EIS analysis of fuel cell electrodes processed by the dispersing agents. (f) PPD change of HT-PEMFCs after 2 h of operation at 0.2 A cm^{-2} under water vapor pressure = 48kPa$_{abs}$.
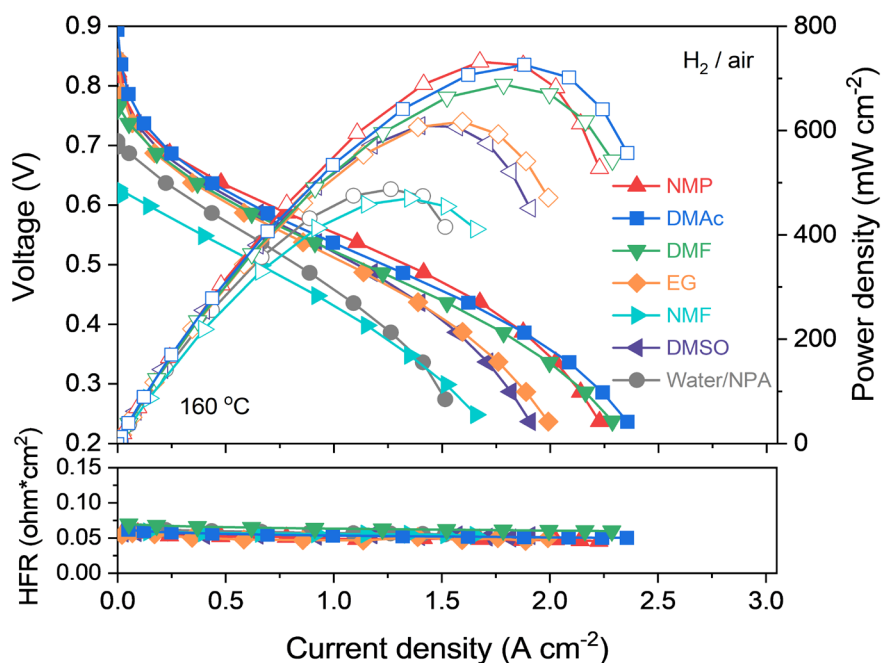
Figure 4-12. Polarization curves and high frequency resistance (HFR) of the MEAs after the AST test. The AST condition: left the single cell under humidified N_2/N_2 gas with water vapor pressure of 47 kPa for two hours.

Table 4-3. OCV of the MEAs before and after AST

Dispersing agent	OCV (V)		
	H_2/O_2	H_2/air	
	Before AST	Before AST	After AST
DMSO	0.95	0.86	0.84
Water/NPA	0.94	0.86	0.71
EG	0.96	0.92	0.86
NMF	0.92	0.86	0.64
DMAc	0.95	0.90	0.89
DMF	0.95	0.89	0.76
NMP	0.93	0.85	0.84

The durability of the HT−PEMFCs was evaluated by an accelerated stress test (AST) under partially humidified conditions (P_{H2O} = 47 kPa) (Figure 4−12). MEAs processed from DMSO, DMAc, EG, and NMP exhibit improved performance after the 2 h of AST due to the proper phosphoric acid redistribution,[31] while, by contrast, the fuel cell performance of the MEAs processed by DMF, water/NPA, and NMF decreased. Figure 4−11(f) summarizes the PPD change after the AST. The PPD changes follow the mechanical robustness of the ionomer, consistent with the previous observation that the low mechanical integrity of ionomers can cause premature failure of the catalyst−ionomer interface.[8] Also the mechanically unstable electrode accelerates membrane degradation, as significantly lower open−circuit voltage was obtained after the AST for DMF−, NMF−, and water/NPA−processed MEAs (Table 4−3).

4.2.4 Conclusion

In conclusion, this study shows the impact of dispersing agents on the microstructure of a protonated phosphonated ionomer. Because pore formation does not occur with the PFSA-only ionomer, the dispersing agent's effect on fuel cell performance is different from that with conventional low temperature fuel cells.[32] This study also shows that the water uptake and proton conductivity of the dispersion cast ionomer are related to the H-bonding interaction of the liquid media. On the other hand, the mechanical properties of the water swollen ionomer are affected by several factors, including electrophilicity, porosity, and water uptake. Moreover, we were able to ascertain that the initial fuel cell performance is influenced primarily by the porous structure, and the durability of the fuel cells is affected by the mechanical robustness of the ionomer. NMP, DMAc, and DMF are the best choices for electrode processing, considering the fuel cell performance and durability. This study highlights the importance of dispersing agents on ionomer processing for HT-PEMFCs and may stimulate more in-depth research on the fundamental relationship between the parameters of dispersing agents and the properties of the cast ionomers.

4.2.5 References

[1] van de Witte, P. J. D. P., Dijkstra, P. J., Van den Berg, J. W. A., & Feijen, J., **1996**, *Journal of membrane science*, *117*(1-2), 1-31.
[2] Susanto, H., & Ulbricht, M., **2009**, *Journal of Membrane Science*, *327*(1-2), 125-135.
[3] Rangou, S., Buhr, K., Filiz, V., Clodt, J. I., Lademann, B., Hahn, J., ... & Abetz, V., **2014**, *Journal of Membrane Science*, *451*, 266-275.
[4] Sinturel, C., Vayer, M., Morris, M., & Hillmyer, M. A., **2013**, *Macromolecules*, *46*(14), 5399-5415.

[5] Son, J. G., Gotrik, K. W., & Ross, C. A., **2012**, *ACS Macro Letters*, *1*(11), 1279−1284.

[6] Altena, F. W., & Smolders, C. A., **1982**, *Macromolecules*, *15*(6), 1491−1497.

[7] Lodge, T. P., Hanley, K. J., Pudil, B., & Alahapperuma, V., **2003**, *Macromolecules*, *36*(3), 816−822.

[8] Kim, Y. S., Welch, C. F., Mack, N. H., Hjelm, R. P., Orler, E. B., Hawley, M. E., ... & Johnston, C. M., **2014**, *Physical Chemistry Chemical Physics*, *16*(13), 5927−5932.

[9] Kusoglu, A., & Weber, A. Z., **2017**, *Chemical reviews*, *117*(3), 987−1104.

[10] Zhang, J., Zhu, W., Huang, T., Zheng, C., Pei, Y., Shen, G., ... & Guiver, M. D., **2021**, *Advanced Science*, *8*(15), 2100284.

[11] Kim, Y. S., **2021**, *ACS Applied Polymer Materials*, *3*(3), 1250−1270.

[12] Berlinger, S. A., McCloskey, B. D., & Weber, A. Z., **2018**, *The Journal of Physical Chemistry B*, *122*(31), 7790−7796.

[13] Tarokh, A., Karan, K., & Ponnurangam, S., **2019**, *Macromolecules*, *53*(1), 288−301.

[14] Wang, Z., Tang, H., Li, J., Zeng, Y., Chen, L., & Pan, M., **2014**, *Journal of Power Sources*, *256*, 383−393.

[15] Ma, C. H., Yu, T. L., Lin, H. L., Huang, Y. T., Chen, Y. L., Jeng, U. S., ... & Sun, Y. S., **2009**, *Polymer*, *50*(7), 1764−1777.

[16] Atanasov, V., Lee, A. S., Park, E. J., Maurya, S., Baca, E. D., Fujimoto, C., ... & Kim, Y. S., **2021**, *Nature Materials*, *20*(3), 370−377.

[17] Lim, K. H., Lee, A. S., Atanasov, V., Kerres, J., Park, E. J., Adhikari, S., ... & Kim, Y. S., **2022**, *Nature Energy*, *7*(3), 248−259.

[18] Choi, B., Langlois, D. A., Mack, N., Johnston, C. M., & Kim, Y. S., **2014**, *Journal of The Electrochemical Society*, *161*(12), F1154.

[19] Doo, G., Lee, J. H., Yuk, S., Choi, S., Lee, D. H., Lee, D. W., ... & Kim, H. T., **2018**, *ACS applied materials & interfaces*, *10*(21), 17835−17841.

[20] Wang, C., Krishnan, V., Wu, D., Bledsoe, R., Paddison, S. J., & Duscher, G., **2012**, *Journal of Materials Chemistry A*, *1*(3), 938−

944.

[21] Peltonen, A., Etula, J., Seitsonen, J., Engelhardt, P., & Laurila, T., **2021**, *ACS Applied Polymer Materials*, *3*(2), 1078−1086.

[22] Reynolds, W. L., & Lampe, K. A., **1968**, *Journal of Inorganic and Nuclear Chemistry*, *30*(10), 2860−2862.

[23] Burgot, J. L., **1998**, *Analyst*, *123*(2), 409−410.

[24] Woolley, E. M., & Hepler, L. G., **1972**, *Analytical Chemistry*, *44*(8), 1520−1523.

[25] Wada, G., & Takenaka, T., **1971**, *Bulletin of the Chemical Society of Japan*, *44*(10), 2877−2877.

[26] Goldfarb, A. R., Mele, A., & Gutstein, N., **1955**, *Journal of the American Chemical Society*, *77*(23), 6194−6196.

[27] Breant, M., & Dupin, M., **1969**, *Comptes Rendus Hebdomadaires Des Seances De L Academie Des Sciences Serie C*, *269*(4), 306.

[28] Mayer, U., Gutmann, V., & Gerger, W., **1975**, *Monatshefte für Chemie/Chemical Monthly*, *106*, 1235−1257.

[29] Kim, Y. S., Welch, C. F., Hjelm, R. P., Mack, N. H., Labouriau, A., & Orler, E. B., **2015**, *Macromolecules*, *48*(7), 2161−2172.

[30] He, Q., Yang, X., Chen, W., Mukerjee, S., Koel, B., & Chen, S., **2010**, *Physical Chemistry Chemical Physics*, *12*(39), 12544−12555.

[31] Eberhardt, S. H., Toulec, M., Marone, F., Stampanoni, M., Büchi, F. N., & Schmidt, T. J., **2015**, *Journal of the Electrochemical Society*, *162*(3), F310.

[32] Zhang, J., Pei, Y., Zhu, W., Liu, Y., Yin, Y., Qin, Y., & Guiver, M. D., **2021**, *Journal of Power Sources*, *484*, 229259.

4.3 Protonated phosphonic acid proton exchange membranes

4.3.1 Introduction

As a hydrogen fuel cell directly generates electric energy by an oxidation-reduction reaction of hydrogen and oxygen fuels, it has high energy efficiency and is environment-friendly, so it is attracting much attention as a next-generation energy technology for the future environment.[1-5] PEMFC is a fuel cell that uses a polymer membrane as an electrolyte. PEMFC is a high-output fuel cell with a higher current density than other types of fuel cells.[6-8] It has excellent durability, making it a suitable system as a power source for automobiles. PEMFC is divided into low temperature polymer electrolyte membrane fuel cell (LT-PEMFC) and high temperature polymer electrolyte membrane fuel cell (HT-PEMFC) according to the operating temperature.

Due to various reasons, LT-PEMFC has experienced difficulties in commercialization. The polymer electrolyte used in LT-PEMFC is costly perfluorosulfonic acid (PFSA) ionomers, and since the proton conductivity of PFSA polymer electrolyte is highly dependent on water hydration, a water management system such as a humidifier is required for LT-PEMFC.[9-12] HT-PEMFC generally uses a phosphoric acid (PA)-doped PBI-based polymer electrolyte, PA-doped PBI can operate without additional humidification because proton conduction is not dependent on water and protons are well delivered even at low humidity.[13-15] HT-PEMFC significantly reduces MEA performance degradation due to CO poisoning because of the operating temperatures of 120 to 180 °C or higher.[16-18] The activation overpotential also decreases, and the higher the temperature, the lower the mass transfer resistance and the lower the concentration polarization. However, although the HT-PEMFC has a high electrochemical reaction rate in theory, the performance of the actually developed HT-PEMFC does not reach that of the LT-PEMFC. In addition, durability is weak due to

phosphoric acid leakage and harsh operating conditions of temperatures varying from 160 ℃ and high current density conditions.[19-20]

Operation at intermediate temperatures of PEMFCs has several advantages. Compared to LT-PEMFCs, poisoning by impurities such as CO or SO_2 is reduced, and issues related to water management or electrode flooding are reduced.[21] Compared to HT-PEMFCs, it has broad material options due to its relatively low temperature, and it has cost savings by simplifying the stack.[22],[23] However, a suitable polymer electrolyte that can be used at intermediate temperature and low humidity has not been developed.

As a method for synthesizing aromatic polymers, there is superacid-catalyzed condensation of ketones and aromatic compounds, which is a hydroxyalkylation reaction.[14-26] As the intermediate alcohol reacts with another aromatic compound, a high molecular weight polymer with a linear para-substitution main chain is synthesized.[27] In addition, thermochemically and mechanically robust polymers are obtained as a result of the reaction.

Super acid-catalyzed polycondensation reaction offers some advantages like simple one-pot synthesis, metal-free conditions, easy purification and short reaction time, etc.[28] Also, the obtained polymers with high molecular weight have good solubility in common organic solvents and excellent physical and thermal properties.

On the other hand, perfluoroarylenes have ability to undergo a nucleophilic substitution reaction.[29] As shown in Figure 4-13, the fluorine atom in the para position of the perfluorophenyl moieties is highly activated by nearby electron withdrawing fluorine atoms.[30] Therefore, additional functional groups such as sulfonic acid or phosphonic acid can be introduced into the para site of perfluoroaromatic units in the polymer.
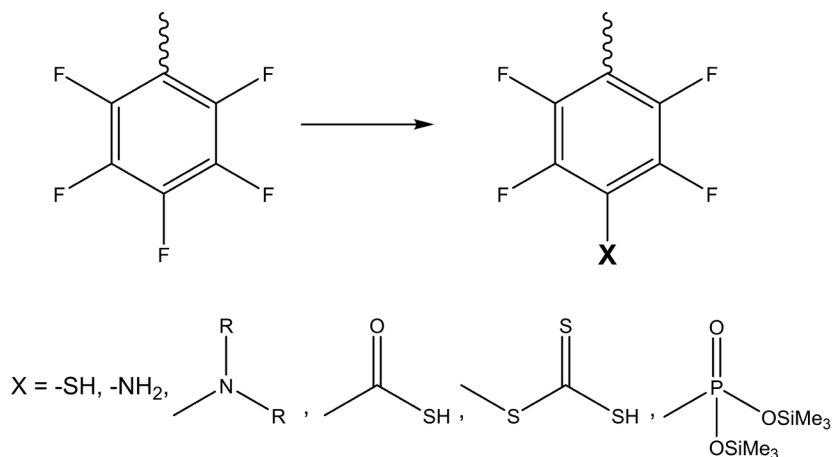
Figure 4-13. Nucleophilic substitution reaction of perfluoroarylenes

Chapter 4.3 describes the fabrication and evaluation of proton exchange membrane (PEM) using protonated phosphonic acid capable of proton conduction even at medium temperature and low humidity. Polymer was synthesized by superacid-catalyzed hydroxyalkylation, and two types of polymers were synthesized by introducing sulfonic acid and phosphonic acid into the para site of the perfluoroaromatic unit in the polymer. By blending the two polymers, a PEM containing protonated phosphonic acid could be synthesized.

4.3.2 Experimental

Materials

For the synthesis of polymer and fabricate the membranes, p-terphenyl (99.5 %) , sodium hydrosulfide hydrate (60 %), chloroform-d (CDCl3, 99.8 % atom % D), and dimethyl sulfoxide-d_6 (DMSO-D6, 99.9 atom % D) were supplied by Sigma Aldrich Chemical Co. Ltd. Perfluoroacetophenone (95%) was supplied by BLD. Dichloromethane (DCM, 99%), methyl alcohol (MeOH, 99.5 %), N,N-dimethylacetamide (DMAc, 99.5 %), hydrochloric acid (1M HCl), acetic acid (99.7 %), hydrogen peroxide (30% H_2O_2), hexane (85 %), dimethyl sulfoxide (DMSO, 99.5 %),

phenolphthalein solution (1 %), sodium chloride (NaCl, 99 %) and sodium hydroxide (NaOH, 98 %) were obtained from Daejung. Trifluoromethanesulfonic acid (98 %)and tris(trimethylsilyl) phosphite (95 %) were supplied by TCI.

Synthesis of pTPPFA

The precursor polymers was synthesized by Friedel-Crafts polyhydroxyalkylations using p-terphenyl and perfluoroacetophenone. The carbonyl monomer is relatively unreactive, whereas the carbinol intermediate formed after the first reaction is more reactive. Therefore, if an excess of carbonyl monomer is added, a high molecular weight polymer can be obtained in a short time by a nonstoichiometric effect due to a large reactivity difference.[31-33] The precursor polymers, pTPPFA, were synthesized by the following method. p-Terphenyl (7 g, 30.4 mmol) with anhydrous DCM 30 ml solution was prepared in a 250 ml round bottle and stirred for 10 min. It was noted that, p-terphenyl shows low solubility in DCM. Subsequently, excess perfluoroacetophenone (12.05, 45.6 mmol) was added to the solution and stirred for 10 min. Then trifluoromethane sulfonic acid (TFSA) used as catalyst was dropwise at 0 °C. The reaction mixture becomes dark green viscous solution after 2 days of reaction at room temperature. The reaction solution was reprecipitated in excess methanol and purified by repeated precipitations with methanol. Finally, the obtained beige solid was dried at vacuum oven. Yield: 13.61 g (95%)

^{1}H-NMR (400 MHz, CDCl$_3$) δ 7.74 (s, 1H), 7.69 (d, J = 8.5 Hz, 1H), 7.48 (d, J = 8.3 Hz, 1H); ^{19}F-NMR (377 MHz, CDCl$_3$) δ −55.89 ~ −65.69 (m), −125.30 ~ −131.33 (m), −147.30 ~ −154.39 (m), −160.70 (dd, J = 36.1, 14.1 Hz).

Synthesis of S100

S100 was synthesized by introducing sulfonic acid at the para position of the perfluoroaromatic group in pTPPFA. The synthesis of S100 was carried out in two steps using literature procedures.

[34] First, to introduce a thiol into the perfluoroaromatic group, pTPPFA (1g, 2.10 mmol repeating units) was dissolved in DMAc (10 ml) at 90 °C. The reaction solution was cooled to room temperature, and sodium hydrosulfide was added (0.65 g, 6.30 mmol) and stirred for 24 hrs. When 1M HCl (10 ml) was slowly added to the reaction mixture, a yellow solid was precipitated, and a solid was obtained by filtering. Yellow solid with acetic acid (10 ml) and 30% hydrogen peroxide solution (7 ml) were prepared for oxidation of thiol group and reaction for 24 hrs at 50 °C and 1 hr at 110 °C. Product was obtained by filtering and purified by dialysis (MWCO = 3,500 Da) in deionized water. Finally, S100 was obtained by freeze-drying. (yield 75 %, 0.837g)
^{19}F NMR (377 MHz, DMSO) δ −57.50 ~ −63.46 (m), −129.42 ~ −131.64 (m), −136.74 ~ −139.28 (m).

Synthesis of P100

P100 was synthesized by literature methods.[35] pTPPFA (0.5g, 1.05 mmol repeating units) and tris(trimethylsilyl) phosphite were introduced into a round bottle equipped with reflux condenser, magnetic bar and heating system. The reaction solution was stirred for 14 hrs at 170 °C under Ar atmosphere. Then product was precipitated in water and refluxed for 4 hrs in water. White solid was treated by 1M HCl for 12 hrs at 50 °C and precipitated in hexane. Finally P100 was obtained by drying at vacuum oven. (yield 85 %, 0.49g)
^{19}F NMR (377 MHz, DMSO) δ −60.23 (s), −130.57 (d, J = 347.8 Hz), −132.42 (s).

Membrane fabrication

All membranes were prepared by solution casting of polymers dissolved in DMSO. Concentration of prepared P100 and S100 solution in DMSO was both 5 wt%. It was noted that the molecular weights of the repeating units of P100 and S100 were almost similar to 538.37 g/mol and 538.45 g/mol, respectively. So, we fixed the molecular weight of the two polymers at 538.40 g/mol, the

same content of S100 and P100 means the same repeating unit in mmol. The manufacturing process of SP55 membrane blended with S100 and P100 at a ratio of 1:1 is as follows. 1 g each of 5 wt% S100 solution in DMSO and 5 wt% P100 solution in DMSO was weighed and the solutions were mixed. The mixture solution was into glass petri dish, then placed in 80°C vacuum oven for 48 hrs. The membranes were peeled off by soaking the petri dish in deionized water. SP55 membranes were obtained after treating in 1M H_2SO_4 for 24 hrs at 80°C and washed with deionized water several times. The SP37 and SP73 membranes, in which S100 and P100 are blended in 3:7 and 7:3 respectively, were prepared in the same way as above.

Characterization and measurements

^1H-NMR, ^{19}F-NMR and ^{31}P-NMR spectra were measured in $CDCl_3$ or DMSO-d6 at 25℃ on a Bruker Ascend™ 400 to confirm successful synthesis of pTPPFA, P100 and S100. Fourier-transform infrared spectroscopy (FT-IR) spectra was obtained using PerkinElmer FT-IR system (Spectrum-GX) to analyze the structure of PEMs. The thermal stability of the membranes were examined by using TA Instrument TGA 2950 with heating rate of 10 ℃/min under N_2 atmosphere. Differential scanning calorimetry was carried out with a TA Instrument DSC Q20-1426 using a heating rate of 10 ℃/ min under N_2 atmosphere. Note that second scans were only shown. Mechanical property of the PEMs was characterized using universal tensile machine (Tinius Olsen H5K-T). Membrane samples (4cm*0.5cm) were prepared to measure the mechanical strength and tested at stretching speed of 10 mm/min. Field Emission Scanning Electron Microscopy (FE-SEM) images to verify morphology and shape of patterned Cu, was taken on an Inspect F50 (FEI, Korea).

The water uptake (WU) were evaluated after immersing the membranes in water at room temperature for 24 hrs. After removing the membrane from the water, excess water on the surface was carefully wiped off and the weight and was measured

for comparison. After membrane was completely dried, the weight of the dried membrane were also measured. As the result, WU was calculated according to the following formula:

$$WU = ((W_{wet} - W_{dry})/W_{dry}) * 100$$

Ion exchange capacity (IEC) value was determined titration. All membranes were dried at 100 °C, overnight before weighing. All samples in H^+ form were weighed, then immersed in 1M NaCl and stirred at RT for 24 h. As an indicator, 1-2 drops of 1% phenolphthalein indicator are used and titrated with 0.1M NaOH solution. The IEC (meq g^{-1}) was calculated based on the following equation:

$$IEC = (V_{NaOH} * C_{NaOH})/W_{dry}$$

Where V_{NaOH} is volume of NaOH, C_{NaOH} is the concentration of NaOH. W_{dry} is the weight of the dried membranes.

The ohmic resistance of the PEMs were measured at different related humidity (25 % ~ 100 %) and different temperature by two-electrode electrochemical impedance spectroscopy (EIS, SI 1260, Solartron) over the frequency range from 10 Hz to 10 MHz with an amplitude of 20 mV. Proton conductivity was calculated by the following equation:

$$\sigma = L/(R \times W \times d)$$

where L was the distance between two electrodes (cm), R was the measured ohmic resistance (Ω), W was the width of the membrane (cm) and d was the width of the membrane (cm).

The oxidative stability of the membranes was tested in Fenton's reagent by assessing the residual weight of each after Fenton's reagent treatment at 80℃.[36] Membranes were immersed in the Fenton's reagent (3 wt% H_2O_2, 4ppm Fe^{2+}) at 80℃ for 8hrs, the residual weight was calculated after washing with DI water and

dried.

MEA preparing and Fuel cell testing

The catalyst loadings of anode and cathode were 0.4 mgPt cm^{-2} and 0.8 mgPt cm^{-2}, respectively and containing ionomers with I to C ratio 0.9. 36BB GDL was used and catalyst layers were prepared with catalyst coated membrane (CCM) method by spraying the catalyst ink on the membrane. All prepared membranes' thickness was ~30 μm.

HT-PEMFC performance was measured with a fuel cell station (Fuel Cell Technologies), after break-in the cell under constant voltage condition (from 0.7 to 0.4 V). Polarization curves of each MEAs were recorded at a cell temperature of 80, 100, 120 ℃ and 150 kPa back pressure under H_2/air atmosphere with 500/1000 sccm flow rate, and 100%, 80%, 60%, 40% humidification were applied during the tests.

4.3.3 Results and discussion

Synthesis and characteristics of pTPPFA, S100 and P100
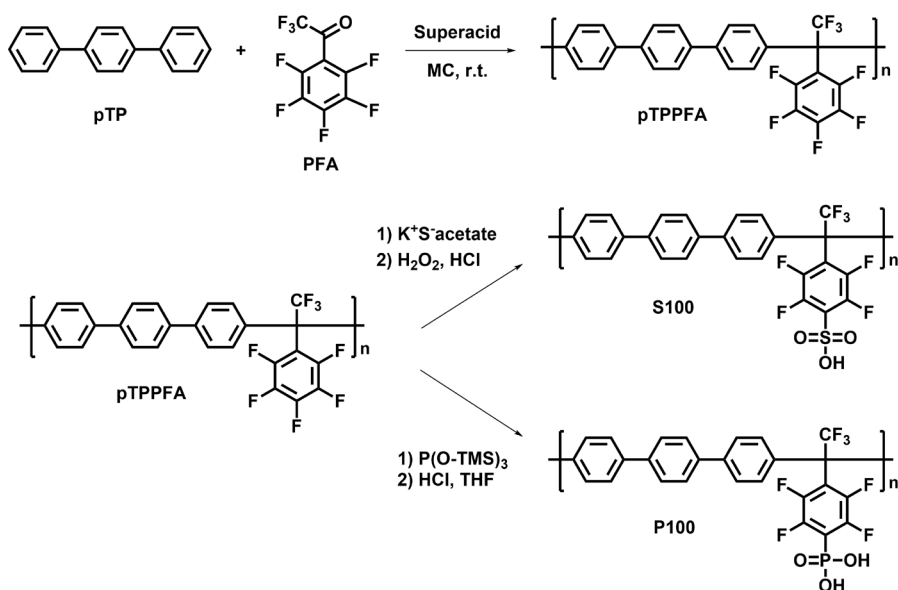
Figure 4-14. Synthesis of pTPPFA and nucleophilic substitution reaction of pTPPFA

      The precursor polymers was synthesized by Friedel-Crafts polyhydroxyalkylations using p-terphenyl and perfluoroacetophenone. The carbonyl monomer is relatively unreactive, whereas the carbinol intermediate formed after the first reaction is more reactive. Therefore, if an excess of carbonyl monomer is added, a high molecular weight polymer can be obtained in a short time by a nonstoichiometric effect due to a large reactivity difference.[37] The synthesis mechanism of pTPPFA is shown in Figure 4-14. The structure of the pTPPFA with molecular weight of 53,000 g/mol was confirmed by ^{1}H-NMR and distinct peaks of the terphenyl backbone were observed at 7.4 ppm to 7.8 ppm as shown in Figure 4-15. The obtained pTPPFA showed good solubility in common organic solvents such as THF, DCM, chloroform, toluene, NMP and DMF. S100 and P100 were obtained

by introducing additional functional groups of sulfonic acid and phosphonic acid to perfluoroarylenes in pTPPFA, respectively. S100 was synthesized by introducing sulfonic acid at the para position of the perfluoroaromatic group in pTPPFA. As shown in Figure 4−16(a), the synthesis of S100 was carried out in two steps using literature procedures.[38] : introduction of a thiol group and thiol oxidation. P100 was also prepared in a two−step procedure as hown in Figure 4−16(b). First, fluorine atoms in the para position in pTPPFA were substituted with phosphonated ester groups by Michaelis−Abuzov reaction and second, trimethylsilyl esters were hydrolyzed by acid treatment.
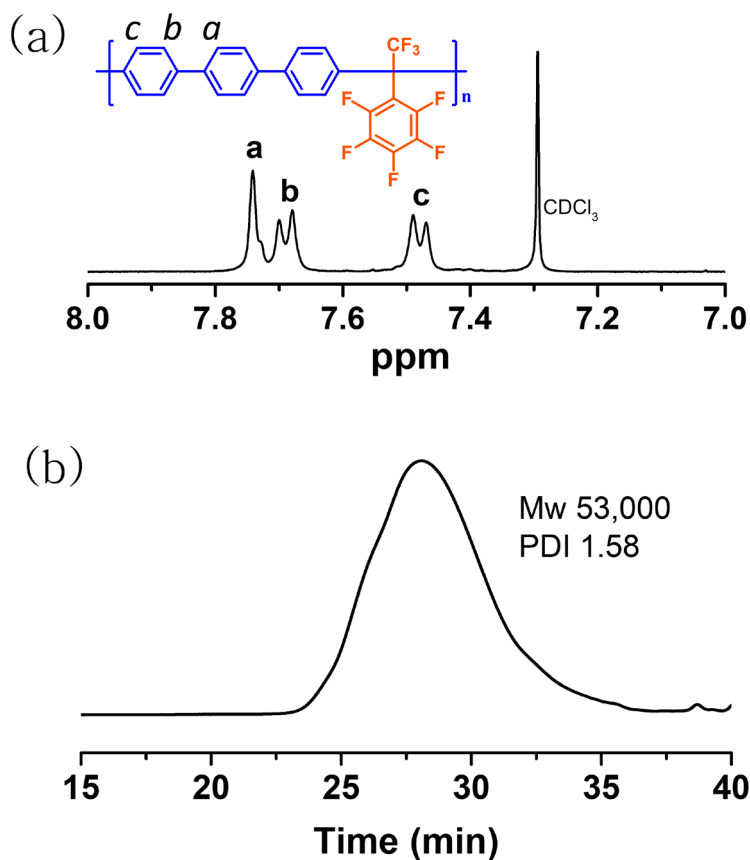

Figure 4−15. (a) ^{1}H−NMR and (b) GPC spectra for pTPPFA
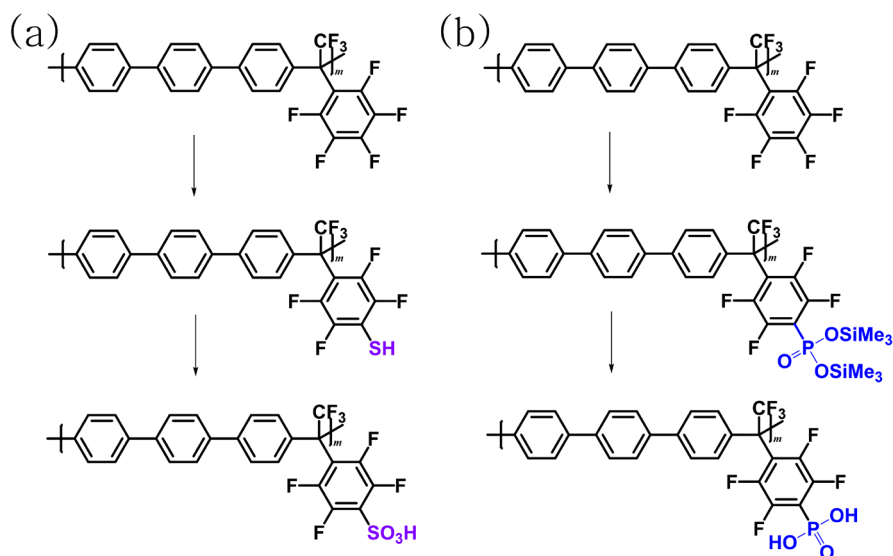
Figure 4-16. Two-step synthesis mechanism of (a) S100, (b) P100

The structure of the pTPPFA, S100 and P100 were confirmed by ^{19}F-NMR and FT-IR. As shown in Figure 4-17, pTPPFA has four fluorine atoms with different environments, so four distinct peaks were identified in ^{19}F-NMR. On the other hand, in S100 and P100, the c peak at the para position completely disappeared, confirming that they were completely substituted with sulfonic acid groups and phosphonic acid groups, respectively.

Figure 4-18 shows the FT-IR spectra for pTPPFA, S100 and P100. The 1216 cm^{-1} signals of pTPPFA were assigned as CF_3 groups. In both S100 and P100, -OH peaks were observed at 3000 to 3800 cm^{-1}, which were detected not only for each acid group but also for the stretching vibration of the O-H of water. Hydrogen bonding of the sulfonic acid groups with the surrounding water molecules of S100 were observed at 1635 cm^{-1} and the stretching vibration of SO_3^- was observed at 1270 cm^{-1}.[39] Hydrogen bonding of the phosphonic acid groups with the surrounding water molecules of P100 were observed at around 1725 cm^{-1}. Also, the stretching vibration of PO_3 and PO were confirmed at 1450 cm^{-1} and 1086 cm^{-1}, respectively.
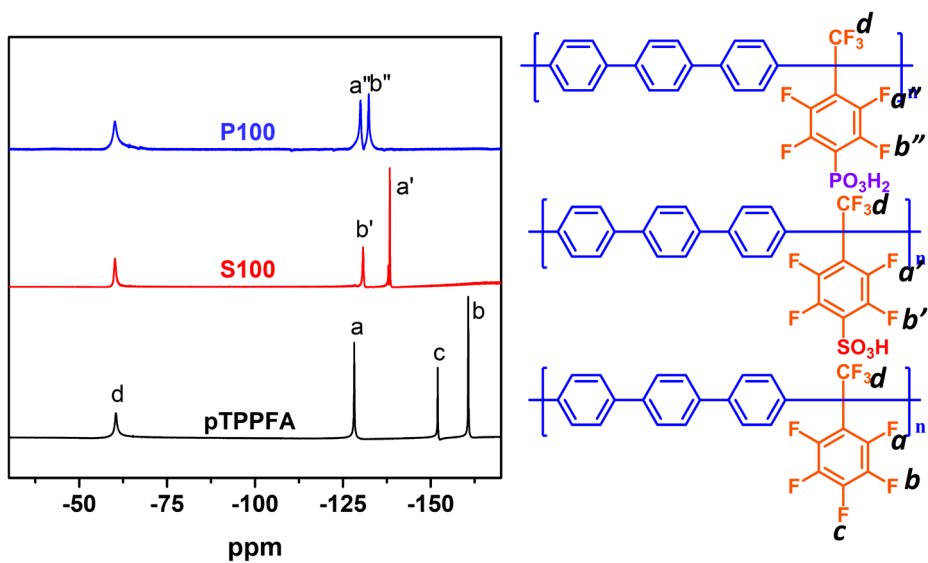
Figure 4-17. ^{19}F-NMR spectra for pTPPFA, S100, and P100
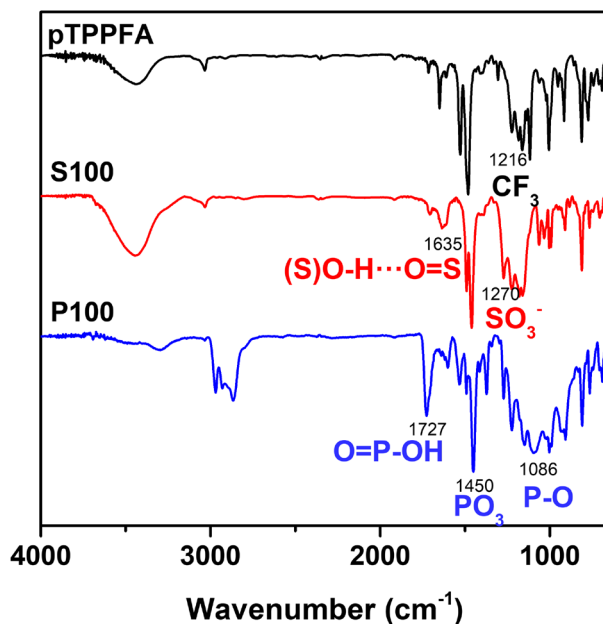
Figure 4-18. FT-IR spectra for pTPPFA, S100, and P100

1 6 9
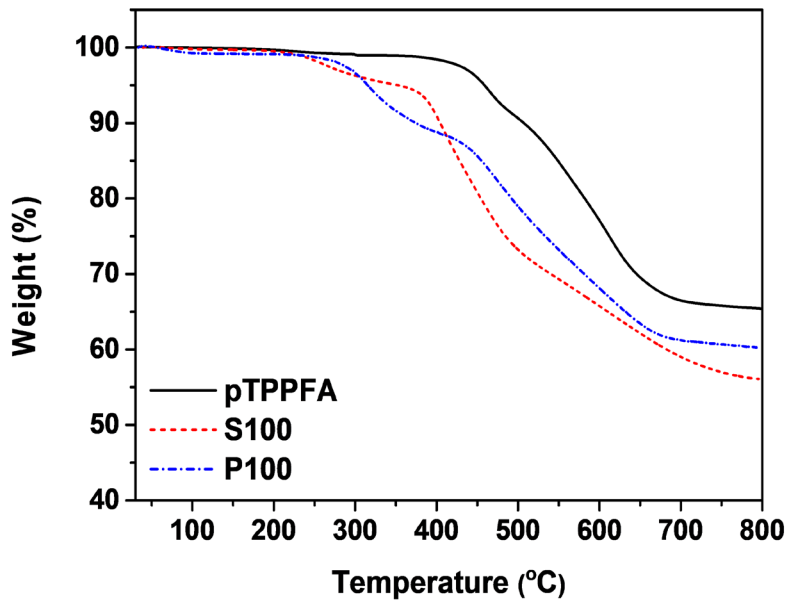
Figure 4-19. Thermal analysis of pTPPFA, S100, and P100

In fuel cells, the thermal stability of PEMs is an important factor related to the durability of PEMFCs. Thermal stability of polymers was examined by TGA, and the TGA curves were shown in Figure 4-19. TGA measurements revealed that, pTPPFA, S100 and P100 showed excellent thermal stability up to 390 ℃, 220 ℃ and 240 ℃, respectively. Dephosphonation of P100 occurred around 340 ℃.[29]

Table 4-4. Theoretical IEC and experimental IEC of S100, SP7E, SP55, SP37 and P100

IEC	S100	SP73	SP55	SP37	P100
Theoretical	1.86	2.41	2.79	3.16	3.71
Experimental	1.71	1.73	1.77	1.79	1.83

[mmol/g]

Membrane fabrication and characteristics

All membranes were manufactured by mixing and solution casting of S100 solution (5% in DMSO) and P100 solution (5% in DMSO). It was noted that the molecular weights of the repeating units of P100 and S100 were almost similar to 538.37 g/mol and 538.45 g/mol, respectively. So, we fixed the molecular weight of the two polymers at 538.40 g/mol, the same content of S100 and P100 means the same repeating unit in mmol. The membrane blended with 50% of S100 and P100, respectively, was named SP55, the membrane blended with 30% and 70%, respectively, was named SP37, and the membrane blended with 70% and 30% was named SP73.

Table 4-4 lists the theoretical and experimental IEC of the membrane. P100 has the same repeating unit molecular weight as S100, but P100 has two protons, so it has a twice higher IEC than S100. IEC measured by titration yielded similar IEC values range from 1.71 to 1.83 mmol/g. The theoretical IEC means the amount of all exchangeable protons ($-PO_3H_2$ / $-PO_3H^-$ / $-PO_3^{2-}$) at pH range from 1 to 14.[40] However, experimental IEC concludes the amount of all exchangeable acid proton. Only the dissociation of the first proton of phosphonic acid affected the experimental IEC.

Figure 4-20(a) shows the photograph of the SP55 membrane. All SP membranes has good rigidity and flexibility, so they were easy to handle. Figure 4-20 (b) and (c) shows the SEM image of SP55 membrane. It was confirmed that SP55 has a dense structure in both the surface and cross section. Also, as shown in Figure 4-20(d), at the EDX analyses of SP55 membrane, it was found that the S and P elements were blended well with the same content, and S100 and P100 were evenly mixed without phase separation.
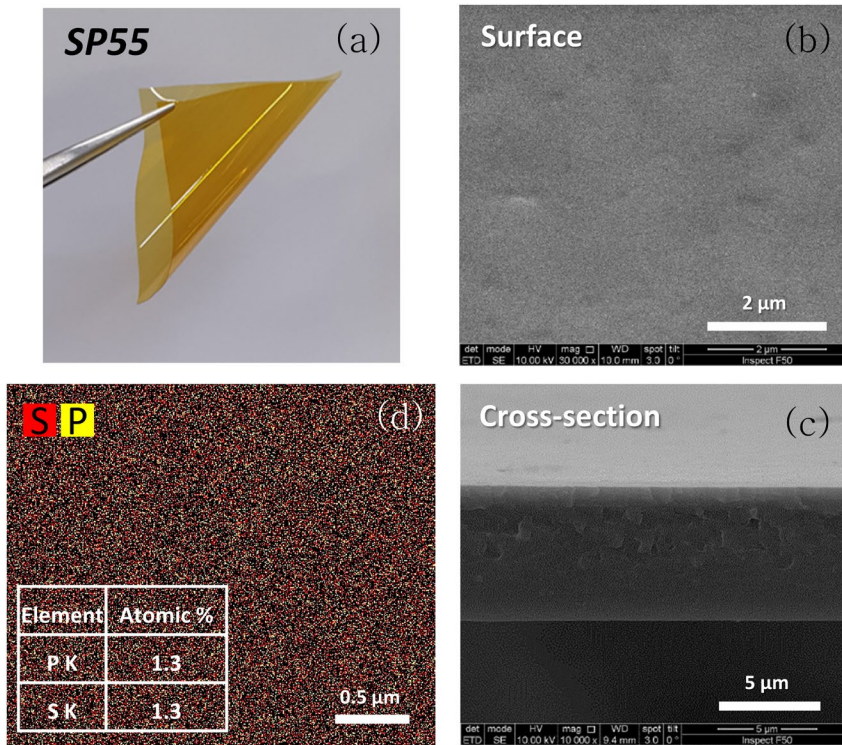
Figure 4-20. (a) SP55 membrane (b) SEM image of SP55 - surface (c) cross section (d) EDX analyses

^{31}P-NMR was measured to confirm the interaction between sulfonic acid and phosphonic acid within the SP membranes, and the NMR spectra are shown in Figure 4-21. A single phosphorus peak was observed at −2.79 ppm for P100. As S100 was added, the electron density of phosphorus was lowered by sulfonic acid, an electron withdrawing group, and shifted to a downfield. Therefore, the peak of phosphonic acid shifted due to the interaction between sulfonic acid.
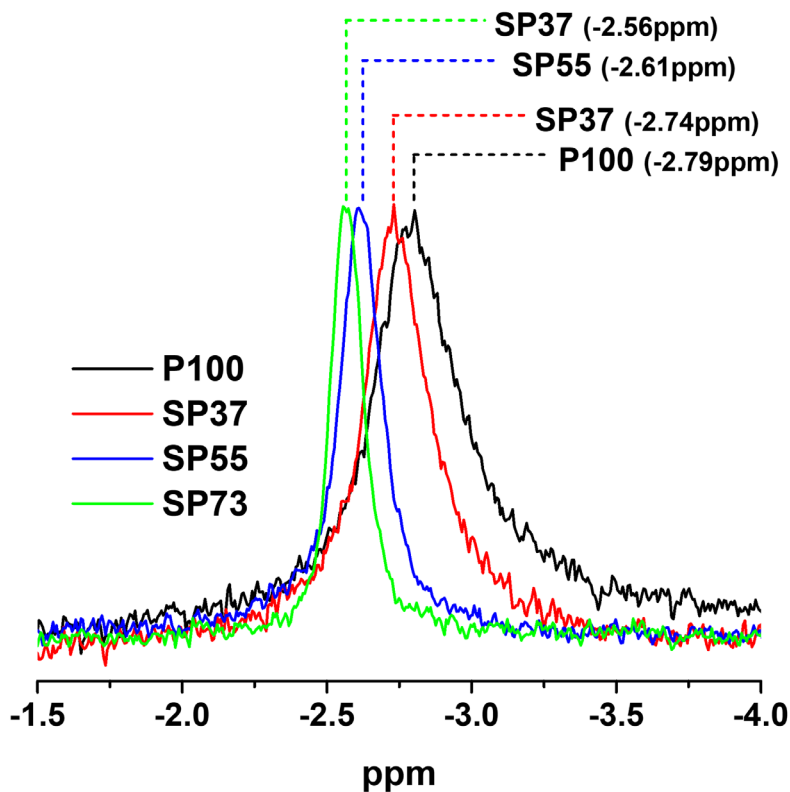
Figure 4-21. ^{31}P-NMR spectra for P100, SP37, SP55 and SP73

Figure 4-22 shows the tensile strength of N212, and SP membranes at dry condition and wet condition. N212 showed tensile strength of 24.7 MPa in dry condition and 16.7 MPa in wet condition, respectively. SP membrane showed much better mechanical strength than N212 due to its rigid aromatic backbone. P100 showed slightly better mechanical strength than S100, and SP55 obtained tensile strength of 43.2 MPa in dry state and 28.0 MPa in wet state. It is expected to contribute to improving the durability of fuel cells with good mechanical strength even in the wet state.
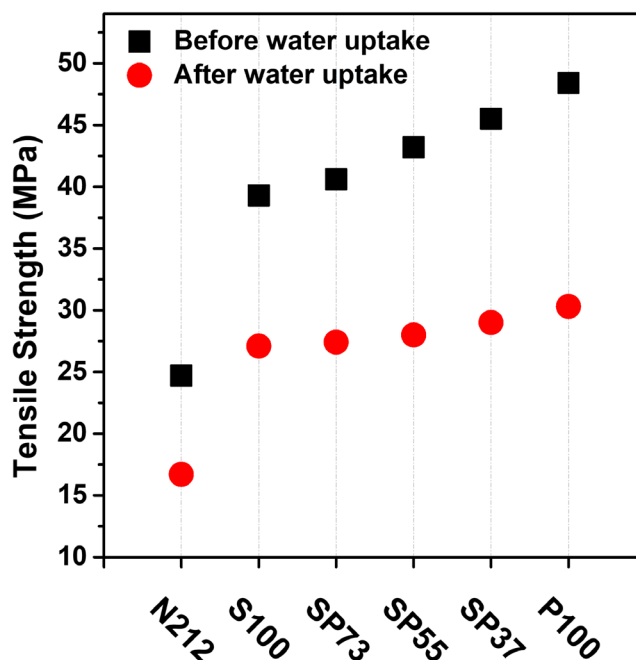
Figure 4-22. Tensile strength of N212, S100, SP73, SP55, SP37 and P100

       The water uptake of N212 and SP membranes at 25 °C and 80 °C was measured and shown in Figure 4-23(a). At 25 °C, N212 showed a water uptake of 17.6 %, and all SP membranes except S100 showed lower water uptake than N212 due to the rigid aromatic backbone. S100 showed the highest water uptake of 19.6% at room temperature due to the good water uptake of sulfonic acid while having a higher IEC than N212. However, even S100 obtained a lower water uptake than that of N212 at 80 °C due to the good water absorption and swelling properties of the relatively more flexible N212. Water uptake decreased as P100 was added to S100, and this is due to the lower acidity of phosphonic acid and extensive intrinsic H-bonding between phosphonic acids.[41] Therefore, phosphonic acid that can interact with water was reduced, resulting in a relatively lower water uptake than that of S100.[41]
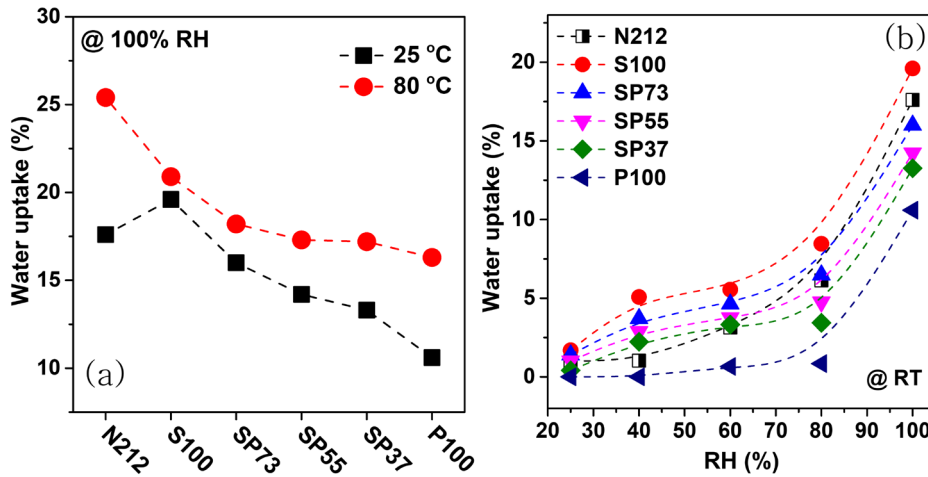
Figure 4-23. Water uptake of the membranes (a) at 25°C and 80°C under 100% RH and (b) at different RH under room temperature

In PEMFC, since humidity has a great influence on the proton conductivity of PEM, the water uptake was measured while changing the humidity from 25% to 100%.(Figure 4-23) Water uptake at all humidity levels showed a trend of P100 < SP37 < SP55 < SP73 < S100. On the other hand, the water uptake of N212 showed a rapid increase compared to that of the SP membrane as the humidity increased, confirming that N212 was more affected by humidity.

The proton conductivity of the membrane as a function of temperature at 100% RH was evaluated. As shown in Figure 4-24(a), P100 showed the lowest proton conductivity at all temperatures, which was attributed to low water uptake and low acidity of phosphonic acid. Other SP membranes obtained higher proton conductivity than N212 at all temperatures. The proton conductivity of the SP membranes showed a tendency of P100 < S100 < SP37 < SP73 < SP55. This is a different trend from water uptake and IEC, at 80°C, SP55 showed the highest proton conductivity of 514.4 mS/cm.
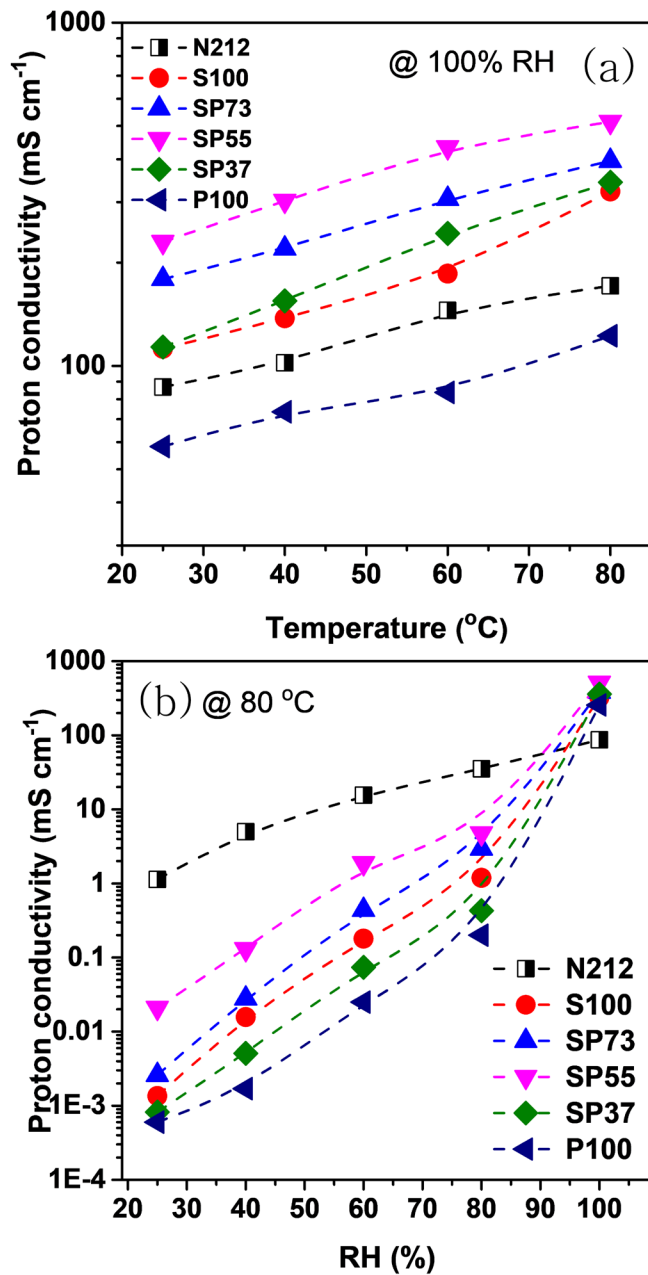
Figure 4-24. (a) Proton conductivity of membranes at 100 % RH with different temperature (b) proton conductivity of membranes at 80 ℃ with different RH %
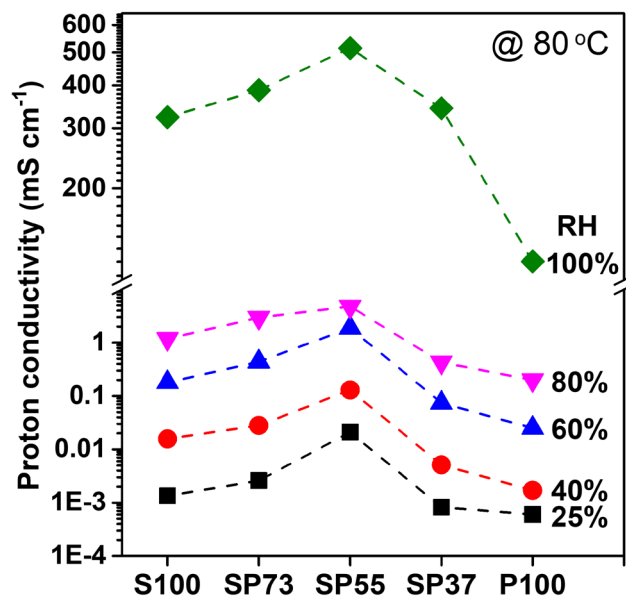
Figure 4-25. Comparison of proton conductivity of membranes with different RH

Water uptake was highest in S100 with the highest IEC, but S100 had the second lowest proton conductivity, and as P100 was added, the conductivity increased and peaked at SP55. This is because sulfonic acid and phosphonic acid interact with each other, and as the acidic proton of sulfonic acid is transferred to phosphonic acid, proton conduction occurs more effectively.

Figure 4-24 (b) shows the proton conductivity as a function of RH at 80℃. Proton conductivity increased as RH increased, and N212 showed the highest proton conductivity at 25% to 80% RH. The relatively high proton conductivity of N212 even at low humidity is due to the formation of channels for ion clusters due to the microphase separation between the hydrophobic and hydrophilic regions of N212, resulting in effective proton transport.[42],[43]
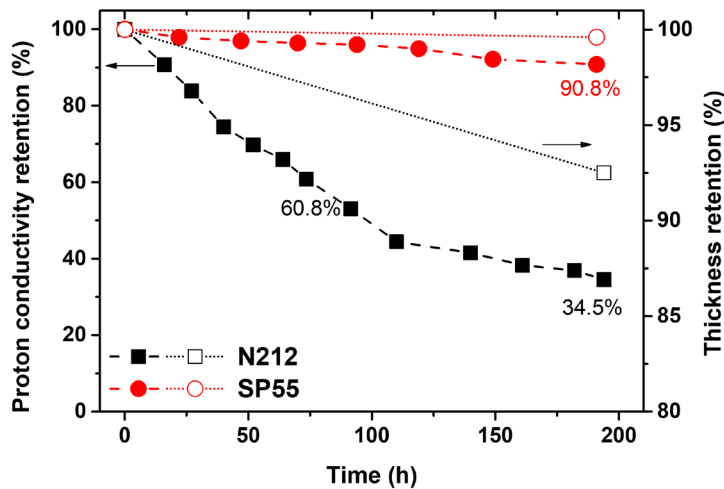
Figure 4−26. Proton conductivity and thickness retention at low humidity (80°C and 50% RH)

Figure 4−25 shows the comparison of proton conductivity of SP membranes with different RH at 80°C. At all RHs, the proton conductivity of SP55 was the best due to the protonated phosphonic acid effect, at 25 RH, 40 RH, 60 RH, 80RH and 100 RH, proton conductivity of 0.021 mS/cm, 0.13 mS/cm, 1.88 mS/cm, 4.77 mS/cm and 514.4 mS/cm, respectively, was obtained. SP73 showed a higher conductivity than SP37, which is considered to be due to the slightly higher content of sulfonic acid with higher acidity.

The durability of the membrane at high temperature and low humidity is directly related to the lifetime of the PEMFC. Therefore proton conductivity and thickness retention test were examined at 80°C and 50% RH for 200 hrs, as shown in Figure 4−26. After N212 was exposed to a high−temperature and low−humidity environment, the proton conductivity rapidly decreased, and after 200 hrs, it decreased to the initial level of 34.5%. Also, as moisture evaporated and shrank, the thickness of N212 also decreased. However, SP55 showed high proton conductivity retention even after 200 hrs due to its relatively rigid structure, and no decrease in thickness occurred. Therefore, SP55 showed much better durability than N212 at high temperature and low humidity.
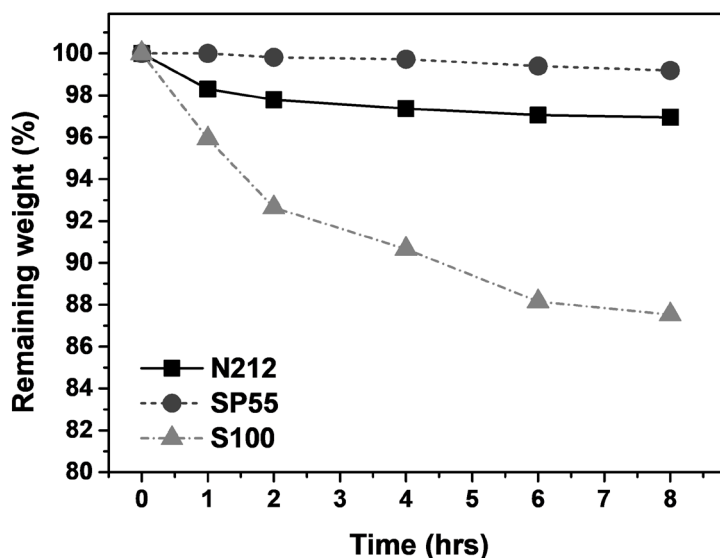
Figure 4-27. Oxidative stability of the membranes

When a very small amount of gas crossovers through the membrane, hydrogen peroxide that can be cleaved with radicals is generated in the catalyst layer, and degradation of ionomers and membranes occurs due to the radicals.[44] Therefore, the oxidative stability of the membranes was tested in Fenton's reagent. Membranes were immersed in the Fenton's reagent (3 wt% H_2O_2, 4ppm Fe^{2+}) at 80℃ for 8hrs, the residual weight was calculated. As shown in Figure 4-27, N212 showed a residual weight of 96.9% after Fenton's test, showing a slight decrease in weight. On the other hand, SP55 showed a higher remaining weight than that of N212 of 99.2%. Recently, a study was reported that phosphonic acid, including fluorine, acts as a radical scavenger,[45] and pentafluorophopsphonic acid of P100 also acts as a radical scavenger, and high oxidative stability was obtained. Also, Nafion is degraded by the main mechanism of ether-linkage dissociation,[46] SP55 does not have such ether-linkage. On the other hand, S100, which does not contain phosphonic acid with fluorine, showed relatively low oxidative stability.

HT-PEMFCs performance

To confirm the effect of protonated phosphonic acid, three combinations of membrane and ionomer were compared, and the combinations can be seen in Table 4-5. First, both the membrane and ionomer are non-protonated combinations using Nafion. Second, SP55 protonated membrane was used only for the membrane and Nafion was used for the ionomer. Third, SP55 membrane and PWN70 with Nafion protonated ionomer were introduced by giving protonated effect to both membrane and ionomer.

Table 4-5. Membrane and ionomer combination numbering for MEAs

	Membrane	Ionomer
1.	Nafion 212	Nafion
2.	SP55 protonated membrane	Nafion
3.	SP55 protonated membrane	PWN70+Nafion protonated ionomer

The temperature and humidity of fuel cell were measured at 80 °C with 100 % RH and 40% RH with lower humidity. After that, the temperature was gradually increased and the humidity was gradually decreased, and measurements were carried out under harsher conditions of higher temperature and lower humidity. Figure 4-28 shows the fuel cell polarization curve and power density curve for combinations 1 to 3. At 80 °C and 100% RH, Nafion, which has good conductivity due to relatively low temperature and high humidity, showed the best PPD of 0.92 W/cm^2. No. 3 combination using protonated membrane and ionomer showed PPD of 0.89 W/cm^2, which was almost the same as No. 1 combination.
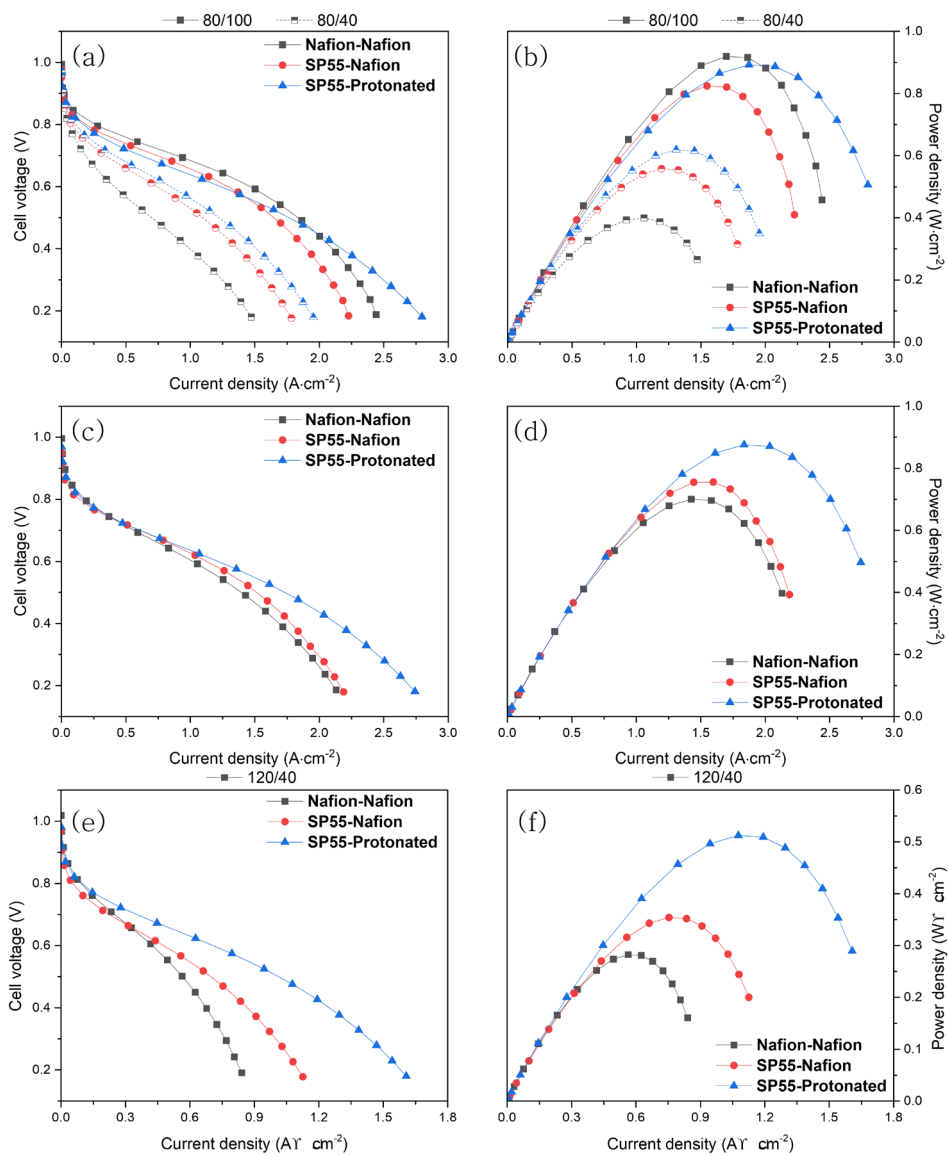
Figure 4-28. Polarization curves and power densities of MEAs with different combination of membranes and ionomers. Black line:Nafion212 membrane, Nafion ionomer, blue line:SP55 membrane, Nafion ionomer, red line:SP55 membrane, protonated ionomer, (a),(b) 80 ℃ at 100% RH and 40% RH (c),(d) 100 ℃, 80% RH (e),(f) 120 ℃, 40% RH.

At 80 °C and 40% RH, as the humidity decreased, the protonated membrane and ionomer effect appeared, protonated membrane and ionomer combination showed better performance than the Nafion combination. When the temperature was subsequently increased and the humidity decreased, Nafion's performance dropped dramatically, while the protonated combination maintained similar peak power densities. Under the conditions of high temperature and low humidity with 120 °C and 40% RH, the protonated combination showed the best PPD, followed by the use of Nafion ionomer for the SP55 membrane. Protonated membrane and protonated ionomer combination showed the best PPD at all temperatures and humidity except for 80 °C and 100% RH. Therefore, the protonated effect confirmed in ionic conductivity was also confirmed in PEMFC, and the effect was the largest at high temperature/low humidity.

4.3.4 Conclusion

In this study, proton exchange membranes with protonated phosphonic acid capable of proton conduction even at medium temperature and low humidity were developed. Polymer was synthesized by superacid−catalyzed hydroxyalkylation, and two types of polymers were synthesized by introducing sulfonic acid and phosphonic acid into the para site of the perfluoroaromatic unit in the polymer. By blending the two polymers, a PEM containing protonated phosphonic acid could be synthesized. SP55 showed the highest proton conductivity of 514.4 mS/cm due to the protonated phosphonic acid effect. Except for 80℃ and 100RH, the combination of protonated membrane and protonated ionomer showed the highest PPD. Therefore effect of the protonated membrane was confirmed at high temperature and low humidity, and a synergy effect was exhibited when used together with the protonated membrane and ionomer.

4.3.5 References

[1] Ijaodola, O. S., El-Hassan, Z., Ogungbemi, E., Khatib, F. N., Wilberforce, T., Thompson, J., & Olabi, A. G., **2019**, *Energy*, *179*, 246-267.

[2] Chandan, A., Hattenberger, M., El-Kharouf, A., Du, S., Dhir, A., Self, V., ... & Bujalski, W., **2013**, *Journal of Power Sources*, *231*, 264-278.

[3] Rosli, R. E., Sulong, A. B., Daud, W. R. W., Zulkifley, M. A., Husaini, T., Rosli, M. I., ... & Haque, M. A., **2017**, *International Journal of Hydrogen Energy*, *42*(14), 9293-9314.

[4] Lü, X., Qu, Y., Wang, Y., Qin, C., & Liu, G., **2018** , *171*, 1273-1291.

[5] Gamburzev, S., & Appleby, A. J., **2002**, *Journal of power sources*, *107*(1), 5-12.

[6] Taner, T., **2015**, *Journal of Fundamentals of Renewable Energy and Applications*, *5*(3), 1-4.

[7] Zhang, G., & Jiao, K., **2018**, *Energy Conversion and Management*, *176*, 409-421.

[8] Ahmed, D. H., & Sung, H. J., **2006**, *Journal of Power Sources*, *162*(1), 327-339.

[9] Nanadegani, F. S., Lay, E. N., & Sunden, B., **2020**, *Electrochimica acta*, *333*, 135552.

[10] Rosli, R. E., Sulong, A. B., Daud, W. R. W., Zulkifley, M. A., Husaini, T., Rosli, M. I., ... & Haque, M. A., **2017**, *International Journal of Hydrogen Energy*, *42*(14), 9293-9314.

[11] Haque, M. A., Sulong, A. B., Loh, K. S., Majlan, E. H., Husaini, T., & Rosli, R. E., **2017**, *International Journal of Hydrogen Energy*, *42*(14), 9156-9179.

[12] Nimir, W., Al-Othman, A., Tawalbeh, M., Al Makky, A., Ali, A., Karimi-Maleh, H., ... & Karaman, C. , **2023**, *International Journal of Hydrogen Energy*, *48*(17), 6638-6656.

[13] Liu, G., Zhang, H., Hu, J., Zhai, Y., Xu, D., & Shao, Z. G., **2006**, *Journal of Power Sources*, *162*(1), 547-552.

[14] Cho, H., Hur, E., Henkensmeier, D., Jeong, G., Cho, E., Kim, H. J., ... & Cleemann, L. N., **2014**, *European polymer journal*, *58*, 135–143.

[15] Chen, H., Wang, S., Liu, F., Wang, D., Li, J., Mao, T., ... & Wang, Z., **2020**, *Journal of Membrane Science*, *596*, 117722.

[16] KP, V. B., Varghese, G., Joseph, T. V., & Chippar, P., **2021**, *International Journal of Hydrogen Energy*, *46*(11), 8179–8196.

[17] Authayanun, S., Mamlouk, M., & Arpornwichanop, A., **2012**, *International journal of hydrogen energy*, *37*(8), 6808–6817.

[18] Jannelli, E., Minutillo, M., & Perna, A., **2013**, *Applied Energy*, *108*, 82–91.

[19] Jeong, Y. H., Oh, K., Ahn, S., Kim, N. Y., Byeon, A., Park, H. Y., ... & Kim, J. Y., **2017**, *Journal of Power Sources*, *363*, 365–374.

[20] Mack, F., Heissler, S., Laukenmann, R., & Zeis, R., **2014**, *Journal of Power Sources*, *270*, 627–633.

[21] Lee, K. S., Maurya, S., Kim, Y. S., Kreller, C. R., Wilson, M. S., Larsen, D., ... & Mukundan, R., **2018**, *Energy & Environmental Science*, *11*(4), 979–987.

[22] Park, J. S., Shin, M. S., & Kim, C. S., **2017**, *Current Opinion in Electrochemistry*, *5*(1), 43–55.

[23] Venugopalan, G., Chang, K., Nijoka, J., Livingston, S., Geise, G. M., & Arges, C. G., **2019**, *ACS Applied Energy Materials*, *3*(1), 573–585.

[24] Guzman-Gutierrez, M. T., Nieto, D. R., Fomine, S., Morales, S. L., Zolotukhin, M. G., Hernandez, M. C. G., ... & Wilks, E. S., **2011**, *Macromolecules*, *44*(2), 194–202.

[25] Olvera, L. I., Guzmán-Gutiérrez, M. T., Zolotukhin, M. G., Fomine, S., Cárdenas, J., Ruiz-Trevino, F. A., ... & Prokhorov, E., **2013**, *Macromolecules*, *46*(18), 7245–7256.

[26] Olah, G. A., Rasul, G., York, C., & Prakash, G. S., **1995**, *Journal of the American Chemical Society*, *117*(45), 11211–11214.

[27] Hernandez, M. C. G., Zolotukhin, M. G., Fomine, S., Cedillo, G., Morales, S. L., Fro¨hlich, N., ... & Ruiz-Trevino, A., **2010**, *Macromolecules*, *43*(17), 6968–6979.

[28] Kasi, B., Murugesan, V., & Kaliaperumal, N., **2019**, *Applied Petrochemical Research*, *9*, 91−100.

[29] Atanasov, V., & Kerres, J., **2011**, *Macromolecules*, *44*(16), 6416−6423.

[30] Kang, N. R., Pham, T. H., Nederstedt, H., & Jannasch, P., **2021**, *Journal of Membrane Science*, *623*, 119074.

[31] Olvera, L. I., Ruiz−Trevino, F. A., Balmaseda, J., Ronova, I. A., Zolotukhin, M. G., Carreón−Castro, M. P., ... & Gavino, R., **2016**, *Polymer*, *102*, 221−230.

[32] Cruz−Rosado, A., Romero−Hernández, J. E., Ríos−López, M., López−Morales, S., Cedillo, G., Ríos−Ruiz, L. M., ... & Vivaldo−Lima, E., **2022**, *Polymer*, *243*, 124616.

[33] Cai, Z., Liu, Y., Wang, C., Xie, W., Jiao, Y., Shan, L., ... & Luo, S., **2022**, *Journal of Membrane Science*, *644*, 120115.

[34] Kang, N. R., Pham, T. H., & Jannasch, P., **2019**, *ACS Macro Letters*, *8*(10), 1247−1251.

[35] Atanasov, V., & Kerres, J., **2011**, *Macromolecules*, *44*(16), 6416−6423.

[36] Lee, K. H., Chu, J. Y., Kim, A. R., & Yoo, D. J., **2018**, *ACS applied materials & interfaces*, *10*(24), 20835−20844.

[37] Olvera, L. I., Ruiz−Trevino, F. A., Balmaseda, J., Ronova, I. A., Zolotukhin, M. G., Carreón−Castro, M. P., ... & Gavino, R., **2016**, *Polymer*, *102*, 221−230.

[38] Kang, N. R., Pham, T. H., & Jannasch, P., **2019**, *ACS Macro Letters*, *8*(10), 1247−1251.

[39] Atanasov, V., Bürger, M., Lyonnard, S., Porcar, L., & Kerres, J., **2013**, *Solid State Ionics*, *252*, 75−83.

[40] Atanasov, V., Oleynikov, A., Xia, J., Lyonnard, S., & Kerres, J., **2017**, *Journal of Power Sources*, *343*, 364−372.

[41] Lafitte, B., & Jannasch, P., **2007**, *Advances in fuel cells* (Vol. 1, pp. 119−185). Elsevier Science.

[42] Hou, J., Yu, H., Wang, L., Xing, D., Hou, Z., Ming, P., ... & Yi, B., **2008**, *Journal of power sources*, *180*(1), 232−237.

[43] Einsla, M. L., Kim, Y. S., Hawley, M., Lee, H. S., McGrath, J. E., Liu, B., ... & Pivovar, B. S., **2008**, *Chemistry of Materials*, *20*(17),

5636-5642.

[44] Tsuneda, T., Singh, R. K., Iiyama, A., & Miyatake, K., **2017**, *ACS omega*, *2*(7), 4053-4064.

[45] Agarwal, T., Adhikari, S., Kim, Y. S., Babu, S. K., Tian, D., Bae, C., ... & Borup, R. L., **2023**, *Journal of Materials Chemistry A*.

[46] Tsuneda, T., Singh, R. K., Kunimatsu, K., Iiyama, A., & Miyatake, K., **2017**, *Electrochemical Society Meeting Abstracts 232* (No. 46, pp. 2030-2030).

Chapter 5. Conclusion

Among water electrolysis technologies, anion exchange membrane water electrolyzers (AEMWEs) are attracting considerable attention as a next-generation water electrolyzer technology because it can produce high-purity hydrogen through use of non-platinum group metal based electrodes at high current densities. Anion exchange membranes (AEMs) are key component of AEMWEs, and its main role is to transfer hydroxide and prevent crossover of gas generated from both the cathode and anode. The ionomer present on the electrode catalyst layer also affects the water electrolysis performance, serving as a binder and effectively delivering hydroxide ions from the catalyst layer to the membrane.

In Chapter 2, anion exchange membranes for water electrolysis with improved mechanical strength and alkaline stability were developed. In order to increase mechanical strength, an interpenetrating cationic network membranes were prepared, and pyrrolidinium and piperidinium, which have high alkaline stability, were introduced as cationic groups. The PiP/xEVOH membranes are capable of high KOH uptake of 60.9% while maintaining excellent mechanical strength of 21.9-55.3MPa. PiP/50EVOH showed excellent ionic conductivity of 66.6 mS/cm at 70℃. Also, PiP/50EVOH which β hydrogens of cation groups exist inside the ring shows excellent alkaline stability than commercially available AEMs. Under 1M KOH conditions, MEA with PiP/50EVOH membrane exhibits a current density of 1.78 A/cm^2 at 2.0V and 70℃. Also, ionic conductivity of BD₃/50EVOH (161 mS/cm at 70℃) was higher than with the commercial available FAA-3 membrane. In addition, high alkaline stability was confirmed as the ionic conductivity was maintained even after immersion in 1M KOH at 70℃ for 310 hours. BD₃/50EVOH membrane exhibited excellent AEMWE performance with the current density of 1.57 A/cm^2 at the potential of 2.0 V in 1 M KOH at 70 ℃,

In Chapter 3, polydiallylammonium−based anion exchange membranes and ionomer for AEMWEs were developed. Diallylammonium produces a pyrrolidinium anion exchange groups with excellent alkaline stability through cyclization polymerization. PDAA−BP(3.39) showed good thermal stability over 180℃, and had a high hydroxide conductivity of 152.4 mS/cm at 80℃. In the AEMWEs performance test, PDAA−BP(3.39) with the highest IEC showed excellent performances of 5.07 A/cm^2 and 9.98 A/cm^2 at 1.8V and 2.0V, respectively. In addition, polydiallylammonium ionomers with a wide range of ion exchange capacities were synthesized by adjusting the chain group, and the effect of the ion exchange capacities on AEMWE performance was confirmed. When applied to AEMWEs, the current density increased as the IEC of PDAA−X,Y increased, but the current density decreased after IEC 3.7 mmol/g. In addition, the greater the hydrophobicity of PDAA−X,Y, the faster the emission of generated H$_2$ gas and the higher current density was shown because the reaction site was not blocked with H$_2$ gas. PDAA−3,8 has an excellent current density of 8.23 A/cm^2 at 2.0V.

High−temperature proton exchange membrane fuel cells (HT−PEMFCs) are tolerant to carbon monoxide poisoning and exhibit increased catalytic activity at elevated temperature. However, Nafion, a typical commercially available proton exchange membrane, shows a rapid decrease in proton conduction at high temperatures due to low humidity. Also, phosphoric acid doped− polybenzimidazole which is widely studied as a proton exchange membranes and ionomers for HT−PEMFCs causes phosphate poisoning of the platinum catalyst. Therefore, the development of membranes and ionomers that can be stably applied to HT− PEMFCs is necessary.

In Chapter 4, ionomers and proton exchange membranes containing protonated phosphonic acid groups were developed for HT−PEMFCs. The protonated phosphonic acid group is capable of proton transport even at high temperature and low humidity. The parameters of the dispersion solvent that affect the microporous

structure of the ionomer were identified, and the effect of the microporous structure of the ionomer on the fuel cell was confirmed. The best parameter that correlates with the visible transmittance is the pKa of the dispersing agent. The cell performance varied drastically, depending on the porous structure of the ionomer. The MEAs processed by NMP, DMAc, and DMF (high level of pores) exhibited the highest peak power density (PPD) ($\sim$700 mW cm^{-2}), while the MEAs processed by DMSO and water/NPA (no pores) showed the lowest PPD ($\sim$540 mW cm^{-2}). Therefore, NMP, DMAc, and DMF are the best choices for electrode processing, considering the fuel cell performance and durability. In chapter 4.3, SP55 showed the highest proton conductivity of 514.4 mS/cm due to the protonated phosphonic acid effect. MEAs with protonated membrane and protonated ionomer showed the highest PPD over N212 at 80 ℃/40RH, 100 ℃/80RH, and 120 ℃/40RH condition. Therefore effect of the protonated membrane was confirmed at high temperature and low humidity, and a synergy effect was exhibited when used together with the protonated membrane and ionomer.

Finally, to summarize, moving towards a hydrogen economy requires simultaneous development of water electrolyzers that produce green hydrogen and fuel cells that generate electricity using hydrogen. Therefore, in this study, anion exchange membrane and ionomer, and proton exchange membrane and ionomer that can be applied to anion exchange membrane water electrolyzers and proton exchange membrane fuel cells, respectively, were developed and evaluated.

국문초록

연료전지 및 수전해용
이온 교환성 고분자 설계 및 융합

      화석연료 중심의 에너지 시스템에서 벗어나 수소를 에너지원으로 활용하는 수소 경제로의 전환이 가속화되면서 수소경제 활성화를 위한 에너지 기술의 중요성이 대두되고 있다. 수소경제의 양면을 이루는 수전해와 연료전지는 수소경제의 기본이 되는 기술이며, 수전해는 전기를 이용하여 물로부터 수소를 생산하는 기술이고, 연료전지는 수소 연료로부터 전기를 생산하는 기술이다. 수전해 기술 중에서 음이온교환막 수전해는 비귀금속 기반 전극의 사용과 고순도의 수소 생산이 가능하여 차세대 수전해 기술로 주목받고 있다. 음이온교환막 수전해에서 음이온 교환 분리막은 막 전극 접합체를 이루는 핵심 요소로, 이온을 전달하며 동시에 양극에서 발생하는 가스의 crossover를 막아준다. 음이온 교환 분리막은 높은 이온전도도와 기계적 안정성을 가져야하고 알칼라인 안정성이 좋아야 한다. 이오노머 또한 수전해의 성능에 영향을 미치는 중요한 요소로, 전극 촉매 층 위에 존재하며 바인더 역할과 동시에 촉매 층으로 이온을 효과적으로 전달해준다.

      제 2장에서는 향상된 기계적 강도와 알칼라인 안정성을 가지는 음이온교환막 수전해용 음이온교환막을 개발했다. 기계적 강도를 높이기 위해 양이온성 고분자 네트워크를 이루는 상호 침투 고분자막을 만들었고, 양이온기로는 환형구조로 알칼라인 안정성이 높은 피롤리디늄과 피퍼리디늄이 도입됐다. 개발된 막은 기존 상용화된 음이온교환막보다 향상된 알칼라인 안정성 및 내구성을 보였다.

      제 3장에서는 다이알릴암모늄 기반의 음이온교환막 수전해용 음이온교환막과 이오노머 개발을 다룬다. 다이알릴암모늄은 고리화중합을

통해 알칼라인 안정성이 우수한 피롤리디늄 음이온 교환기를 만들어낸다. 이를 이용해 제작된 음이온교환막은 수전해 평가에서 2.0V에서 9.98 A/cm^{2}의 높은 전류밀도를 가졌다. 또한 사슬기의 조절을 통해 넓은 범위의 이온교환 용량을 가지는 폴리다이알릴암모늄 이오노머를 합성했으며, 수전해 성능에 미치는 이오노머의 이온교환 용량 효과를 확인했다.

고온 양이온교환막 연료전지는 높은 온도로 인해 일산화탄소로 인한 피독을 줄일 수 있고, 촉매 활성을 높일 수 있다. 고온 양이온교환막과 이오노머로 널리 연구되고 있는 인산이 도핑된 폴리벤즈이미다졸은 백금 촉매의 phosphate 피독을 일으킨다. 따라서 고온양이온 교환막 연료전지에 안정적으로 응용할 수 있는 분리막 및 이오노머의 개발이 대두되고 있다. 제 4장에서는 고온 양이온교환막 연료전지용 양성자화된 포스폰산기를 포함하는 이오노머 연구와 분리막 개발을 다룬다. 양성자화된 포스폰산기는 고온 및 저습에서도 양성자 전달이 가능하다. 본 연구를 통해 이오노머의 미세다공성 구조에 미치는 분산 용매의 파라미터를 밝혀냈으며 이오노머의 미세다공성 구조가 연료전지에 미치는 영향을 확인했다. 양성자화된 포스폰산기를 함유하는 양이온교환막은 나피온보다 좋은 기계적 물성을 나타냈으며 고온 및 저습에서 나피온보다 더 좋은 연료전지 성능이 얻어졌다.

주요어 : 음이온교환막 수전해, 고온 양이온교환막 연료전지, 음이온교환막, 양이온교환막, 이오노머
학번 : 2019-36023